

CR-102,801

May 15, 1970

INVESTIGATION OF THE PREPARATION OF MATERIALS IN SPACE

TASK IV

FIELD MANAGEMENT FOR POSITIONING AND PROCESSING OF FREE SUSPENDED LIQUID MATERIALS

CONTRACT No. NAS 8-24683

MODIFICATION No. 2

CONTROL No. DCN 1-9-54-20055, S2

9101172/62

N70-35742	
(ACCESSION NUMBER)	(THRU)
95	1
(PAGES)	(CODE)
CR-102801	23
(NASA CR OR TMX OR AD NUMBER)	(CATEGORY)

Space Sciences Laboratory

GENERAL  ELECTRIC

SPACE DIVISION

Valley Forge Space Center

P. O. Box 8555 • Philadelphia, Penna 19101

Reproduced by
**NATIONAL TECHNICAL
INFORMATION SERVICE**
Springfield, Va. 22151

INVESTIGATION OF THE PREPARATION OF MATERIALS IN SPACE

TASK IV

**FIELD MANAGEMENT FOR POSITIONING AND PROCESSING
OF FREE SUSPENDED LIQUID MATERIALS**

BY

R. T. Frost

A. Gatti

L. Napaluch

E. Stockhoff

G. Wouch

Final Report

Covering the Period 22 August 1969 — 31 April 1970

Contract No. NAS 8-24683

Modification No. 2

Control No. DCN 1-9-54-20055, S2

Prepared for

**NATIONAL AERONAUTICS AND SPACE ADMINISTRATION
MANUFACTURING ENGINEERING LABORATORY
MARSHALL SPACE FLIGHT CENTER**

May 15, 1970

**Space Sciences Laboratory
GENERAL ELECTRIC COMPANY
P. O. Box 8555
Philadelphia, Pennsylvania 19101**

FOREWORD

This Final Report describes the efforts on Task IV during the period 22 August 1969 to 31 April 1970. The first three tasks under this contract were concerned with the collection and assessment of ideas for the exploitation of the space environment. These tasks were especially concerned with.

- I Growth of high density, highly perfect crystals.
- II. Melting, purification and solidification of materials
- III. Unit separation processes.

Work on these first three tasks is monitored by Dr. E C McKannon, Marshall Space Flight Center, and is reported separately. The work reported herein is concerned with a fourth task

- IV. Field management for positioning and processing of free suspended liquid materials.

The contract monitor is Leroy H. Berge, Marshall Space Flight Center. This work has as its objective the definition in some depth of the physical problems associated with the melting, purification, and solidification of free floating materials in a weightless environment. Another objective of this Task is to define experimental techniques and hardware which will be required in developing new metallurgical and ceramic processes for exploitation of the space environment.

ABSTRACT

Many new processes which can exploit the weightless environment of space have been suggested as possibilities for making improved or unique materials. A large number of these will involve, at some stage, a containerless melt or transfer of molten material. Some of the physics and technology problems associated with these processes are discussed. The range of applicability of some new electromagnetic process control methods is also presented. Development of a servo device for measurement and control of free floating masses is described.

Table of Contents

	Page
I. Introduction	I-1
II. Examples of Weightless Materials Processes	II-1
A. Elimination of Gravitational Phase Separation	II-1
B. Elimination of Thermal Convection	II-3
C. Crucibleless Melting	II-3
D. The Possibility for Solidification in the Absence of Contact with Molds	II-4
E. Shape Formation Through Surface Tension and Inertial and Electromagnetic Fields	II-4
F. Positioning and Handling of Containerless Melts — Theoretical and Experimental Studies	II-5
III. Oscillations of a Free Liquid Spheroid	III-1
A. Mass Limitations	III-2
B. Free Oscillations	III-2
C. Excitation or Damping by Positioning Device	III-5
D. Internal Fluid Currents	III-6
E. Rotations	III-6
F. Sound Wave Generation	III-6
IV. Theory of Electromagnetic Position Control and Body Distributed Currents and Forces	IV-1
A. RF Position Control of Levitated Mass	IV-1
B. Vector Potential Induced in Conducting Sphere by Uniform Oscillating Magnetic Field	IV-1
V. Force Measurements and Techniques	V-1
A. Measurement of Large Forces	V-1
B. Measurement of Small Forces	V-1
C. Measurement of Stability of Sphere Position Within Positioning Coils When Servo Loop is Inactivated	V-5
VI. Position Sensing and Control Servo	VI-1
A. Introduction	VI-1
B. Description of Servo Circuits	VI-1
C. Dynamic Analysis of Loop	VI-4
D. Position Sensing Considerations	VI-5
E. Spinning a Conductive Sphere	VI-7

VII.	General Requirements for Space Experiment Facilities	VII-1
A.	Introduction	VII-1
B.	Material Properties – General Considerations	VII-2
C.	Melting Power Required to Supply Surface Radiated Power Loss	VII-2
D.	Basic Equations for Acceleration and Heating	VII-5
	1. Development of Relations Involving only Material and Driving Coil Parameters	VII-7
	2. General Behavior of Force and Power Skin Depth	VII-8
	3. Regimes of x and Range of Parameters	VII-9
	4. Small x Power and Force Relations	VII-9
	5. Positioning Control at Small x	VII-9
	6. Positioning at Large x	VII-13
E.	Frequency Choice for Facilities	VII-13
F.	Heating and Temperature Control	VII-16
G.	Position Sensing	VII-18
VIII.	References	VIII-1
Appendix A	Measurement of Small Forces	A-1
Appendix B	Dielectric Positioning	B-1
Appendix C	Superposition of Forces and Distributions Contributed by Two Coils	C-1
Appendix D	Electrostatic Positioning of a Dielectric	D-1
Appendix E	Reflected Impedance Due to Eddy Currents	E-1
Appendix F	Electric Displacement Current in Dielectrics	F-1
Appendix G	Co-variant Solution of Electromagnetic Eddy Current Problem	G-1

List of Illustrations

	Page
III-1	Shape Oscillation Periods Free Floating Melt III-1
III-2	Hydrodynamic Modes III-2
III-3	Damping Constants for the Aperiodic Modes III-5
III-4	Fluid Currents Due to Magnetostriction III-6
IV-1	Dependence of the Force of Repulsion on the Ratio of the Sphere Radius to Skin Depth IV-2
IV-2	Radial Component of Magnetic Field per Unit Magnetic Induction in Aluminum Sphere of Radius $R_2 = 0.4125$ Inches at Colatitude $\theta = 45^\circ$, Showing Penetration of Field into Sphere as a Function of Skin Depth IV-6
IV-3	Radial Component of Magnetic Field per Unit Magnetic Induction in Aluminum Sphere Radius $R_2 = 0.4125$ Inches at Colatitude $\theta = 45^\circ$, Showing Penetration of Field into Sphere as a Function of Skin Depth IV-7
IV-4	θ Component of Magnetic Field per Unit Magnetic Induction in Aluminum Sphere of Radius $R_2 = 0.4125$ Inches at Colatitude $\theta = 45^\circ$, Showing Penetration of Field into Sphere as a Function of Skin Depth IV-8
IV-5	θ Component of Magnetic Field per Unit Magnetic Induction in Aluminum Sphere of Radius $R_2 = 0.4125$ Inches at Colatitude $\theta = 45^\circ$, Showing Penetration of Field into Sphere as a Function of Skin Depth IV-9
IV-6	Positive Cycle Average of Current Density per Unit Magnetic Induction versus Radial Distance from Center of Aluminum Sphere 0.4125 Radius for $\theta = 90^\circ$ IV-11
IV-7	Radial Component Force/Volume per Magnetic Induction Squared for Aluminum Sphere $R_2 = 0.4125$ Inches at $\theta = 45^\circ$ as a Function of Skin Depth IV-13
IV-8	θ Component Force/Volume per Unit Magnetic Induction Squared for Aluminum Sphere $R_2 = 0.4125$ Inches at $\theta = 45^\circ$ as a Function of Skin Depth IV-14
V-1	Large Force Measuring Apparatus V-2
V-2	Results for Cu and Al at a Coil Current Level of 1.4 rms Ampere V-2
V-3	Results for Cu at Various Frequencies V-3
V-4	Results for Al at Various Frequencies V-3
V-5	Acceleration per Unit Exciting Coil Current Squared V-4
V-6	Tilt Table Assembly for Measurement of Small Forces V-6
V-7	Coil Current versus Position for Constant Force at 10 kHz on Aluminum Sphere V-7
V-8	Force versus Current at Various Distances V-8
VI-1	Positioning Coils on Tilt Table VI-2
VI-2	Electronic Breadboards for Position Servo VI-2
VI-3	Block Diagram of Position Servo Electronics VI-3
VI-4	Position Sensing Characteristic VI-3
VI-5	Force Measuring Apparatus Tilt Table and Pendulum VI-5
VI-6	Bodie Plot of the Important Frequencies VI-6
VI-7	Solid Copper Sphere Supported on Ball Bearing Centered Among Four Coils which Generated a Rotating Magnetic Field VI-7

VII-1	Skin Depth versus Frequency for Several Common Metals and Molten Glass . . .	VII-3
VII-2	Ratio $F_1(x)/G_1(x)$ and the Functions $F_1(x)$ and $G(x)$	VII-8
VII-3	Eddy Current Power Absorbed by a Free Floating Specimen	VII-10
VII-4	Rigid Positioning of Free Floating Object During Acceleration as High as $10^{-4}g$.	VII-12
VII-5	Power as a Function of Driving Frequency for Metals and Semiconductors . .	VII-14
VII-6	Acceleration as a Function of Driving Frequency for Metals and Semiconductors	VII-15
VII-7	Power as a Function of Driving Frequency for Molten Glass	VII-17
VII-8	Minimum Heating Power Required to Achieve Melting Temperature for Several Metals of Interest	VII-18
A-1	Maximum Density of all Particles with Diameters Greater than s for Several Classes of Clean Room	A-3
A-2	Preventing a Sphere from Rolling Freely	A-3
A-3	Layout of Apparatus for Measurement of Small Forces with a Minimum of Electromagnetic Field Distortion	A-4
A-4	Sphere Suspension	A-5
C-1	Average Power as a Function of Phase Difference	C-2
D-1	Hollow Glass Sphere Filled with Water for Test of Electrostatic Repulsion with One Pointed Electrode	D-1
D-2	Hollow Glass Sphere Filled with Water for Test of Electrostatic Repulsion with Four Pointed Electrodes	D-2
F-1	Plots of $\rho/\kappa_e\epsilon_0 = (2\pi/Q) f$ with Dashed Lines a Molten Glass Region	F-2

I. INTRODUCTION

The prospect of the availability of manned experimental facilities in the nearly weightless environment of near earth orbit opens up a number of exciting possibilities for basic studies in metallurgical and ceramic processing. Even at this point in time it appears likely that some of these experiments can lead to basic new insights into phenomena related to materials processing methods and, hopefully, to future commercial exploitation of new methods for production of selected products of high value. As space transportation costs are reduced with development of the space shuttle and reuseability concepts, the range of feasible materials processes will increase rapidly as products of lower dollar value per pound can be considered. It goes without saying that initial experiments should emphasize heavily the acquisition of new basic knowledge and that for some time in the future only commercial products having an extremely high monetary worth per unit weight can be considered for pilot production studies.

II. EXAMPLES OF WEIGHTLESS MATERIALS PROCESSES

In two symposia which NASA has held at the Marshall Space Flight Center, a large number of specific suggestions have been made for new types of processes or for improvements in existing materials preparation methods which may be applicable in the future to commercial production of uniquely valuable products of relatively modest weight. This report will not attempt to summarize these ideas for exploitation of the removal of weight forces. The reader is referred instead to the published proceedings of these symposia, which also include many other references to zero gravity space processing suggestions, and related work. We will here summarize only some suggested new processes which make use of the following categories of phenomena attending the removal of weight forces

1. The elimination of buoyant separation of melt phases of different densities
2. The elimination of thermal convection currents.
3. The possibility for crucibleless melting of metals and ceramics.
4. The possibility for solidification in the absence of contact with molds.
5. Shape forming with surface tension and electromagnetic field forces.

We can think of many processes which exploit these new possibilities either singly or in combination.

A. Elimination of Gravitational Phase Separation

Under the first category, namely the elimination of gravitational separation of melt phases of different densities, we can consider the following candidate products, which are a partial listing of ideas suggested to date:

1. The preparation of new alloys from immiscible melts.
2. The preparation of mixtures of metals with metal oxides, carbides, nitrides, etc.
3. The preparation of foams of metals or glasses.

The occurrence of two-liquid immiscibility in the hypermonotectic alloys at temperatures above the monotectic introduces structural considerations. Given time enough, the two liquids will separate into two layers placed according to density, with the lighter layer water on top. It is quite possible, however, to have the two liquids existing as an emulsion with tiny droplets of one liquid suspended in the other liquid. Which of the two situations, the layer or the emulsion, will be obtained during a given heating and cooling cycle will depend upon the physical characteristics of the alloy system concerned, upon the conditions of formation of the second liquid, and upon the opportunity afforded for the segregation of the two liquids. The possibility of circumventing the buoyant segregation of the two liquids in the weightless environment offers the possibility of preparing mixtures of these melts with controlled concentration of the mixture of solid phases.

A well known example of an alloy system exhibiting liquid immiscibility beyond the monotectic point at sufficiently high temperatures is the Cu-Pb alloy system (II-1). For weight percentages of lead above the monotectic composition point, cooling from sufficiently high temperature will cause breakdown into two liquid layers. The Cu-rich layer forms the top layer and the Pb-rich layer the bottom layer. Some interesting systems are systems such as Cu-W which are virtually insoluble in each other both in the liquid and solid state. One again gets a two layer system and the bottom layer W solidifies first at the freezing point of W, the top layer freezing at the freezing point of Cu. Of interest would be the preparation of an emulsion of W and Cu which would be readily accomplished in the weightless state and examination of the properties of the mixture produced upon solidification.

The preparation of many mixtures of metals with metal oxides, carbides, nitrides, etc., involves components with widely different densities. The solubility of oxides, nitrides, etc. in metals is often measured in parts per million. Vigorous stirring will cause mixing but within minutes or even seconds there is separation due to density differences. In a weightless situation, there would be no tendency to segregate due to density differences. Electromagnetic positioning devices discussed in this report would also aid in stirring the components to achieve the dispersion qualities desired. The preparation of dispersions of many substances not contemplated on the Earth could be considered here, such as unique cermet-like materials for structural and electronic applications.

Some examples of these mixtures which have been suggested are rare earth oxide dispersions in superalloys (II-2), oxides of fissionable materials in metallic reactor fuel elements, and dispersions of small particles of glass in a matrix having a different index of refraction to form phototropic materials or Christiansen filters. However, with the possibility of producing many different mixtures as discussed above, there is a unique opportunity for developing totally new materials not contemplated by present technology.

The possibility of producing foams of metals or glasses in the weightless environment offers the possibility of producing very light materials with good service properties. One of the major problems in foam production is the problem of drainage. In the weightless operation, the problem of foam drainage will be eliminated, even though other problems will remain, such as the collapse of bubbles due to surface tension forces or drainage in thin films through suction by Plateau's border.

Some suggestions for application of foam materials are crushable structures, battery electrodes, the production of very light materials with high temperature capability, high strength properties, and imitation of natural products like wood (II-3). Wood has good properties under compression in that it is composed of cells. When the yield point is reached the cells are crushed upon further application of load. This reduces the buckling of these materials. The design of materials with cell like structure would be a very useful imitation of nature.

B. Elimination of Thermal Convection

The effect of thermal convection in forming dislocations in crystals grown from melts has been described by Utech (II-4) and Grodzka (II-5). Hamalainen (II-6) has also described frozen Bénard convection cells in thin alkali halide crystals. This work demonstrates the importance of thermal convection upon the crystal structure obtained. The effect of thermal convection during glass formation on the homogeneity of glasses has been discussed by Deeg (II-7). It seems likely that, in many other cases, the effects of thermal convection may have as yet unrecognized effects.

C. Crucibleless Melting

Limited studies of the potential for crucibleless melting of metals have been performed in terrestrial experiments where small spherules of metals have been levitated and melted by use of radio frequency induction fields (II-8 through II-22). The objectives of this work have generally fallen under one of the following categories

1. Melting and reaction of refractory or reactive metals, some of which are contaminated by any contact with crucible.
2. Formation of an alloy completely free from segregations.
3. Observation of subcooling below the normal freezing point, which can be achieved routinely with some metals.

The method has not found commercial application for several reasons. First, levitation is not practicable for poor conductors. Secondly, the required levitation power is often so high as to preclude separate control of specimen temperature. In other words, a reduction in RF heating of the specimen will cause loss of levitation or pouring from the bottom of the specimen. Instabilities are sometimes encountered, and, in any event, the mass of material which can be prepared is severely limited. Since levitation is the most obvious property of the weightless space environment, we can for the first time consider a whole range of new processes of this type and their potential application to preparation of large quantities of material.

Removal of the requirements for levitation of a crucibleless melt means that we can have complete latitude in heating of the specimen and its temperature control during solidification. Materials can be prepared which are nonconductors, and many suggestions have been made for new glass processes which should be possible in the space environment.

Besides the possibility for reacting and melting materials without crucible contact, a corollary is the ability to provide super heating to reactive and high melting metals for which skull melting techniques must currently be used. This opens up the possibility for precision casting of these materials which cannot at present be accomplished with the negligible superheat available in skull melting.

D. The Possibility for Solidification in the Absence of Contact with Molds

In terrestrial levitation experiments, extreme degrees of subcooling before solidification are often observed (II-23). Walker has achieved subcooling for a number of materials in glass-lined crucibles. In some cases, the degree of subcooling is believed to approach that at which homogenous nucleation occurs. The possibility exists that some materials may form new phases if solidified in the absence of heterogenous nucleation caused by crucible or mold contact. For example, a new phase of gallium, denoted as Gallium 3, has recently been prepared in minute quantities at a temperature of -30° centigrade (II-24).

The possibility for forming glasses from materials which normally crystallize through heterogenous nucleation has been discussed in papers by Olsen (II-25) and Happe (II-26). Since the nature of such products cannot be anticipated at present, it is clear that containerless solidification experiments must initially be proposed with emphasis upon obtaining basic information rather than with any attempt to anticipate commercial applications.

It has been suggested by Witt (II-27) that the difficulty encountered in pulling thin filaments of single crystal material from melts in studies by Monsanto Research would be greatly relieved if it were possible to suspend a crucibleless melt of boron, for example, and apply forces to the melt which would oppose forces due to withdrawing a boron fiber at a rate allowing single crystal formation.

The possibilities for formation of near perfect spheres by solidification of melts under the sole action of their own surface tension has also been suggested.

E. Shape Formation Through Surface Tension and Inertial and Electromagnetic Fields

Deeg (II-28) has suggested possibilities of fire polished glass surfaces for spherical or spheroidal surfaces which could be formed by centrifugal action in a freely suspended rotating melt. Rotations to produce an oblate spheroidal form of given eccentricity can be easily imparted to a floating mass by means of the orthogonal coil sets discussed in a following section.

Alternatively or in conjunction with inertial forces produced by rotation, electrostatic fields can be applied to perturb the spheroidal shape. If the electric field at the surface of a conductor is represented by E , the local curvature imparted to the surface will be given by

$$\sigma \left(\frac{1}{r_1} + \frac{1}{r_2} \right) = p + \frac{E^2}{8\pi} \kappa (\kappa - 1)$$

where r_1 and r_2 are the radii of curvature in two orthogonal directions, p is the internal pressure, σ is the surface tension, and κ is the dielectric constant. Where only slight departures from spheroidal form are required, design of suitable electrodes to furnish fields to produce a desired shape may be feasible.

F. Positioning and Handling of Containerless Melts - Theoretical and Experimental Studies

A large number of the suggested new processes in weightless processing of metals and ceramics involve at some stage a floating molten mass out of contact with crucibles or molds. A floating mass of this type, held together solely by its own surface tension force and free to oscillate in shape, rotate and support internal fluid currents which might be driven by these or other applied forces, represents a phenomenon with which we have had little experience. Such phenomena are briefly encountered in shot tower processes and in free falling liquid streams, but here the effects of air resistance and, usually, lack of time to establish equilibrium exist.

The following section outlines preliminary results on investigation of some physical problems associated with the melting, handling, and solidification of such freely floating masses. The study of the basic physics involved in such processes leads quite naturally to a definition of the experimental facilities which will be required to handle a range of suggested processes. This section also describes some preliminary development of some new physical hardware concepts which will be required in such facilities.

III. OSCILLATIONS OF A FREE LIQUID SPHEROID

The mathematical physics of small shape oscillations in a liquid mass under the sole action of surface tension and viscous and inertial forces was treated by Lord Rayleigh (III-1), and more recently by Chandrasekhar (III-2). The extension of this work to include large oscillations and large viscosity have been made by Benedikt (III-3) and Reid (III-4). For reasonably small oscillations, Figure III-1 gives the oscillation frequency and time decay constant for shape oscillations in which the shape is alternately a prolate and oblate spheroid. This is the simplest mode of oscillation. More complex shape oscillations can also occur; for a given material the oscillation frequency will be greater and the decay time shorter than for the mode for which Figure III-1 applies. The mathematical expressions for the frequency and decay time for a given oscillation mode are available from the classical literature (III-5).

Figure III-2 illustrates the first three hydrodynamic modes. We can describe these modes most easily by expressing the distance from the center of mass to the liquid surface r as a function of colatitude θ in the way shown at the bottom of the figure. For the zero mode, the radius vector equals a constant a_0 multiplied by the 0-order Legendre polynomial which is simply unity. For this mode, the mass is a perfect sphere with no distortion. For the second hydrodynamic mode, which represents a shape oscillation between prolate and oblate spheroid, we must add to the original radius a term $a_2 P_2(\cos \theta) \cos \omega_2 t$. The center drawing in Figure III-2 illustrates this shape at a given instant of time. The shape oscillates sinusoidally between oblate and prolate. This oscillation mode can be either excited or damped by application of the magnetostriction forces through excitation of position control coils.

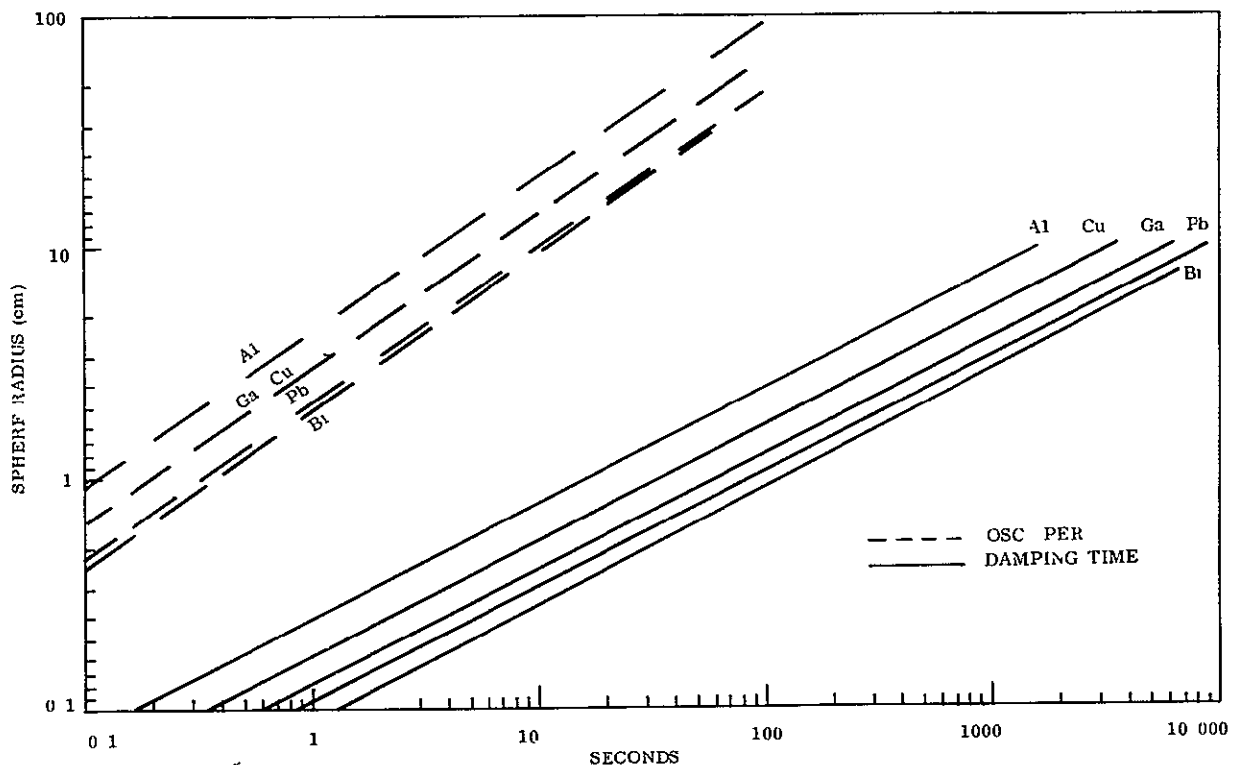


Figure III-1. Shape Oscillation Periods Free Floating Melt

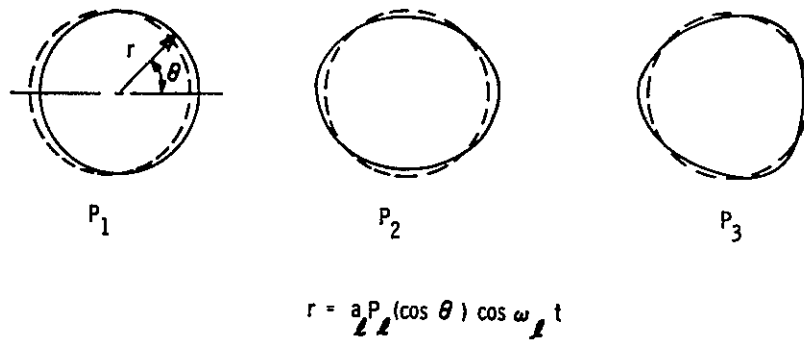


Figure III-2. Hydrodynamic Modes

A. Mass Limitation

Mass limitations arising from excitation of oscillations are described in Reference III-6. Liquid metal masses at least as large as tens of kilograms under control accelerations of $10^{-4}g$ can be considered without worrying about rupture of the mass due to the necessity of position control in practical cases.

As discussed in the following section, studies have been made of methods for position control of a free floating spheroid of liquid. The method which will be described in detail involves the use of electromagnetic fields provided by three orthogonal sets of coils excited by high frequency currents. Regardless of the method used for position control for such free floating liquid masses, it can be anticipated that excitation of shape oscillations and internal fluid currents will occur.

If the position control coils along a given axis are excited asymmetrically, e.g., if we excite only one, then we will obtain a net translational force which excites both the first and third mode. The third mode resembles an eggplant and can be treated similarly to the second mode. The first mode, shown as P_1 in Figure III-2 represents pure translation of a spherical shape and must be treated differently from the other modes. The reason for this is that the frequency corresponding to the first mode is zero and, for this particular term in the sum, we should replace the sinusoidal time term by a term linear in time.

B. Free Oscillations

The free oscillations of a viscous liquid globe under the action of surface tension forces alone are of interest in determining the natural frequencies of the system where resonances can occur. The basic problem we consider here is a fluid sphere of incompressible, viscous fluid under the action of surface tension alone and the small oscillations of the fluid about its spherical form. Lamb (III-5) had discussed this problem in detail for inviscous fluids. Since we are considering small departures from an equilibrium spherical state of an incompressible fluid, we can describe the deformed surface of the configuration by the equation

$$r = R [1 + \epsilon Y_{\ell}^m (\theta, \Phi)]$$

for the deformations of the liquid surface.

The function ϵ is a function of time and here the dependence of the velocities and other quantities on time enters explicitly. It is supposed that

$$\epsilon = \epsilon_0 e^{-\sigma t}$$

where ϵ_0 is a constant and σ is composed of a real part expressing the damping of oscillation due to viscous forces and an imaginary part expressing the oscillatory nature of the deformations about the spherical form

$$e^{-\sigma t} = e^{-t/\tau} e^{-i2\pi f t}$$

where τ is the damping time and f is the frequency of the oscillation.

The angular frequencies of oscillation are given by

$$(2\pi f)^2 = \sigma_{\ell;0}^2 = \ell(\ell-1)(\ell+2) T_1 / \rho R^3$$

where

$\sigma_{\ell;0}$ = the angular oscillation frequency for inviscous liquids

ℓ = the degree of the surface harmonic $Y_{\ell}^m(\theta, \Phi)$

R = the radius of the undeformed sphere

ρ = density of the fluid

T_1 = surface tension/unit length

$$Y_{\ell}^m(\theta, \Phi) = P_{\ell}^m(\cos \theta) \left\{ g_{\ell}^m \cos m \Phi + h_{\ell}^m \sin m \Phi \right\}$$

where the P_{ℓ}^m are the associated Legendre polynomials.

For small oscillations of viscous fluids about their spherical form, the problem is to determine the $\sigma_{\ell, \nu}$'s or the frequencies of oscillation for a coefficient of kinetic viscosity ν . This involves solving the linearized equations of motion.

$$\frac{\partial \vec{u}}{\partial t} = -\nabla \left(\frac{\delta P}{\rho} \right) - \nu \nabla \times (\nabla \times \vec{u})$$

$$\nabla \cdot \vec{u} = 0$$

where \vec{u} = velocity, P = pressure, ρ = density, and t is time, subject to the following prescribed boundary conditions:

1. At the deformed surface of the drop, the radial component of the velocity must be equal to the velocity of the surface itself.
2. The tangential stresses vanish at the surface.
3. The normal component of the viscous stress is $-P_{rr} = T_1 (1/R_1 + 1/R_2)$. Here R_1 and R_2 are the principal radii of curvature taken positive when directed inward.

Reid (III-4) has discussed this problem and he obtains the characteristic equation for the frequencies of oscillation:

$$\frac{\alpha^4}{q^4} + 1 = \frac{2(\ell - 1)}{q} \ell + (\ell + 1) \left[\frac{q - 2\ell Q_{\ell+1/2}(q)}{q - 2Q_{\ell+1/2}(q)} \right]$$

where $Q_{\ell+1/2}(q)$ is written in terms of spherical Bessel functions as $J_{\ell+3/2}(q)/J_{\ell+1/2}(q)$.

Here we have

$$\alpha^2 = \frac{\sigma_{\ell;0} R^2}{\nu}$$

$$\frac{\sigma_{\ell;\nu}}{\sigma_{\ell;0}} = \frac{q^2}{\alpha^2}$$

We can solve the characteristic equation and get the $\sigma_{\ell;\nu}$'s. The following results are obtained:

As $q \rightarrow \infty$, the limiting case of small viscosity

$$\sigma_{\ell;\nu} = (\ell - 1)(2\ell + 1) \nu / R^2 \pm i \sigma_{\ell;0}$$

which is Lamb's result.

2. The characteristic equation admits solutions of two types, depending on a value of α called the critical value α_c .
 - a. If $\alpha^2 > \alpha_c^2$ then damped oscillations will occur.
 - b. If $\alpha^2 < \alpha_c^2$, two aperiodic modes of decay appear.

Figure III-3, from Chandrasekhar's book, illustrates the aperiodic decay constants in terms of the undamped angular frequency $\sigma_{l,0}$ and the physical properties of the liquid spheroid.

C. Excitation or Damping by Positioning Device

Excitation of the position control coils can be used either to initiate or to damp translational motions of the floating mass and shape oscillations as well as any rotations which may occur. The position control and shape oscillation problem is most easily treated by considering individual hydrodynamic modes of a liquid sphere under the action of surface tension forces and the electromagnetic forces due to internal eddy currents.

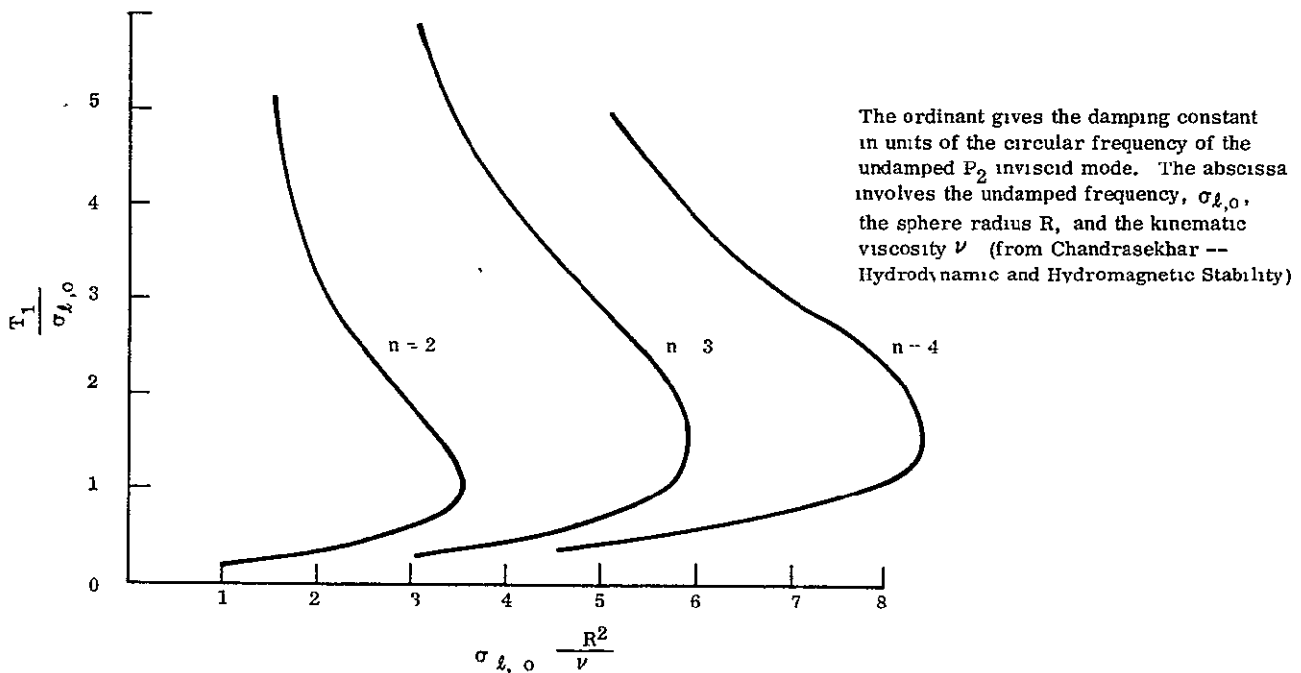


Figure III-3. Damping Constants for the Aperiodic Modes

D. Internal Fluid Currents

In addition to generation or damping of surface oscillations and translational motions, we can stimulate circulating currents within the floating mass by magnetostrictive forces. Figure III-4 shows a simple current pattern which can be stimulated by exciting a single control axis. These fluid currents can be oriented in various directions by exciting various sets of coils. These currents will be useful for stirring of alloys or dispersions and will also affect bubble motion in an important way.

At the higher frequencies, the pressure gradient resulting from the magnetostrictive forces which drive the steady state fluid currents will be concentrated in a thin surface layer centered about the equatorial plane with respect to the excitation axis. After the coils are excited, an equilibrium will be quickly reached in which this driving pressure gradient is balanced by viscous forces. At lower frequencies where the skin depth becomes an appreciable fraction of the sphere radius, the flow patterns will be altered somewhat. The quasiequilibrium shape of this spheroid will be influenced not only by the magnetostrictive forces which drive the fluid currents, but also by the dynamics of the circulating dense fluid. Since magnetostrictive forces can be applied in an arbitrary manner and translational acceleration of the mass can be suppressed by simultaneous excitation of opposite members in coil pairs, we see that considerable freedom exists for electromagnetic shaping of the floating mass in various symmetric or asymmetric configurations.

E. Rotations

If we consider an orthogonal pair of excitation coils to be excited with a phase quadrature so as to produce a rotating magnetic field, we can calculate that the spheroid will be caused to rotate in the manner of the rotor of an induction motor. By proper choice of excitation for various pairs of the positioning coils, angular velocity can be imparted to the floating spheroid in any desired direction and with any speed consistent with configurational stability of the mass. This will be limited by the stability furnished by the action of surface tension. Oscillational instability can occur for higher rotational speeds, and damping due to viscosity will play a key role in prevention of buildup of catastrophic oscillations. Conversely, properly phased excitation of a given pair of coils can be used to remove an angular velocity orthogonal to both coil axes if such rotation is not desired.

F. Sound Wave Generation

The high frequency variation of magnetostriction forces can be used to generate sound waves within the floating mass if we desire to go to high level excitation. This might be useful, for example, to prevent agglomeration of oxide dispersion particles within the mass.

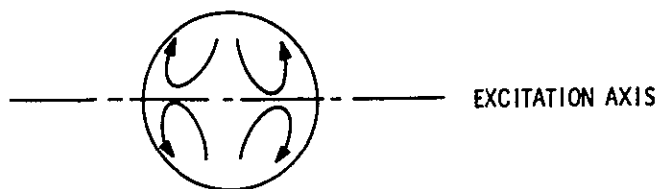


Figure III-4 Fluid Currents Due to Magnetostriction

IV. THEORY OF ELECTROMAGNETIC POSITION CONTROL AND BODY DISTRIBUTED CURRENTS AND FORCES

The present section describes theoretical developments pursued in order to examine a few idealized basic problems which have immediately applicable results and which can be logically extended to obtain solutions to other problems. The objectives of these theoretical development are (1) to understand the electric currents induced in material bodies of selected composition when these bodies are immersed in electromagnetic fields, (2) to understand the forces exerted on freely suspended material bodies by electromagnetic fields, and (3) to determine the interaction of material bodies with the electromagnetic field sources through mutual inductance and capacitance so as to describe how the positioning and control devices must function.

A. RF Position Control of Levitated Mass

For three-axis position control of the levitated specimen in zero-g environment, three pairs of centering coils can be used, each pair with an axis orthogonal to the other two. The theory of the forces delivered to the levitated mass resulting from excitation of any one of the coils has been studied by Okress (IV-1). The theory has been generalized for multiple turn coils by Fromm and Jehn (IV-2). Since relatively small forces are required for centering, it is expected that quite low RF powers will suffice.

Figure IV-1 (from Fromm and Jehn) shows a cross section of a levitation coil used in present one-g experiments. In a zero-g experiment, one can utilize relatively weak currents in a few turns and provide stability by the addition of a separately powered coil lying above the sphere, and similarly other sets of coils in a position, to impart forces in all three orthogonal directions. Excitation of any one of the coils would cause a repulsion away from it so that a total of six coils in three orthogonal sets would do the job.

Figure IV-1 shows the way in which the force of repulsion depends on the dimensionless parameter X , the ratio of sphere radius to skin depth. The restoring forces on the levitated object will be concentrated within a "skin depth" given by the formula in the figure. Here, f is the frequency, γ is the conductivity, and μ is the permeability. Larger forces are available, at a given power, by the use of higher frequency or lower resistivity materials. To some extent, the distribution of the body forces can be adjusted by adjustment of the frequency, in the sense that the skin depth may be made to penetrate through the body of the specimen by going to a sufficiently low frequency. This would allow imparting of restoring forces with minimum distortion of the surface shape of the specimen. If separate facilities are provided for resistance oven or RF heating, separate control could be achieved for melting and stirring, the latter achieved by use of the high intensity RF fields.

B. Vector Potential Induced in Conducting Sphere by Uniform Oscillating Magnetic Field

The first problem considered is that of a conducting sphere in a uniform time harmonic magnetic field. The solution of this problem is applicable to the study of melting conducting materials by induction, fluid currents produced by electromagnetic forces, fluid oscillations due to electromagnetic forces, studies of bubble motion driven by fluid currents, the generation of acoustic

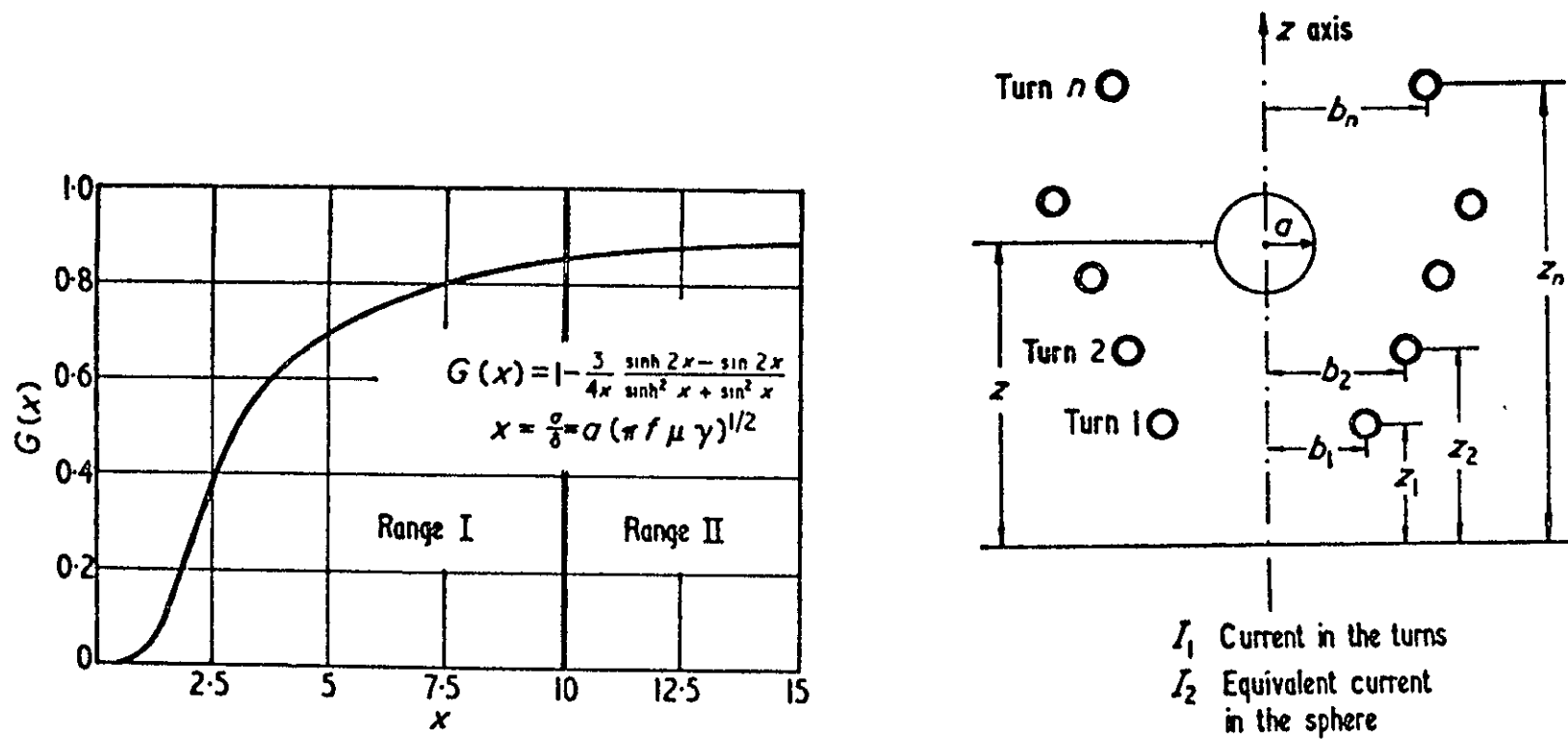


Figure IV-1. Dependence of the Force of Repulsion on the Ratio of the Sphere Radius to Skin Depth

waves, and many other topics of interest. This solution is also the first step in understanding positioning forces exerted on the sphere by nonuniform fields, since it can be used to construct a first-order solution for force exerted by fields having gradients, as will be shown in following sections.

The problem considered is a sphere of uniform conductivity σ immersed in a time harmonic uniform magnetic field $\vec{B}_A = B_0 \hat{k} \cos \omega t$, where B_0 is the amplitude of the applied field, $\nu = \omega/2\pi$ is the frequency of the applied field, and \hat{k}_0 is the unit vector in the z direction. Mathematically the problem can be formulated as the following boundary value problem:

$$\nabla^2 \vec{A}_e = 0 \text{ outside the sphere}$$

$$\nabla^2 \vec{A}_i - \mu \sigma \partial \vec{A}_i / \partial t = 0 \text{ inside the sphere}$$

and boundary conditions:

$$\text{As } r \rightarrow \infty, \vec{A}_e \rightarrow \vec{A}_A$$

$$\text{As } r \rightarrow 0, \vec{A}_i \text{ remains finite}$$

$$\text{At } r = a, \hat{n} \cdot [(\nabla \times \vec{A}_i) - (\nabla \times \vec{A}_e)] = 0$$

$$\hat{n} \times [1/\mu_i \nabla \times \vec{A}_i - 1/\mu_o \nabla \times \vec{A}_e] = 0.$$

Here \vec{A} is the vector potential and the magnetic induction \vec{B} is just $\nabla \times \vec{A}$.

Thus

$$\vec{B}_A = \nabla \times \vec{A}_A \text{ is the applied magnetic field}$$

$$\vec{B}_e = \nabla \times \vec{A}_e \text{ is the total external magnetic field}$$

$$\vec{B}_i = \nabla \times \vec{A}_i \text{ is the magnetic field within the sphere, and solving the boundary value posed above for } \vec{A}_e \text{ and } \vec{A}_i \text{ gives } \vec{B}_e \text{ and } \vec{B}_i.$$

The above problem has been treated by Smythe (II-20) and others. We have extended the treatment of Symthe to include the field inside the sphere, the instantaneous forces acting at all points on and within the sphere, and the time averaged forces acting at all points on and within the sphere. Rather than present the detailed solution to this problem which can be found in the above reference, we shall outline the solution and discuss the results and our extension in detail. An alternate solution in terms of the co - variant form of field equations is given in Appendix G.

To simplify the mathematical solution of the problem, it is convenient to replace $\vec{B}_A = B_0 \cos \omega t \hat{k}$ by $B_A = B_0 e^{j\omega t} \hat{k}$, where $e^{j\omega t} = \cos \omega t + j \sin \omega t$, where $j = \sqrt{-1}$.

We can then write

$$\nabla_i^2 \vec{A} - j \omega \mu \sigma \vec{A} = 0.$$

We must remember that in the solutions we must multiply by $e^{j\omega t}$ and take the real part as the actual solution.

The vector potential \vec{A}_A of \vec{B}_A can be written in spherical polar coordinates as $\vec{A}_A = \frac{1}{2} B_0 r \sin \theta \hat{\Phi}$, where $\hat{\Phi}$ is the unit vector in the Φ direction. Since the exciting vector potential has only a $\hat{\Phi}$ component, we expect the currents induced in the sphere to have only a $\hat{\Phi}$ component, and hence the vector potential \vec{A}_i to have only a $\hat{\Phi}$ component. Since the total external vector potential is due to the applied field and the induced currents, we then have the vector potential external to the sphere; \vec{A}_e must also have only a $\hat{\Phi}$ component. The results obtained by Smythe (II-20) after writing $\nabla^2 \vec{A} = 0$ and $\nabla^2 \vec{A} - j\omega\mu\sigma \vec{A} = 0$ in spherical polar coordinates and solving the boundary value problem by separation of variables are:

$$\vec{A}_e = \left[\frac{1}{2} B_0 r \sin \theta + D B_0 \sin \theta / r^2 \right] \hat{\Phi}$$

$$\vec{A}_i = \frac{1}{2} B_0 C r^{-\frac{1}{2}} I_{3/2} \{ (jp)^{\frac{1}{2}} r \} \sin \theta \hat{\Phi}$$

where

$$D = \frac{(2\mu + \mu_0) v I_{-1/2} \{v\} - \left[\mu_0 (1 + v^2) + 2\mu \right] I_{1/2} \{v\}}{(\mu - \mu_0) v I_{-1/2} \{v\} + \left[\mu_0 (1 + v^2) - \mu \right] I_{1/2} \{v\}} a^3$$

and

$$C = \frac{3\mu v a^{3/2}}{(\mu - \mu_0) v I_{-1/2} \{v\} + \left[\mu_0 (1 + v^2) - \mu \right] I_{1/2} \{v\}}$$

Here we have I_n as the symbol for the Bessel function of order $n, p = \sigma\mu\omega$ and $v = (jp)^{1/2} a$. The skin depth δ is a basic parameter of the solution and

$$\delta = \sqrt{\frac{2}{\sigma\mu\omega}} = \sqrt{\frac{2}{p}}$$

If we consider the conducting sphere as not permeable so that $\mu = \mu_0$, then C further simplifies to become

$$C = \frac{3 a^{3/2}}{v I_{1/2} \{ v \}}$$

Explicit Analytical Expressions for Body Distributed Currents and Forces

Eddy Currents

An expression for the magnetic potential \vec{A} and the current density j is available from the work of Smythe (II-20) as outlined above.

Figures IV-2 and IV-3 show the results of calculations of the radial component of the magnetic field inside a conducting sphere placed in a previously uniform oscillating magnetic field. The ordinants give the radial component of the magnetic field inside this sphere (B_{ir}) normalized to the unperturbed value B of the external field. The parameters labeling the various curves are the ratio of sphere radius R_2 to skin depth δ . As noted above, the skin depth is determined by the angular frequency ω , the sphere conductivity σ , and the permeability μ . High frequencies and good conductivity correspond to small depths of penetration δ of the electromagnetic field into the sphere and, correspondingly, to large values of the parameter R_2/δ . We see that for large skin depth ($R_2/\delta = 0.1$), the field penetrates far inside the sphere and is, in fact, nearly uniform throughout the sphere. For high frequencies and good conductivity ($R_2/\delta = 13$), the field dies out rapidly inside the surface of the sphere and, in fact, reverses sign as we proceed inward.

Figures IV-4 and IV-5 show similar calculations for the θ -component of the magnetic field computed from $\text{curl } \vec{A}_i$.

The force density is obtained in terms of the curl of this expression and the current density for the case of unit permeability. The current density is given by

$$j_\phi = -\frac{ip}{\mu} A_\phi = -\frac{ip}{\mu} \frac{B_0}{2} \frac{3a^{3/2}}{\sqrt{ipr}} \frac{\sin \theta}{\sqrt{\frac{2}{\pi v}}} \sqrt{\frac{2}{\pi v}} \left[\cosh v' - \frac{1}{v} \sinh v' \right]$$

where we have written the Bessel functions in terms of hyperbolic functions with the notation

$$B_0 e^{i\omega t} = \text{applied field}$$

$$p = \sigma \omega \mu$$

$$\sigma = \text{conductivity}$$

$$\mu = \text{permeability}$$

$$v = \sqrt{ip} a$$

$$a = \text{sphere radius}$$

$$v' = \sqrt{ip} r$$

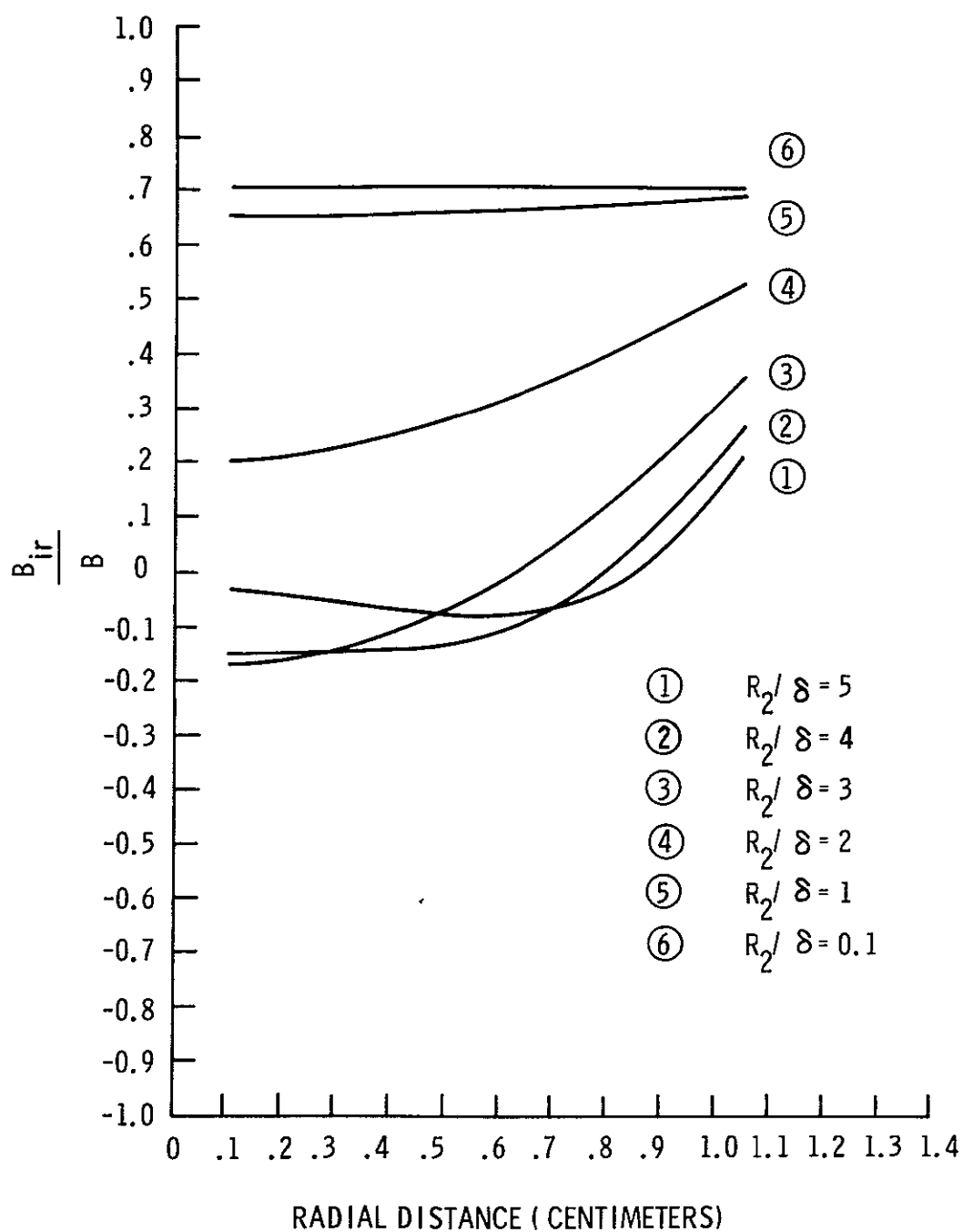


Figure IV-2. Radial Component of Magnetic Field per Unit Magnetic Induction in Aluminum Sphere of Radius $R_2 = 0.4125$ Inches at Colatitude $\theta = 45^\circ$, Showing Penetration of Field into Sphere as a Function of Skin Depth

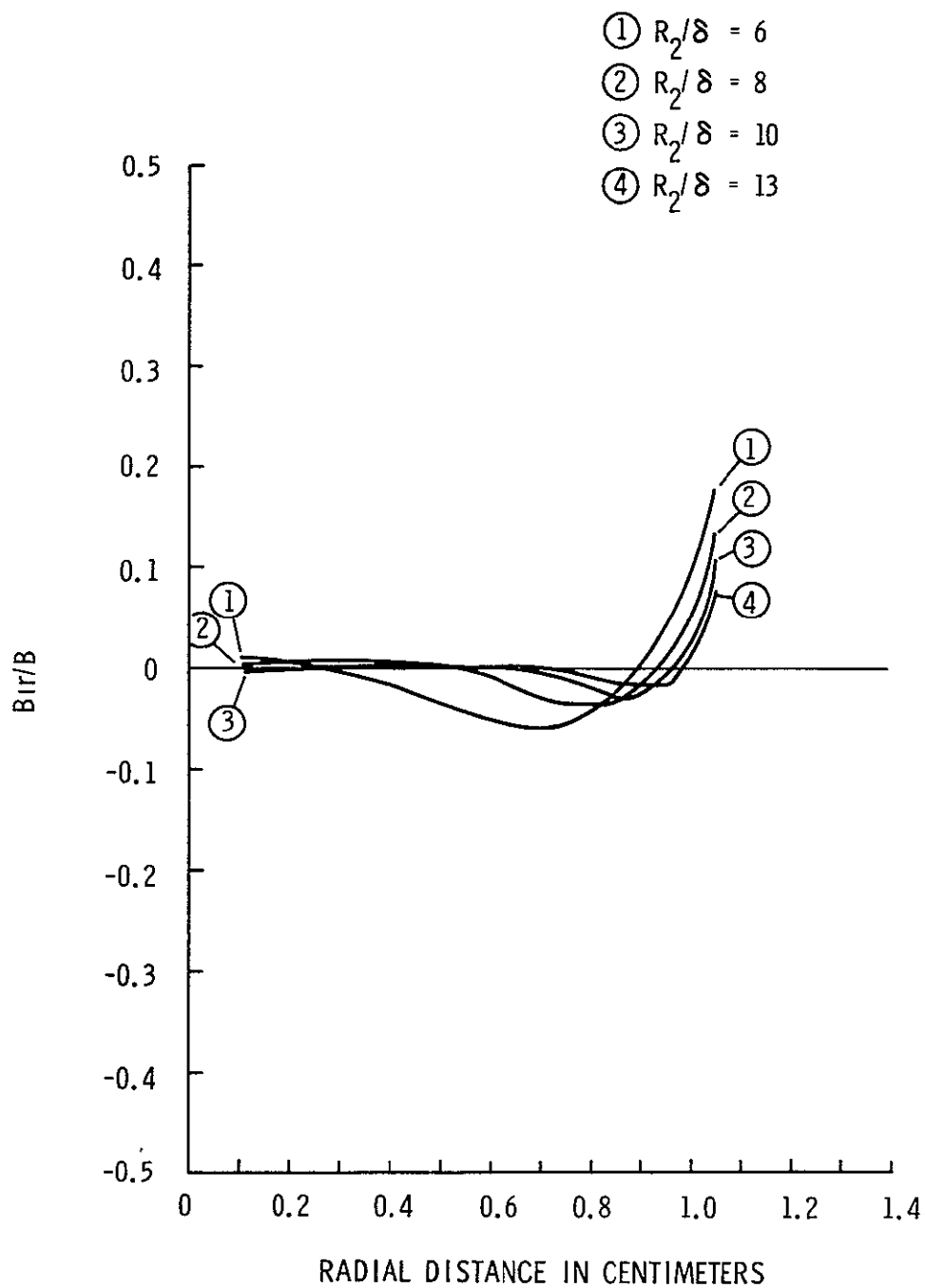


Figure IV-3. Radial Component of Magnetic Field per Unit Magnetic Induction in Aluminum Sphere of Radius $R_2 = 0.4125$ Inches at Colatitude $\theta = 45^\circ$, Showing Penetration of Field into Sphere as a Function of Skin Depth

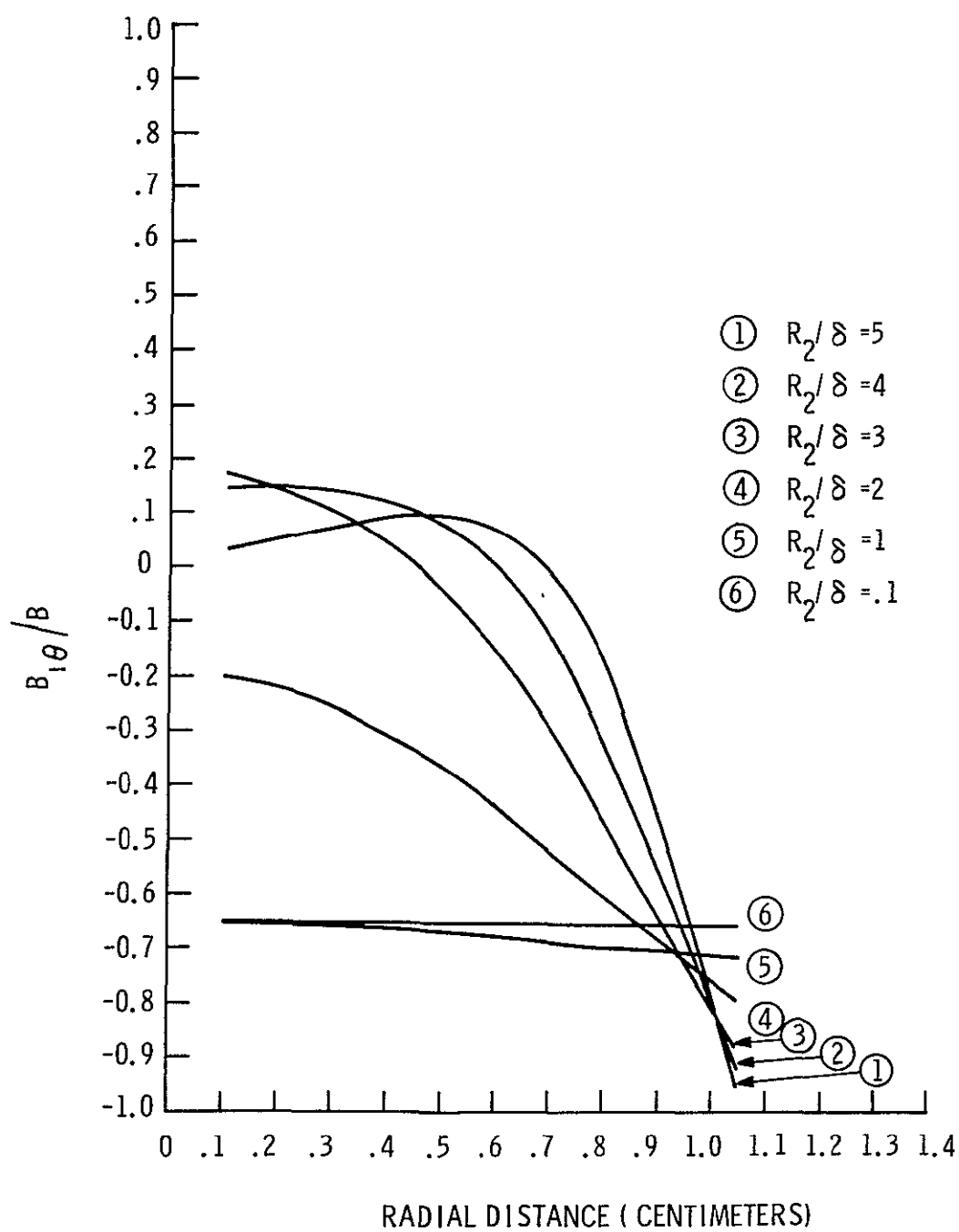


Figure IV-4. θ Component of Magnetic Field per Unit Magnetic Induction in Aluminum Sphere of Radius $R_2 = 0.4125$ Inches at Colatitude $\theta = 45^\circ$, Showing Penetration of Field into Sphere as a Function of Skin Depth

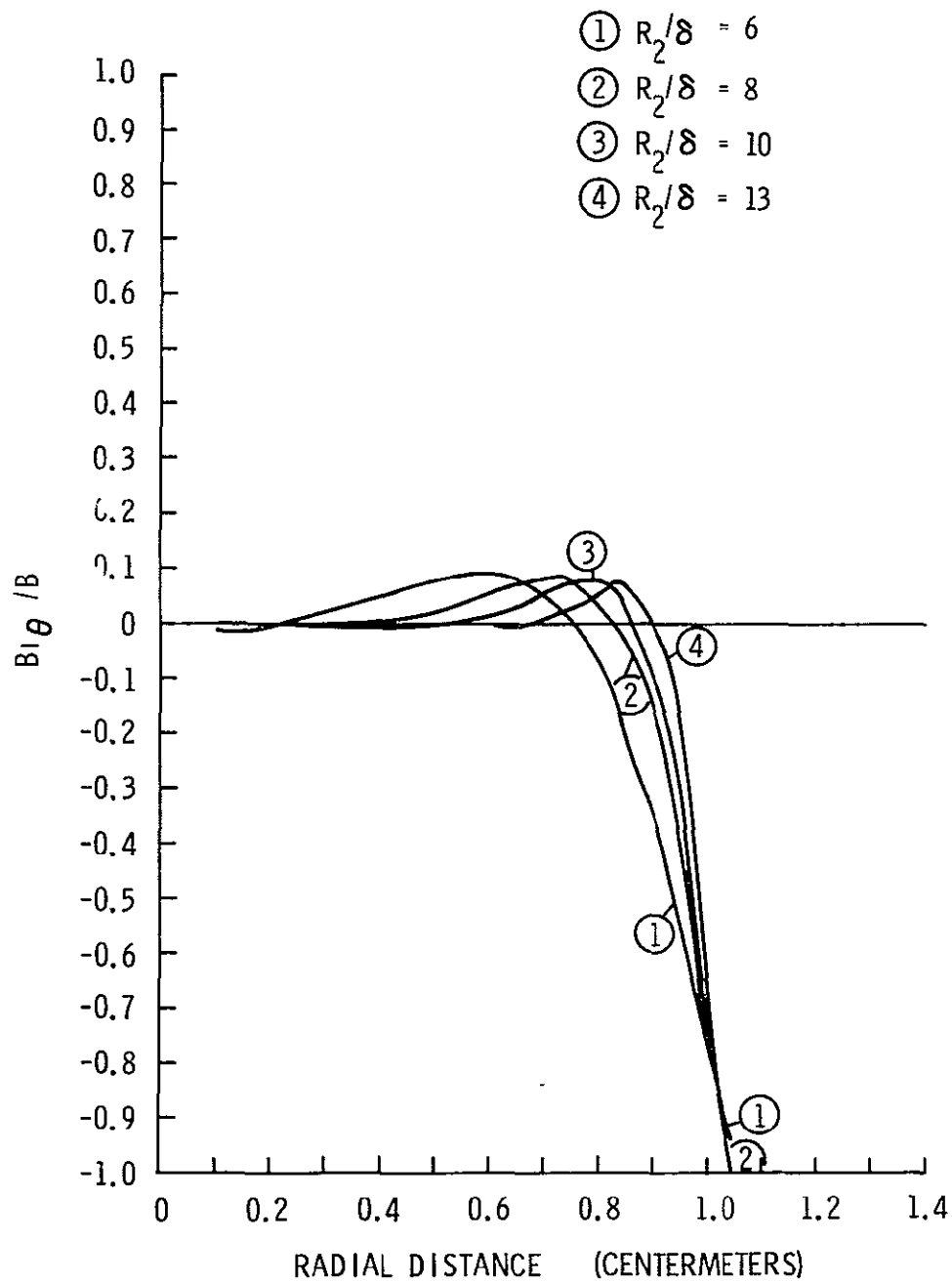


Figure IV-5. θ Component of Magnetic Field per Unit Magnetic Induction in Aluminum Sphere of Radius $R_2 = 0.4125$ Inches at Colatitude $\theta = 45^\circ$, Showing Penetration of Field into Sphere as a Function of Skin Depth

If we use the notation

$$\xi = \sqrt{\frac{p}{2}} a \quad \xi' = \sqrt{\frac{p}{2}} r \quad \delta = \sqrt{\frac{2}{p}}$$

we have

$$\sinh v = \sinh \xi \cos \xi + i \cosh \xi \sin \xi$$

$$\cosh v' = \cosh \xi' \cos \xi' + i \sinh \xi' \sin \xi'$$

It is necessary to obtain the real part of both the current density and the magnetic field before multiplying to obtain the force density. For this it is useful to use the notation.

$$\begin{aligned} \alpha &= \sinh \xi \cos \xi & \alpha_r &= \sinh \xi' \cos \xi' & \gamma &= \cosh \xi' \cos \xi' \\ \beta &= \cosh \xi \sin \xi & \beta_r &= \cosh \xi' \sin \xi' & \eta &= \sinh \xi' \sin \xi' \end{aligned}$$

in terms of which the current density becomes

$$j_\phi = \frac{3 B_0 a \sin \theta}{2\mu r \delta (\alpha^2 + \beta^2)} (Y - i X)$$

where we have utilized the abbreviations

$$X = -\alpha F + \beta E$$

$$Y = \alpha E + \beta F$$

and

$$E = \gamma - \eta - \frac{\delta}{r} \alpha_r$$

$$F = \gamma + \eta - \frac{\delta}{r} \beta_r$$

Figure IV-6 shows results of calculations for the current density inside a conducting sphere for several values of skin depth. These have been calculated by taking the time derivative of the

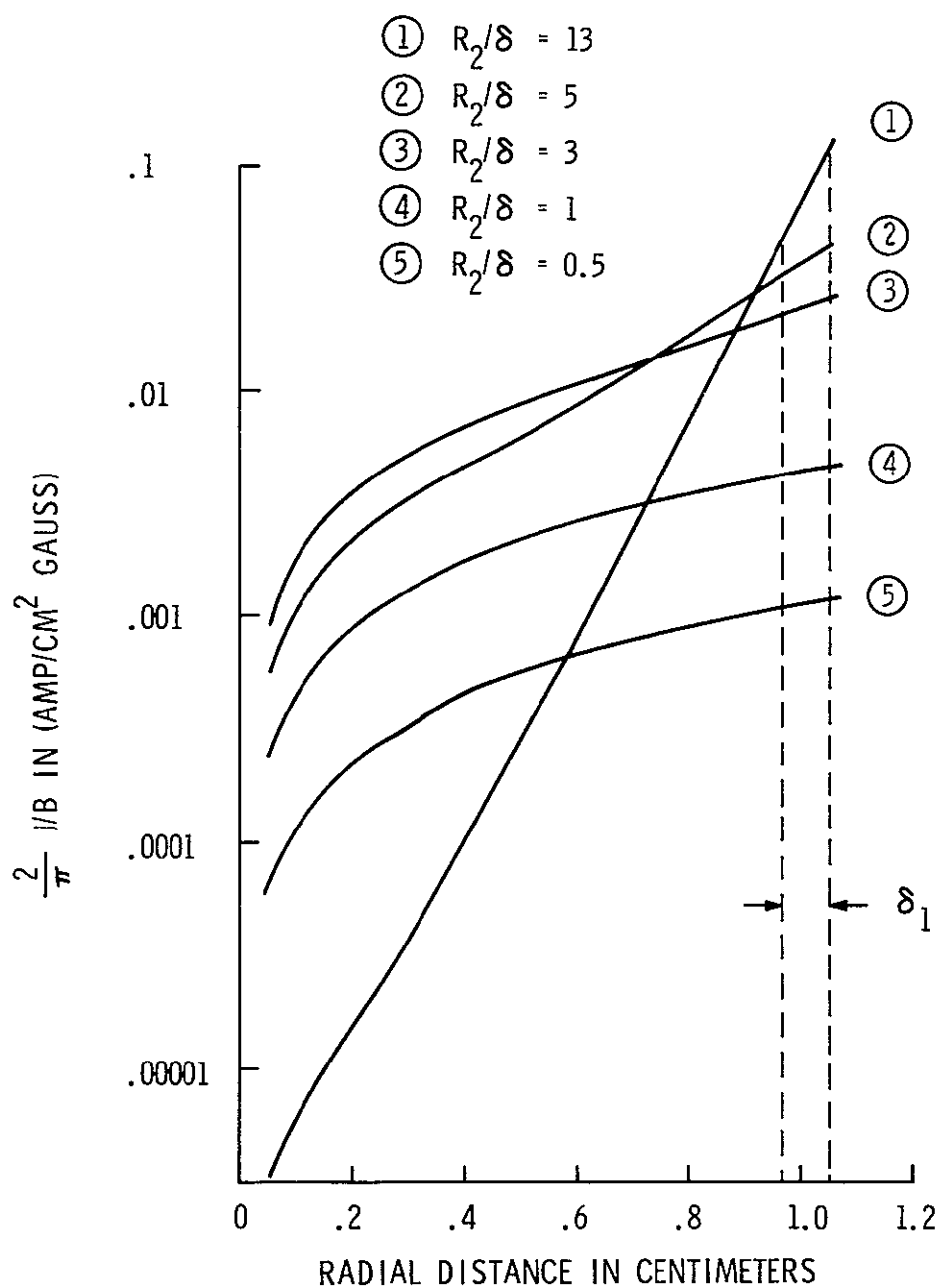


Figure IV-6 Positive Cycle Average of Current Density per Unit Magnetic Induction versus Radial Distance from Center of Aluminum Sphere 0.4125 Radius for $\theta = 90^\circ$

magnetic vector potential. Since the magnetic vector potential has only an azimuthal component A_ϕ , these eddy currents flow in concentric circles whose centers lie along a line passing through the center of the sphere in the direction of the impressed magnetic field.

We can then write the force density as

$$\mathbf{f} = \mathbf{R}(\mathbf{j}) \times \mathbf{R}(\text{curl } \mathbf{A}) \quad \text{where } \mathbf{R}(\quad) \text{ denotes "real part of ..."}$$

or

$$f_r = \frac{9}{4} \frac{B_o^2 a^2 \sin^2 \theta}{\mu r^2 (\alpha^2 + \beta^2)^2} \quad Y \frac{\partial X}{\partial r}$$

$$f_\theta = \frac{9}{2} \frac{B_o^2 a^2 \sin \theta \cos \theta}{\mu r^3 (\alpha^2 + \beta^2)^2} \quad YX$$

These expressions may be useful in considering the resultant circulating fluid currents within a molten sphere. We note immediately that the force field is nonconservative, as might be expected for time dependent electromagnetic forces.

Figure IV-7 shows results of calculations for the radial component of the body distributed force density for several values of skin depth. We see, for example, that for a skin depth of 1/10 the sphere radius (curve 6), the magnetostrictive force dies off extremely rapidly as we proceed into the sphere. Although small radial outward forces are encountered for some regions within the sphere, the pressure is expected to be positive throughout the interior of the sphere so that we need not be concerned with cavitation.

Figure IV-8 shows results of similar calculations for the θ component of the Lorentz force.

NOTE: POSITIVE DIRECTION TAKEN TOWARD SPHERE CENTER SO THAT
A POSITIVE RADIAL FORCE IS COMPRESSIVE

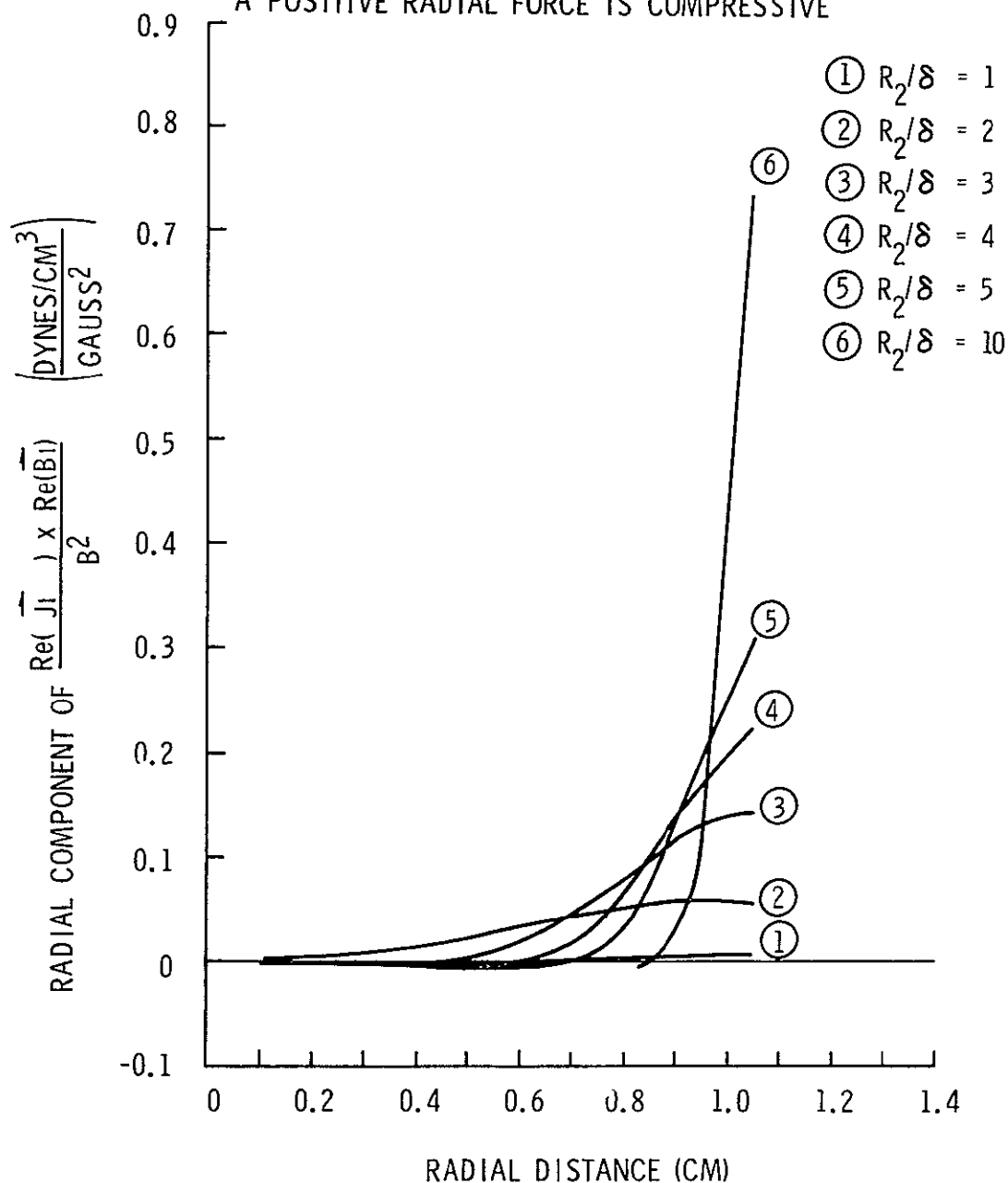


Figure IV-7. Radial Component Force/Volume per Magnetic Induction Squared for Aluminum Sphere $R_2 = 0.4125$ Inches at $\theta = 45^\circ$ as a Function of Skin Depth

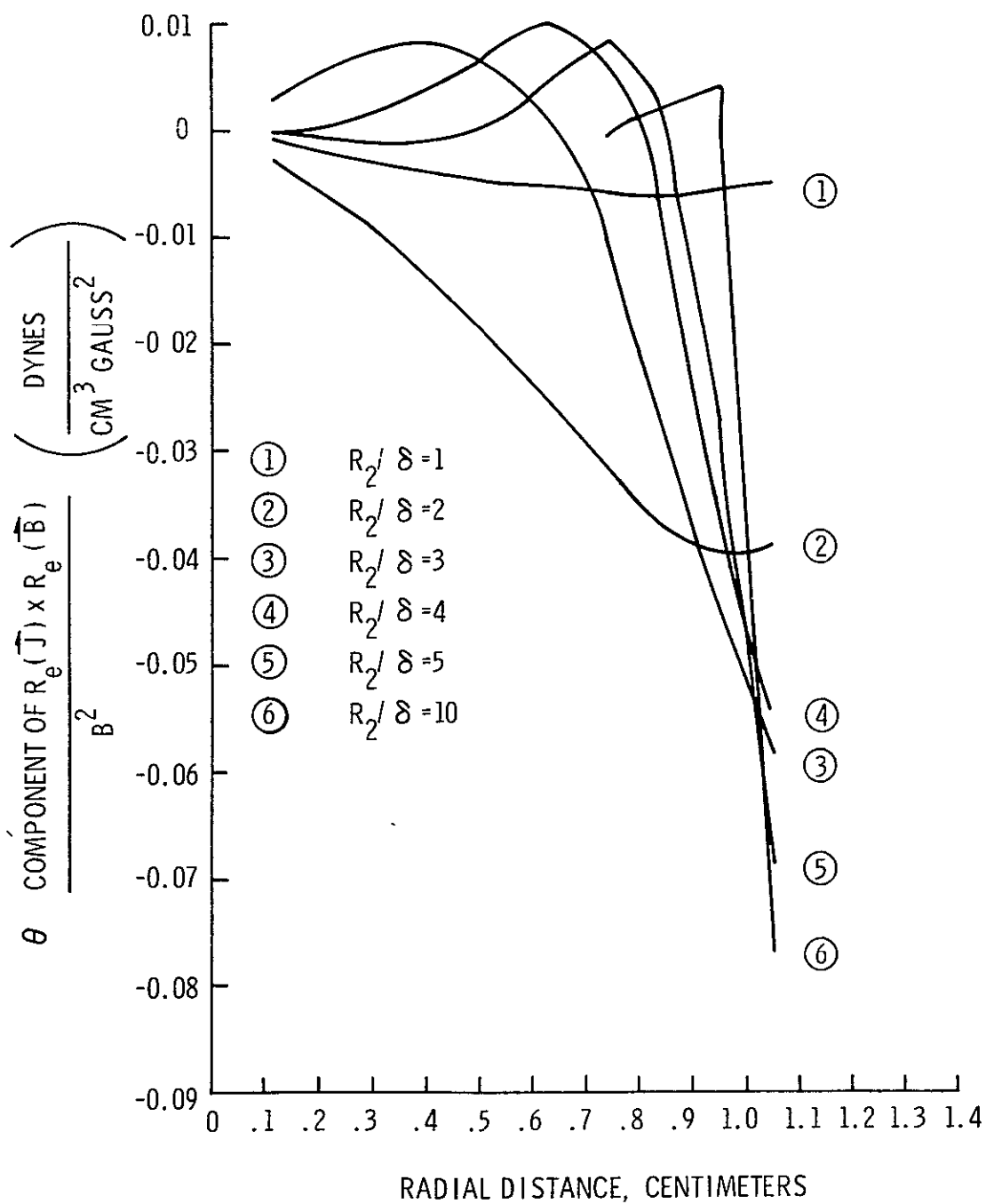


Figure IV-8. θ Component Force/Volume per Unit Magnetic Induction Squared for Aluminum Sphere $R_2 = 0.4125$ Inches at $\theta = 45^\circ$ as a Function of Skin Depth

V. FORCE MEASUREMENTS AND TECHNIQUES

Force-of-repulsion measurements were made to support calculations on the fundamental physical phenomena and the electronic circuitry. It is important to make actual measurements in addition to calculations because of nonlinearities, which will be discussed later. Since the electromagnetic forces depend upon the square of the field amplitude, the forces due to the separate positioning coils will not add linearly, but will depend, in a complex way, on the relative phase of excitation of the coil pairs, as discussed in Appendix C. These force measurements fall into two categories (1) large forces obtained in a general survey, and (2) small forces of the order of dynes, which are closer to the positioning forces actually anticipated in zero-gravity materials processing experiments.

A. Measurement of Large Forces

A simple, magnetically damped beam balance was modified to support any one of several spheres above a coil of wire, as shown schematically in Figure V-1. The coil was raised and lowered to vary the spacing between the coil and sphere. The sphere was relatively motionless as the balance was returned to a balanced condition for each position of the coil. The circuit employed to pass current through the coil is also shown in Figure V-1. The 10-kHz signal from the signal generator was amplified by a power amplifier and applied to the coil, the variable capacitor, and to the one-ohm resistor connected in series. The capacitor was set to tune the combination to the applied frequency and the resulting current was observed by reading the voltage generated across the resistor. With this apparatus, forces were measured for several different coil-to-sphere distances (center-to-center) for each of several spheres with a limiting accuracy of approximately ± 30 dynes. Materials employed for the spheres were copper, aluminum, Inconel, Dowmetal, and tungsten-carbide steel. Results for copper and aluminum at a coil current level of 1.4 rms ampere are given in Figure V-2 with the forces normalized to one ampere turn.

The same apparatus was used to obtain the data given in Figures V-3 and V-4, which are similar to those in the preceding figure, except that a different coil was used and data for three different frequencies are shown, viz. 10 kHz, 1 kHz and 100 Hz. The currents used were about 0.2 rms ampere for 10 kHz and about 0.7 rms ampere for 1 Hz and 100 Hz. The broken lines in Figures V-3 and V-4 are the results of calculations based upon the assumption that currents within the sphere are excited by a uniform oscillating magnetic field. There is some inconsistency in computing the net translational force for the case in which the applied field is uniform. This partially explains the discrepancy shown in the figures. If the field were uniform, no net force would exist. The procedure used in the calculation was to compute the currents in the sphere for the case of the uniform field and to assume that these currents were acted upon by the actual field near the coil so that a net force was obtained.

B. Measurement of Small Forces

Figure V-5 gives results of calculations over a wider range of skin depths and sphere-to-coil distances. We see that the force is maximum for a sphere-to-coil distance approximately 30 percent of the coil radius. These calculations assume that the magnetic dipole moment induced in the sphere is the same as would be induced by a uniform field. In actuality, the dipole moment might be

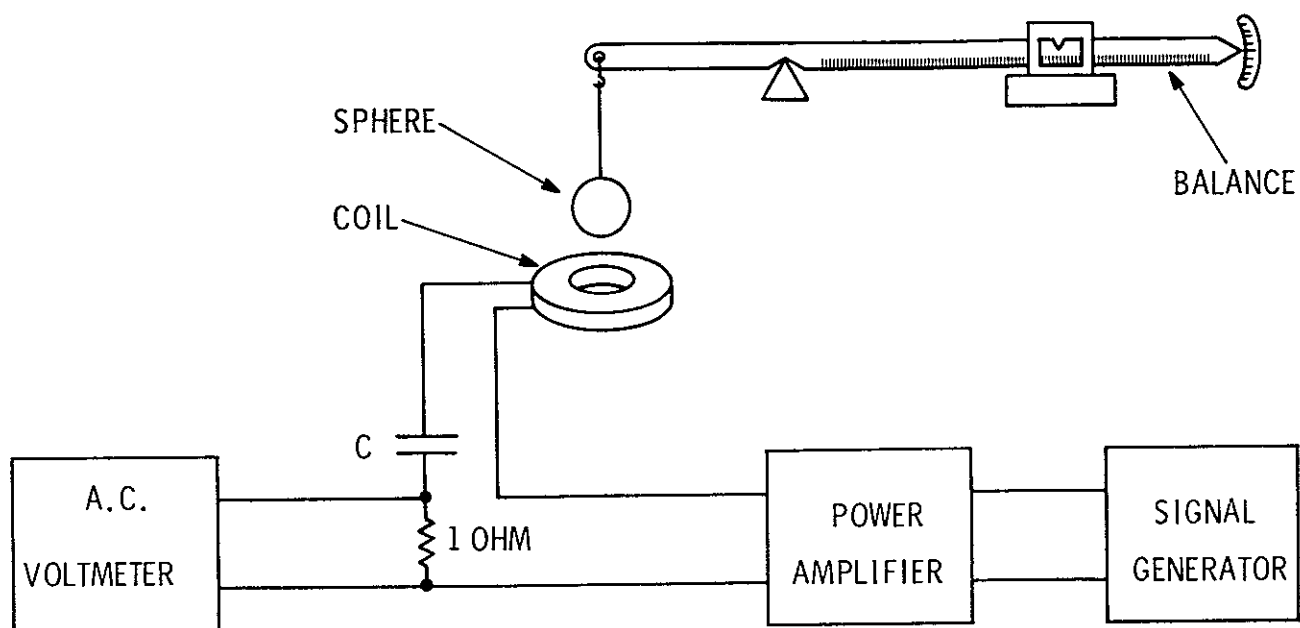


Figure V-1. Large Force Measuring Apparatus

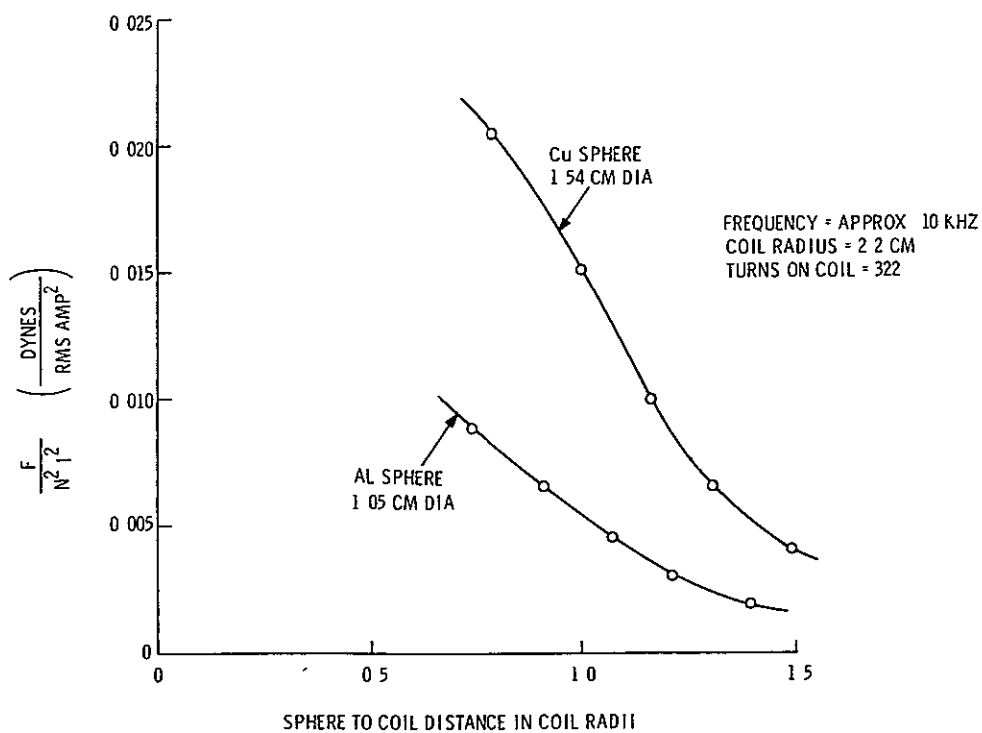


Figure V-2. Results for Cu and Al at a Coil Current Level of 1.4 rms Ampere

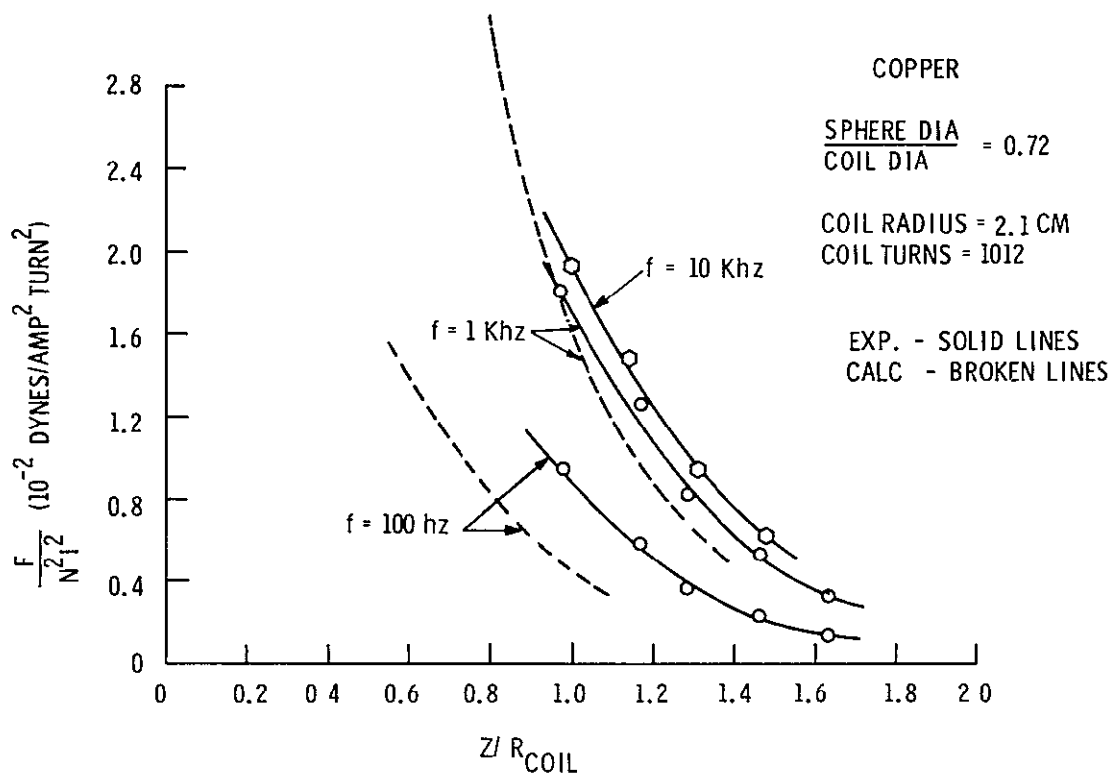


Figure V-3. Results for Cu at Various Frequencies

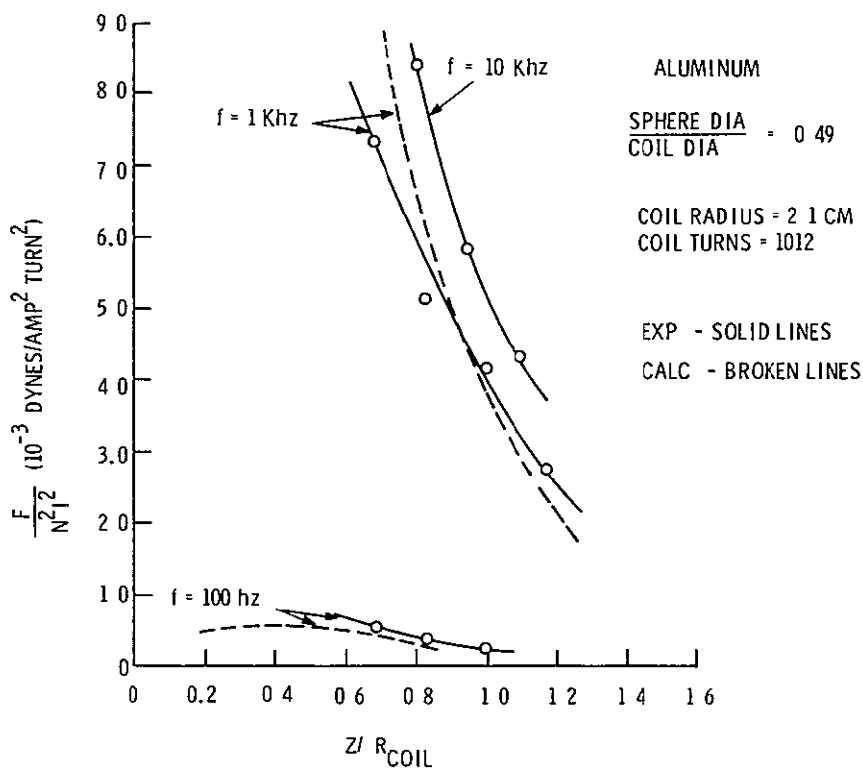


Figure V-4. Results for Al at Various Frequencies

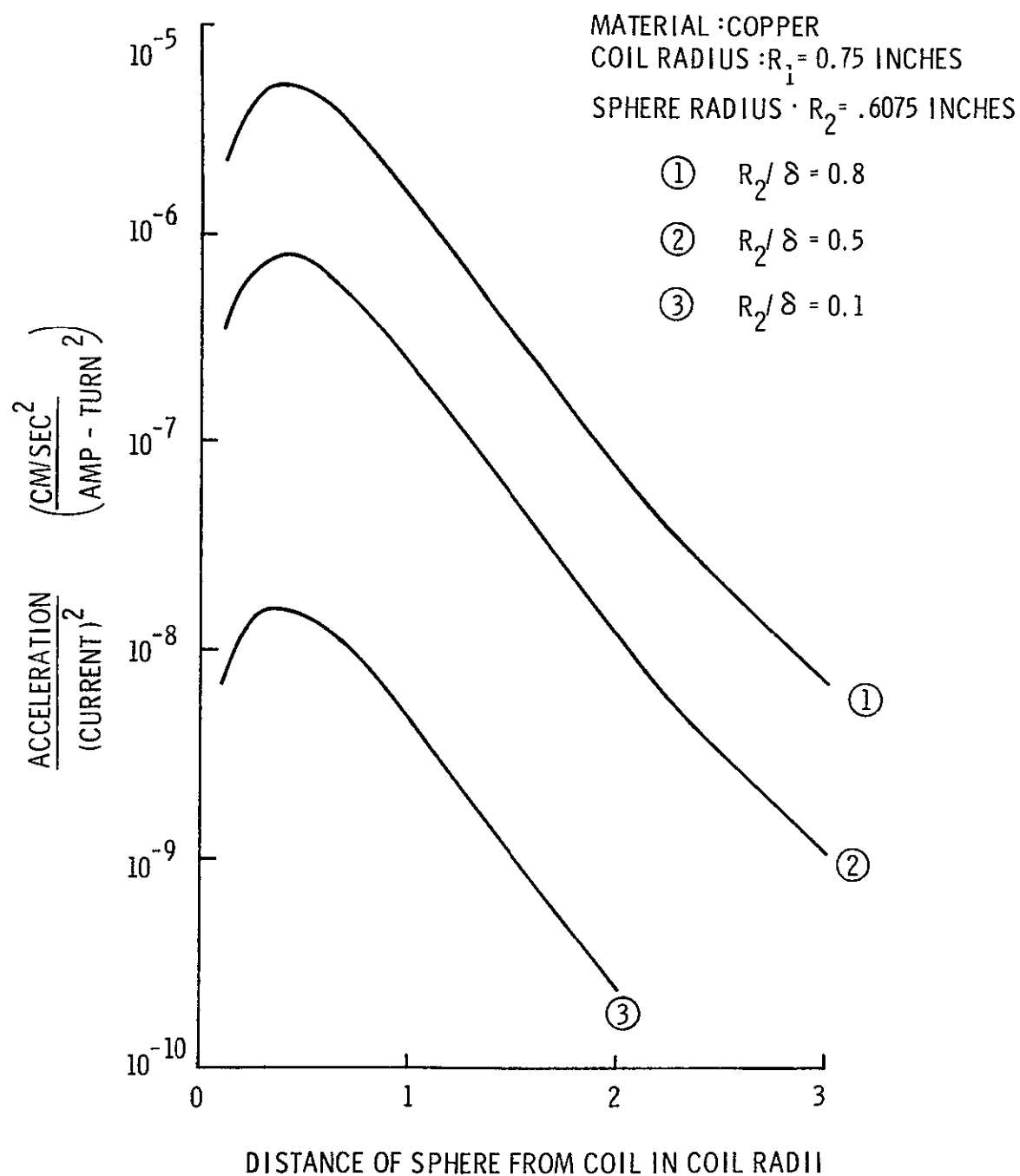


Figure V-5. Acceleration per Unit Exciting Coil Current Squared

significantly different in positions close to the coil where the field gradient becomes severe. Thus, we can expect that the actual position of this maximum will be shifted.

A piece of plate glass 0.5-inch thick, 2-feet long, and 1-foot wide was equipped with three micrometer screw heads which permitted controlled tilting of the glass in one direction in increments of 3.9×10^{-5} radian for each 0.001-inch division. The vernier micrometer heads allowed tilt measurements to one-tenth of this value or 3.9×10^{-6} radian. A transparent box approximately 45 inches tall was placed on the glass plate and the same aluminum sphere as used previously was suspended from the top of the box by a fine wire, see Figure V-6. The same coil as used previously, (see Figure V-3 and V-4) was placed near the sphere to obtain the data given in Figure V-7 at 10 kHz. The procedure used with the apparatus was to observe the position of the sphere on the reticle of a telescope, tilt the table a small amount, and apply current sufficient to return the sphere to its original position. The amount of tilt and the mass of the sphere indicated the force required and the current in the coil was read as described above. The accuracy of the force measurements with this technique is approximately ± 0.5 dyne, and most of this uncertainty is provided by the limit to which the position of the sphere may be read. Swinging of the sphere, which hampered observation of the sphere's position, was eliminated by attaching a lightweight probe to the bottom of the sphere in line with the wire supporting it. The probe extended about 1/8 inch into some 2,000 centistoke silicone oil. This produced a degree of damping somewhat less than critical. By taking vertical "slices" of the data of Figure V-7, the information shown in Figure V-8 was obtained.

This tilt-table apparatus was also used to measure small forces applied to spheres as they roll on an optically flat piece of glass. This technique was not used extensively because the sensitivity was usually no greater than ± 0.5 dyne and only under ideal conditions was it as low as ± 0.05 dyne. The advantage of such a technique is to permit the sphere to range over a wider area, unrestrained by any supporting wire. A disadvantage is that a nearly perfect sphere and dust free surfaces are required.

C. Measurement of Stability of Sphere Position Within Positioning Coils When Servo Loop is Inactivated

Since the force between a given positioning coil and the floating conducting mass is repulsive, the force fields of three orthogonal pairs of positioning coils will create a potential well centered about the common intersection of their axes when all coils are excited. A two-dimensional analog of this potential well has been examined by exciting two orthogonal coil sets whose axes were horizontal. The conducting aluminum sphere was suspended on a long pendulum. The arrangement was such that, with the coils deactivated, the ball was positioned at the intersection of the two coil-pair axes. With the coils activated, oscillations of the sphere were initiated by physically touching the ball. With the two members of each coil pair connected in phase or 180 degrees out of phase, a potential well was observed having a pincushion shape. This means that the oscillations were of lower amplitude when they were parallel to either coil-pair axes than when the plane of the oscillations made an angle of 45 degrees with both coil-pair axes. The period of the pendulum of course depended upon both the plane of oscillation and the amplitude and ranged between 1.5 to 2.0 seconds. The natural frequency of the pendulum (~ 10 feet long) was 3.5 seconds. With the members of coil pairs connected in phase, very little restoring force was apparent for ball positions

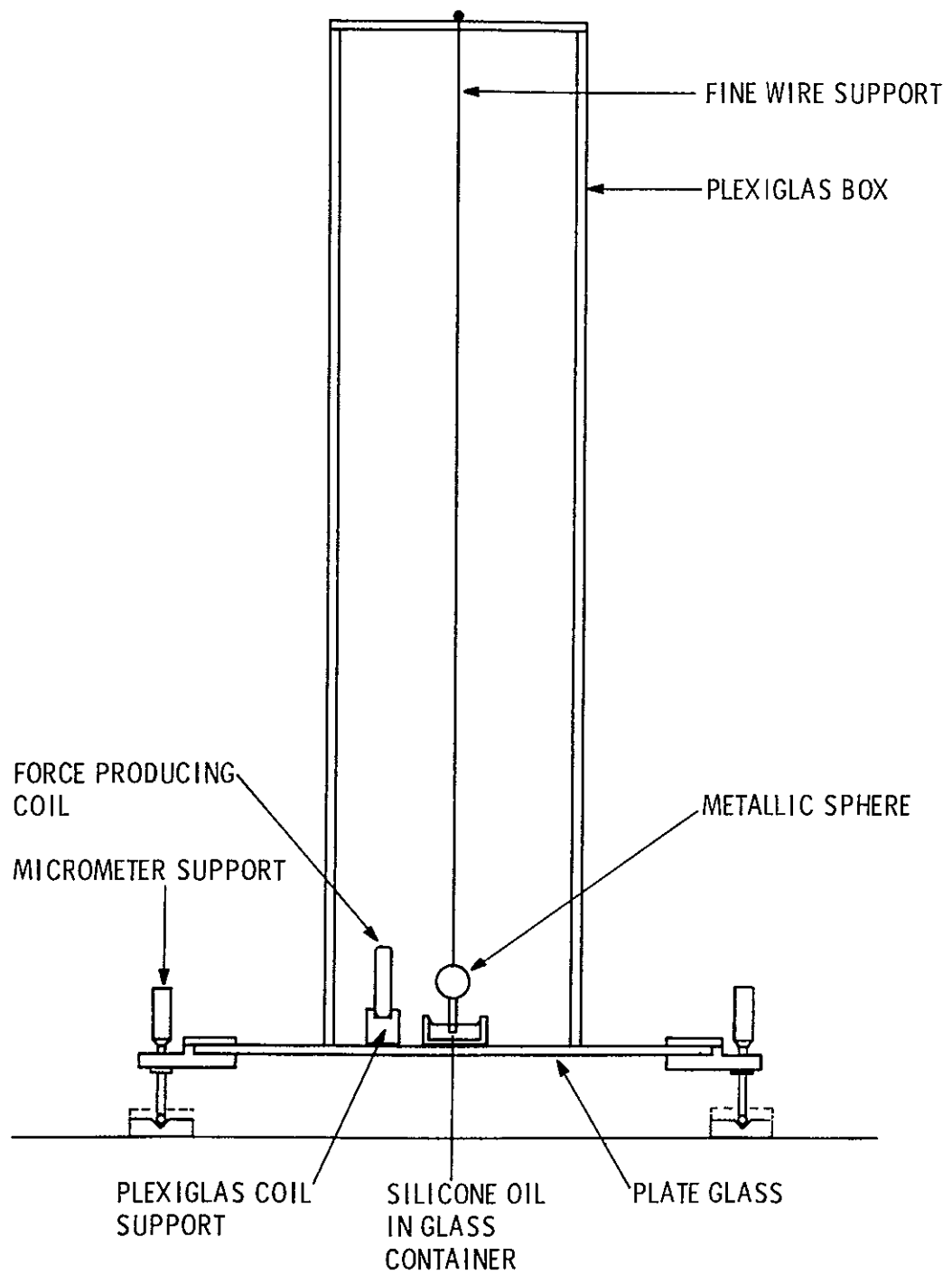


Figure V-6. Tilt Table Assembly for Measurement of Small Forces

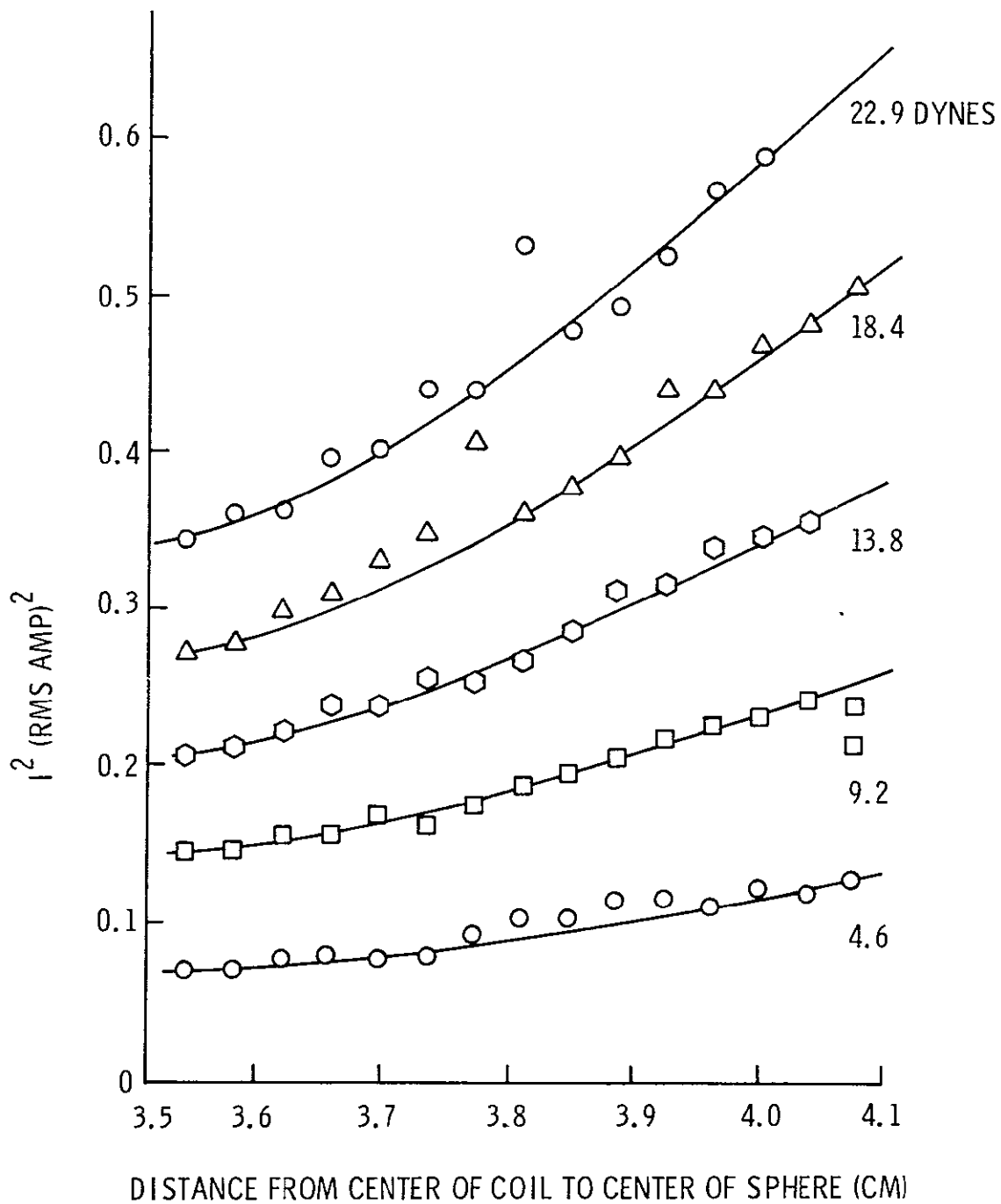


Figure V-7. Coil Current versus Position for Constant Force at 10 kHz on Aluminum Sphere

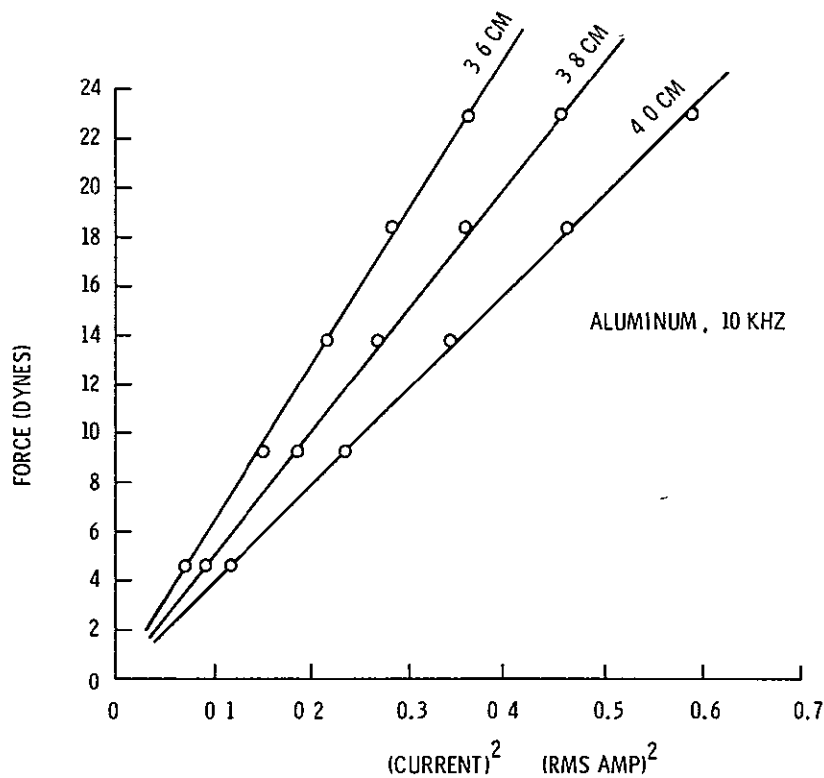


Figure V-8. Force versus Current at Various Distances

near the well center, and the nature of the oscillations were to some extent comparable to the case where the potential well would be a box with rather stiff reflecting boundaries. With the coils connected out of phase, the restoring forces had a "softer" nature, thus demonstrating the nonlinearity of force addition. It is well known that the axial field near the center of the Helmholtz coil pair varies approximately with the cube of the displacement from the center position. This would give a force varying as the 6th power of displacement from the center and would be qualitatively similar to the force variation observed with the coils connected in phase.

Measurement of small forces by a number of alternate methods was explored analytically and, to some extent, experimentally. A summary of this work is given in Appendix A

VI. POSITION SENSING AND CONTROL SERVO

A. Introduction

The present section describes development work on a servo device for position sensing and control of a free floating conducting mass. It was found that the eddy currents induced in the conducting sphere cause significant changes in the inductance of the coils used to generate the electromagnetic field. A circuit was developed to sense the change in this inductance as the ball moves relative to the coil. The ball position signals obtained in this way are then processed, including signal differentiation to detect ball velocity, and then used to control the coil excitations in a servo loop. Proper mixing of the ball position and velocity errors, and adjustment of gain and frequency characteristics in the servo loop allow for automatic restoring of the ball to a central position equidistant from all coils and removal of any residual velocity relative to the coils. Although, as noted earlier, the floating ball can be trapped in the potential well created by the coils when they are excited, there is essentially no damping of position oscillations. In order to provide for quiescent conditions in which drift of the floating mass can be corrected, damping in an automatic manner is considered essential. For some applications, such as the casting of perfect spheres, accurate removal of drift velocity will be essential so that position control forces may be removed during solidification.

B. Description of Servo Circuits

The control system hardware for position and damping is illustrated in Figures VI-1 and VI-2. Figure VI-3 is a block diagram showing details of the electronics employed in the loop (single axis) and the signal flow paths. The operation of the loop is as follows.

The coils shown at the left of Figure VI-3 are accompanied by shunt resistors which provide a signal proportional to coil current. The excitation voltage and the current signals are amplified individually and drive zero cross-over circuits in the logic block. The output of the logic circuit is a series of pulses which drive the switches, one coil switching (+) reference and one coil switching (-) reference into two summers. The duty cycle of the switches is proportional to the phase angle between the current in the coil and the excitation voltage. This phase angle is related to the position of the ball relative to the coil, as shown in Figure VI-4. Therefore, if the ball is centered between the coils, the coils have identical phase shifts and the (+) and (-) reference switches have equal duty cycles. The resultant average seen by the error summers is zero. Also, the multiplier outputs are equal and both coils have identical excitation voltages from the power amplifiers. The conditions up to now indicate a quiescent state with no disturbances to the ball.

Assume the ball occupies a position nearer to the coil shown in the upper channel of Figure VI-3. From Figure VI-4, we find this coil's current to be shifted up in phase, and the lower coil, which is further from the ball, is shifted down in phase. Under these conditions, the (+) reference switch duty cycle decreases and the (-) reference switch cycle increases. The error in the upper channel becomes (+) at the summer output (the summer inverts), and the modulator increases the signal to the power amplifier and the upper coil. This acts to repel the ball back toward the center position. Even though the lower summer's output goes (-), the modulator is so biased and driven that its

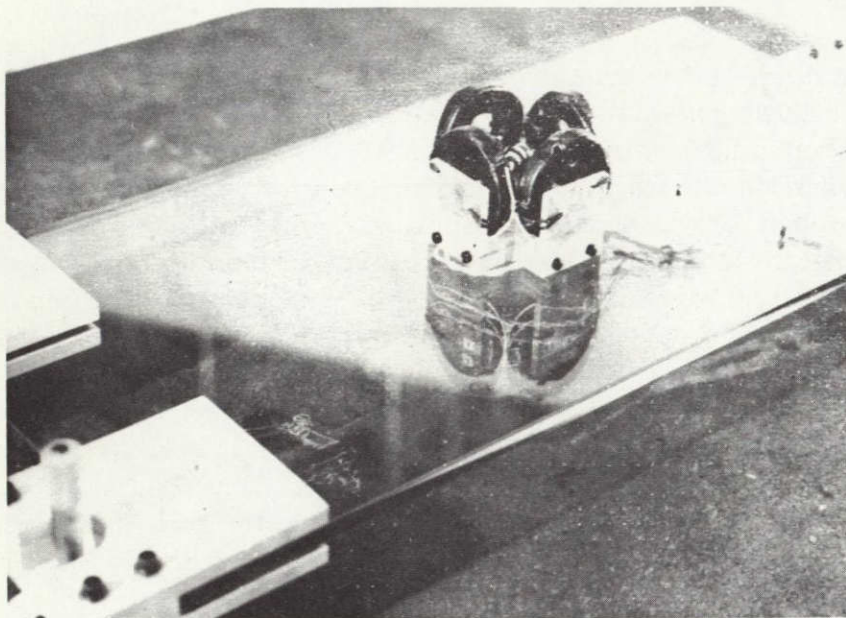


Figure VI-1. Positioning Coils on Tilt Table

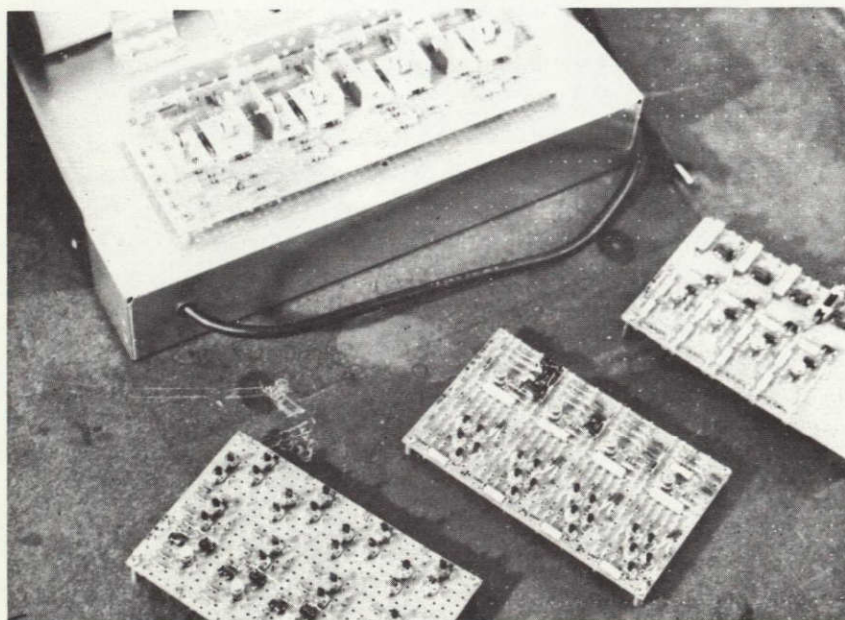


Figure VI-2. Electronic Breadboards for Position Servo

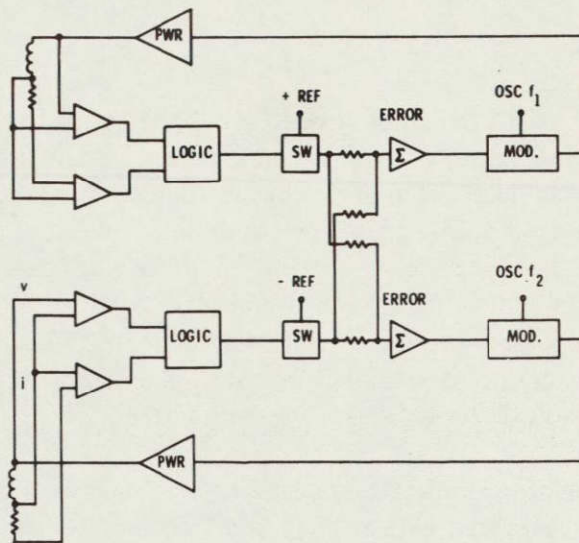


Figure VI-3. Block Diagram of Position Servo Electronics

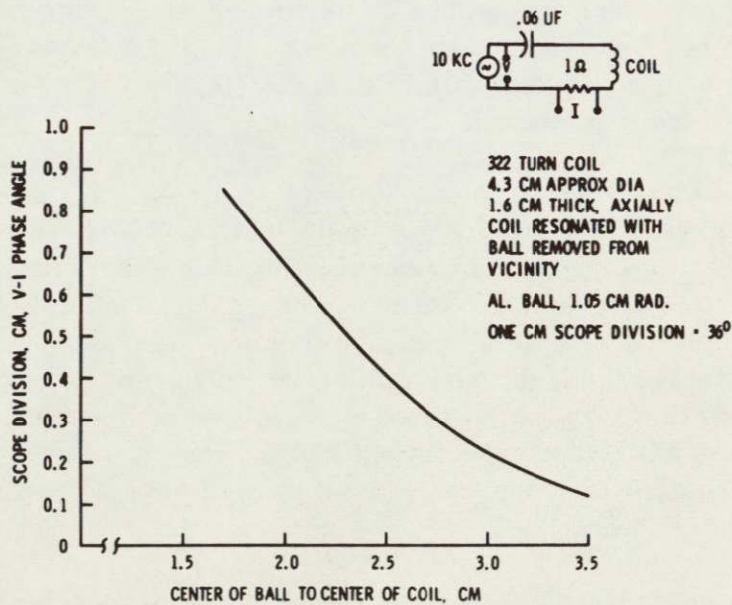


Figure VI-4. Position Sensing Characteristic

output does not go much below the level it has when the ball is at the quiescent position. This ensures the presence of a minimum signal from which to get phase and hence position information from that coil.

C. Dynamic Analysis of Loop

So far, discussion has been confined to the static properties of the control system. The individual elements of the system, shown in Figure VI-3, in general, take a certain time to react, or more accurately, the transient behavior is some function of time. Looking at the position sensing first, we find that phase angle relates to position. The phase angle is sampled and summed each half cycle so that, at 10 kHz, position data lags position by about 25 μ seconds. The voltage and current amplifiers have no delay networks and, in fact, have several MHz bandwidths. To reduce ripple in the position information, ripple filters are employed at the summers and at the modulators. The value of their cut-off frequencies are determined by allowable ripple and loop bandwidth. Representative values are 300 or 400 Hz for a 100 kHz operating frequency.

The summers contain, in addition to a ripple filter, a lead network which is required for damping the loop. This lead network has associated with it a lag at a frequency of about ten times the lead frequency. The exact frequency of the lead network is determined by the gain and bandwidth requirements for given load dynamics, the value in this case being about one Hertz.

The last electronic time constant belongs to the resonated coil which, at 10 kHz, has a Q of about 25, and therefore, a frequency bandwidth of about 400 Hz. The final dynamic consideration is the load, in this case, the sphere of mass m . The coil exerts a force $f = ki^2$ for small signals so the change in force per change in current is $2ki \nabla i$. We see immediately the square law property of the force, which means the overall loop gain is proportional to the current. At a given current, however, the force can be represented by $k' \nabla i$. The transfer function of a mass without viscous force is simply $X(s) = f(s)/ms^2$, where X represents distance. This signifies a double lag (-40 dB per decade) passing through the point $1/m$ at 1 radian per second.

From the above, it is seen that there is no viscous damping; therefore, it is necessary to provide damping in the control loop. This necessity is met by the lead which is placed at the summer. In addition to these transient responses of the various elements, each element has a static gain. The electronic gains, once set, are fixed, but the position sensing and repulsion forces vary. Figures VI-4 and V-7 show the relations between phase angle and position, and between force, current and position. The most variable element is the force which is not only a function of i^2 but of the axial distance between coil and ball. Therefore, the loop characteristics must be determined for a range of static gains. Assuming that the ball stays reasonably well centered in the present loop, this gain variation nominally is about 10 to 1, the higher gain being with the ball deliberately decentered causing a high coil current to flow.

A deviation in these dynamic and static gains occurs when the mass is a pendulum bob, as shown in Figure VI-5. This deviation is due to a different load transfer function which now is affected by a gravity induced restoration force and its attendant natural frequency of vibration. This transfer function for the pendulum mass is $X(s) = f(s)/m[s^2 + g/L]$, where L is the pendulum length and g is the acceleration due to gravity.

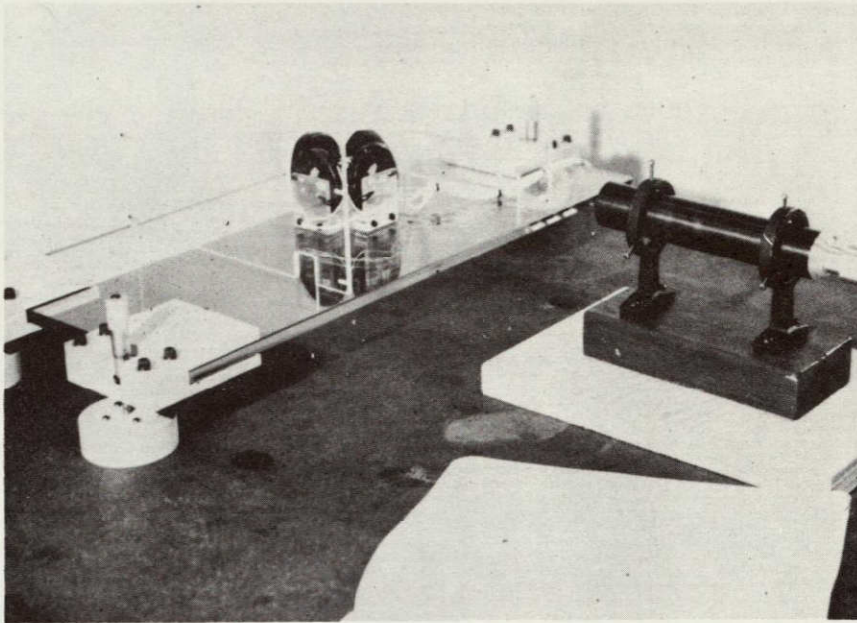


Figure VI-5. Force Measuring Apparatus Tilt Table and Pendulum

The total dc transfer is

$$G = 2.86 \times .35 \times 20 \times .1 \times 2.12 = 4.24 \text{ volts per volt.}$$

$$20 \log_{10} 4.24 = + 12.6 \text{ dB.}$$

A Bode plot of the important frequencies appears in Figure VI-6 for these gains and break frequencies. In actual practice, both the resonance frequency and the gain were higher than calculated which placed the 0-dB crossover at a somewhat higher frequency and thereby caused an underdamped condition.

D. Position Sensing Considerations

Experience with the servo showed position sensing as the most critical task. The task here is made difficult because (1) the coil excitation changes in amplitude about 3:1 from the servo output, and (2) the other coils couple strongly into it. The position sensing logic rejects all but a small amount of this disturbance, but the residual approaches the sensitivity level for adequate position sensing. Some improvement can be made with the existing circuit; but to incorporate spinup, levitation and electromagnetic heating, other approaches offer significant improvement and greater flexibility. For instance, position sensing, a small signal function, can be made independent of the force coils, a power function, in power, frequency and geometry. Some of the more promising approaches are as follows:

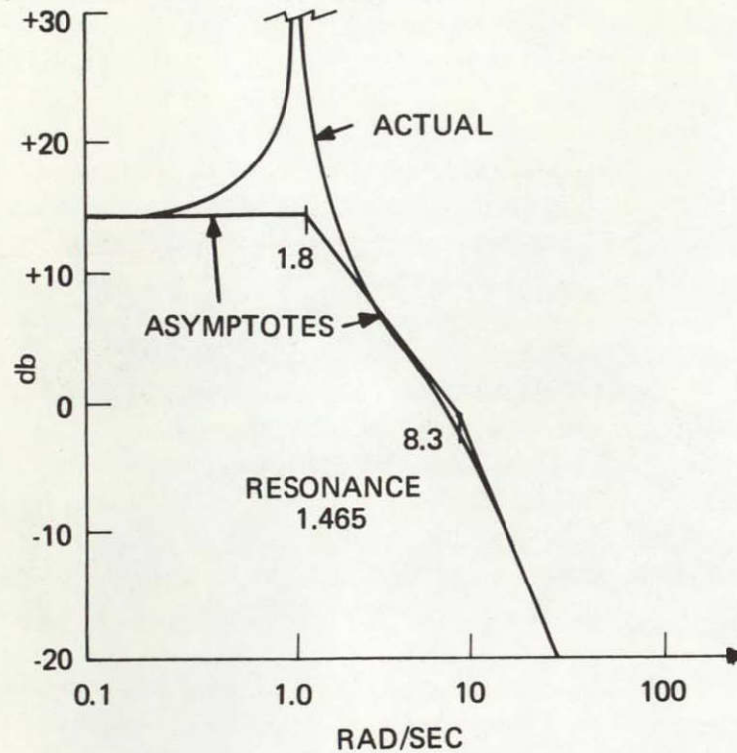


Figure VI-6. Bode Plot of the Important Frequencies.

1. Synchronous detection of current to eliminate all other frequencies.
2. Balanced bridge with synchronous detection, single frequency excitation for all coils.
3. Time-sequencing one axis at a time with momentary deactivation of all other fields.

The position sensing and control device described above has been thoroughly tested and has proven itself capable of quickly damping sphere motions and restoring the sphere to the center position where it remains at zero relative velocity. The stiffness and damping constant of the loop can be easily adjusted. In the experiments carried out under the present contract, initial ball displacements were of the order of 1 cm from the center position, corresponding to horizontal accelerations on the order of $5 \times 10^{-3}g$. Thus, control loop stiffness in terms of applied field strengths was significantly higher than would be required in a near zero-gravity velocity facility. Testing of these devices in a drop tower would be desirable at operating levels more closely approaching those of interest to a zero-gravity space facility. Use of minimum restoring forces may be important for applications where shape deformation of the suspended mass is to be avoided.

A five minute color movie was prepared documenting results of position control and damping characteristics.

E. Spinning a Conductive Sphere

An aluminum sphere (2.1-cm diameter) and a copper sphere (3.1-cm diameter) were each set into rotation while supported by a small ball bearing among the four positioning coils previously made for the servo-control demonstration. The four coils were energized at 60 Hz, with the field generated by each pair of coils about 90 degrees out of phase with that generated by the other pair. The apparatus is shown in Figure VI-7. With the rotating field at the position of the copper sphere approximately 50 oersted, each sphere was easily rotated at a constant rate about one revolution per second by balancing the torque generated by the field against that provided by the drag of the ball bearing.

Each sphere was then hung from a 300-cm long wire, which had a torsion constant of 5.8 dyne-cm/radian, to measure the torque imparted to the sphere by the rotating field. For a field strength of about 30 oersteds at a frequency of 220 Hz, the stationary aluminum sphere received a torque of 25 dyne-cm and the copper sphere received 120 dyne-cm.

These experiments were later repeated with the ball suspended from a long thin wire. Spin up with horizontal forces furnished primarily by the coils was observed to be stable until wire windup was encountered.

A glass sphere (described in Appendix D) was filled with a saturated aqueous solution of sodium chloride and also given a torque. With a field strength of 35 oersted at 10 kHz, the torque imparted to the assembly was 0.07 dyne-cm.

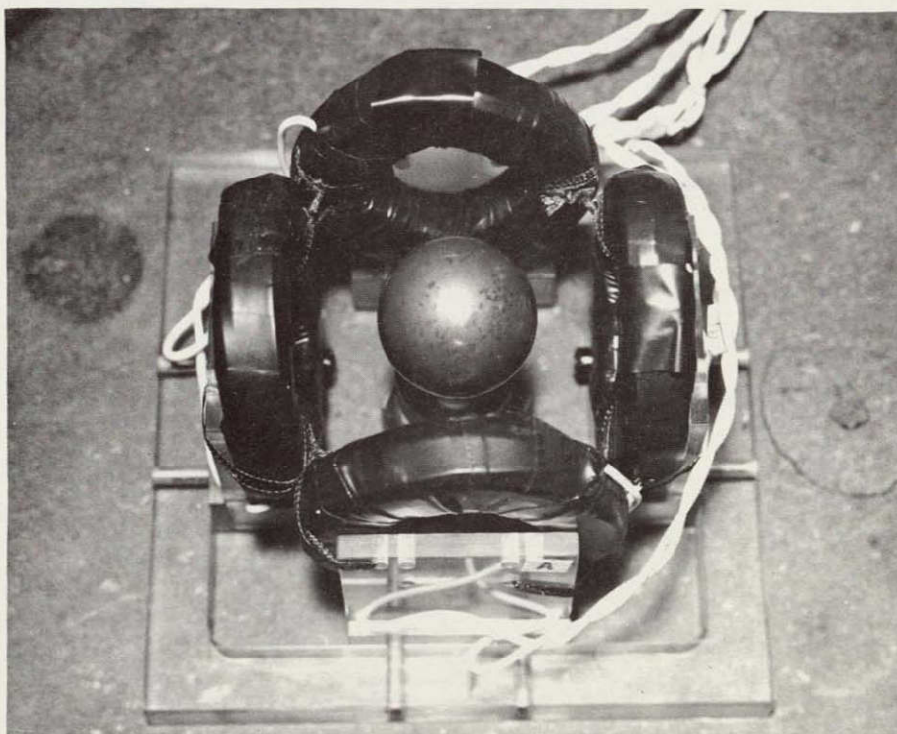


Figure VI-7. Solid Copper Sphere Supported on Ball Bearing Centered Among Four Coils which Generated a Rotating Magnetic Field

VII. GENERAL REQUIREMENTS FOR SPACE EXPERIMENT FACILITIES

A. Introduction

Each of the proposals for exploiting the weightless feature of the space environment in metallurgic and ceramic processing of course requires an individual study of facility requirements in terms of heating power, instrumentation, size of facility, etc. Since a large number of these suggestions involve the handling of a floating molten mass out of contact with crucibles or molds, it is nevertheless possible to define, even at this stage, facilities which will be capable of accepting a large number of candidate new weightless processing experiments. The following describes the beginning of a study to define the physical requirements for a wide range of potential new crucibleless melting and solidification experiments in order to define limits to the range of variables which can be handled in one or more facilities which may be practicable for early incorporation in the post Apollo program.

Some of the physical variables which are important in defining the required experimental facilities are summarized below

Process Variable	Facility Requirement
Melting temperature	Heating power
Size of batch	
Heating rate	
Requirements for vacuum or controlled atmosphere	Processing chamber and accessories, starting material, handling devices
Requirements for pre-melting of pre-cast specimens or for crucibleless mixing and reaction	
Cooling rate	Position control, free floating volume
Solidification temperature	
Processing time	
Purity requirements	
Requirements for absence of contact with crucible of melt during some part of the process	

Requirements for stirring	} Electromagnetic or electrostatic fields, provision for rotation of melt
Requirements for shaping or molding	
Likelihood and nature of included bubbles	Requirements for stirring and bubble detection/ elimination technique

We must translate some of these rather general process requirements into a definition of the facilities required to handle a wide range of processes. The requirements on facilities imposed by position control, position sensing, heating, processing time, free floating volume required for the specimen, maximum permissible accelerations in terms of shape distortions, etc. are of course all related. We first discuss these requirements separately, however, in the course of a detailed discussion, the interdependence of these requirements will become obvious and the region of intersection of the various experiment requirements in terms of facilities will, in most cases, define the required facilities within fairly specific limits.

B. Material Properties — General Considerations

Electromagnetic waves of any frequency (greater than those which might better be called slowly varying dc fields) falling upon a conducting material of zero resistivity would behave as light falling upon a mirror; all of it would be reflected. If the conducting material has a non-zero resistivity, then the electromagnetic waves penetrate the material, losing energy in the process, and the depth by which the amplitude of the wave has diminished to $1/e$ or 0.37 of its initial value is the attenuation distance or the skin depth. This skin depth, δ , depends upon the properties of the material and the frequency of the waves as follows:

$$\delta = \frac{1}{\sqrt{\pi f \sigma \mu}}$$

where f is the frequency of the wave in cps or Hz, σ is the conductivity of the material in mhos/meter (one mho/meter is equivalent to a resistivity of 100 ohm-cm), μ is the magnetic permeability of the material in Newtons/ampere² ($\mu = 4\pi \times 10^{-7}$ Newton/ampere² if the relative permeability is unity), and δ is the skin depth in meters. The skin depth has been plotted in Figure VII-1 for several materials and a wide range of frequencies. Here it may be noted that the skin depths achieved in aluminum and copper in work discussed elsewhere in this report ranged from 0.8 cm at 100 Hz to 0.5 mm at 10 kHz.

C. Melting Power Required to Supply Surface Radiated Power Loss

Table VII-1 presents the melting points of various materials and the total power required for a sphere of 10 cm² surface area to overcome radiation loss at the melting point. This is an important factor in selecting materials for experimentation and in designing apparatus to melt these materials.

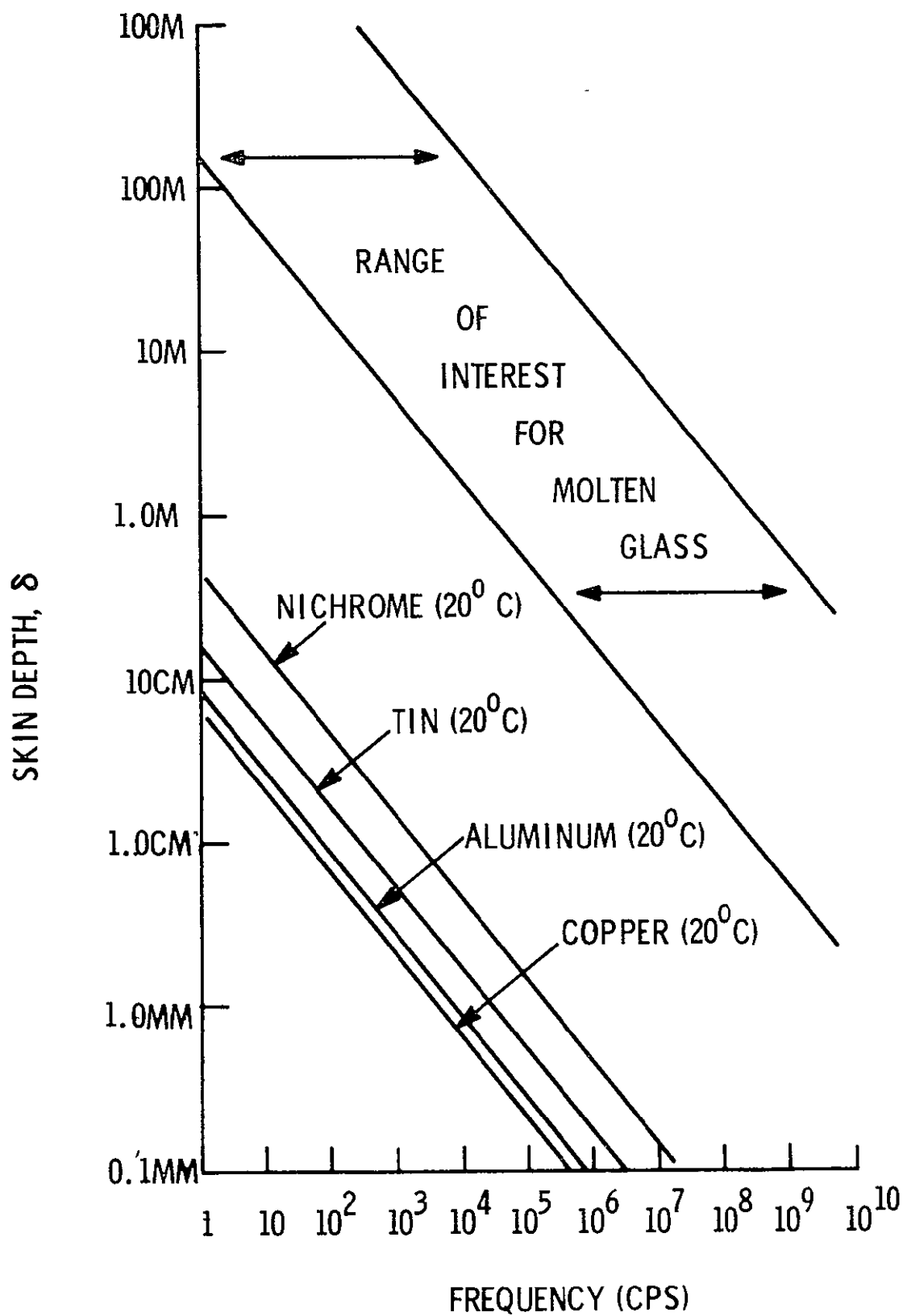


Figure VII-1. Skin Depth versus Frequency for Several Common Metals and Molten Glass

Table VII-1. Physical Properties

Substance or Element	T Melt (C)	T Melt (^o K)	Surface radiation loss for 10 cm ² and unity emissivity*
Ti	1800	2073.16	1.04 x 10 ³
Be	1283 (Top)	1556.16	3.32 x 10 ²
Zr	1857	2130.16	1.17 x 10 ³
W	3370	3643.16	1 00 x 10 ³
Mo	2620	2893.16	3.97 x 10 ³
Cr	1890	2163.16	1.24 x 10 ³
Ta	2996	3269.16	6 47 x 10 ³
PbTe	917	1190.16	1.13 x 10 ²
Steel	1537 (Top)	1846.16	6.58 x 10 ²
Ni	1455	1728.16	5.05 x 10 ²
Ga	29.78	302.94	.48

$$* \sigma = 5.668 \times 10^{-12} \text{ watts/cm}^2 (\text{°K})^4$$

D. Basic Equations for Acceleration and Heating

The development of a set of parameters to discuss processing and positioning of materials can be most easily made by considering the relatively simple system of a single coil and a material sphere. The same parameters are also the most useful in discussing more complicated systems with more than one coil, as will be shown below.

The processor and designer wishes to relate the power absorbed by the material and the force exerted on the material in terms of material properties. For a single loop and a material sphere, the force exerted by the loop on the sphere along the axial line of the loop is

$$F \text{ (dynes)} = \frac{3}{50} \pi^2 I_1^2 A(y) G(x) \left(\frac{R_2}{R_1} \right)^3 \quad (1)$$

and the eddy current power absorbed by the sphere from the field is

$$N \text{ (watts)} = 3 \pi R_2 \rho_e H^2 F_1(x) \quad (2)$$

where

I_1 is the current in amperes

y is the distance along the axis of the loop in terms of loop radius z/R_1 , where z is the distance along the axial line

R_1 is the loop radius

R_2 is the sphere radius

x is the ratio of sphere radius to skin depth R_2/δ

δ is the skin depth

$$A(y) = \frac{y}{(1 + y^2)^{3/2}}$$

H^2 is the magnetic field intensity from the loop along the axis

$$G(x) = \left[1 - \left(\frac{3}{4x} \right) \left(\frac{\sinh 2x - \sin 2x}{\sinh^2 x + \sin^2 x} \right) \right]$$

$$F_1(x) = \frac{x (\sinh 2x + \sin 2x) - \cosh 2x + \cos 2x}{\cosh 2x - \cos 2x}$$

ρ_e = the resistivity in ohm-meters.

For a single loop

$$H^2 = \frac{I_1^2}{4R_1^2} \left\{ \frac{1}{(1+y^2)^3} \right\} \quad (3)$$

so that

$$N = \frac{3\pi}{4R_1^2} \left\{ \frac{1}{(1+y^2)^3} \right\} R_2 \rho_e I_1^2 F_1(x) \quad (4)$$

It can be shown that for more complicated arrangements the equations have the same form so that as an example for two equal coaxial loops carrying equal alternating currents

$$F = \frac{3}{50} \pi^2 I_1^2 G(x) B(y) \left(\frac{R_2}{R_1} \right)^3 \quad (5)$$

where

$$B(y) = \left\{ \frac{1}{(1+y^2)^{3/2}} \pm \frac{1}{(1+y_1^2)^{3/2}} \right\} \left\{ \frac{y}{(1+y^2)^{5/2}} \pm \frac{y_1}{(1+y_1^2)^{5/2}} \right\}$$

Here the distance z is measured positive upward from the plane of the first loop and z_1 is measured positive downward from the plane of the second loop. Then

$$\frac{z}{R_1} - \frac{z_1}{R_1} = y - y_1 = \frac{S}{R_1}$$

where S is the distance between the planes of the loops.

Thus the same parameters used to discuss the single loop and material sphere can be used to discuss more complicated systems and the mathematical complexity is reduced to a minimum by considering the simplest system

1. *Development of Relations Involving only Material and Driving Coil Parameters*

The parameters y , x , etc., used in the above equations are very suitable for computation purposes, but the designer wants to speak of force and power in terms of current, frequency, and the material parameters. Looking at Equations 1 and 4, it is evident that even for the single loop there are many parameters in each equation even with the dimensionless parameters x and y . Thus, the problem of speaking coherently about many materials and their behavior under applied fields and plotting results is fairly complicated

The problem was attacked in the following manner. First the distance dependence factor was removed. The force curve has a peak close to $y = 0.4$. Comparisons were made then at $A(y = 0.4)$. The loop radius was fixed at $R_1 = 0.75$ inches or 1.905 centimeters. This converts Equation 1 to $F = \text{constant} \cdot I_1^2 G(x) R_2^3$ and Equation 4 to $N = \text{constant} \cdot R_2 \rho_e I_1^2 F_1(x)$. For positioning it is more convenient to speak about accelerations, g , imparted to the sphere; since the mass of the sphere is $m = 4\pi \rho_g R_2^3$ where ρ_g is the density, we have

$$g = \frac{F}{4\pi R_2^3 \rho_g} \quad (6)$$

and after putting these into consistent units we have

$$g \text{ (newtons/kilogram)} = \frac{0.0452 G(x) I_1^2}{\rho_g} \quad (7)$$

$$N \text{ (watts)} = (4.16) \cdot 10^3 \rho_e I_1^2 R_2 F_1(x) \quad (8)$$

where here ρ_g is the density in kilograms/meters³

ρ_e is the resistivity in ohm meters, and I_1 is the current in amperes. The parameter x is just R_2/δ where

$$\delta = \left(\sqrt{\pi \mu \sigma \nu} \right)^{-1}$$

and μ is the permeability, σ is $1/\rho_e$ the conductivity, and ν is the frequency of the applied field so that

$$x = R_2 \sqrt{\pi \mu \sigma \nu} \quad (9)$$

The relations of Equations 7, 8, and 9 then form a consistent set for discussing different materials in the field of a single loop.

For a close wound coil we can replace I_1 by NI_1 without an appreciable error, where N is the number of turns in the coil. Calculations based on this approximation for a very close wound coil have been shown to agree fairly well with experimental results (previous quarterly).

2. General Behavior of Force and Power with Skin Depth

It can be seen from Equations 7, 8 and 9 that the following results are obtained. The acceleration imparted to a sphere at a fixed distance from the loop depends upon the sphere radius, the square of the loop current, the permeability of the sphere material, the conductivity (or resistivity) of the sphere material, and the frequency employed in the loop through the complicated function G and inversely upon the density of the sphere material. The eddy current power absorbed by the sphere from the field depends upon the resistivity, the square of the loop current, the sphere radius and also the sphere radius, permeability, conductivity, and the frequency employed through the complicated function $F_1(x)$.

For a given material the ratio of power to acceleration N/g is just

$$\text{constant} \cdot \left(\frac{F_1(x)}{G(x)} \right)$$

Figure VII-2, taken from Fromm and Jehn's article, shows $F_1(x)$, $G(x)$ and $F_1(x)/G(x)$ versus x

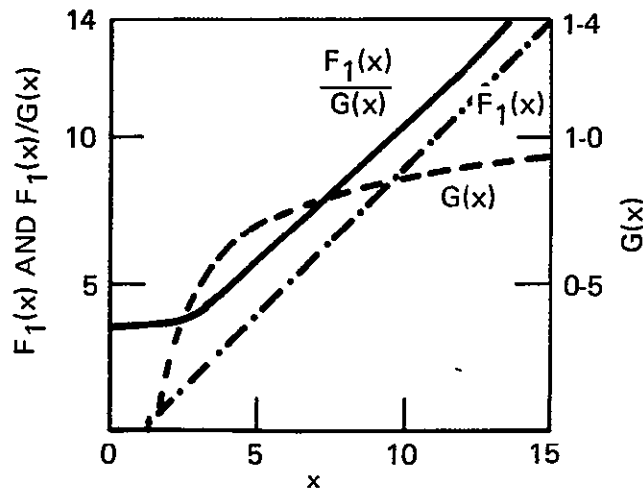


Figure VII-2. Ratio $F_1(x)/G_1(x)$ and the Functions $F_1(x)$ and $G(x)$

3 Regimes of x and Range of Parameters

Referring to Figure VII-2, we see that we can speak essentially of three different regimes in x (ratio of sphere radius to skin depth). These are the regimes $x \leq 1$, x from 1 to about 10, and $x > 10$. For a given material, $x = R_2 \sqrt{\pi \mu \sigma \nu} = \text{constant} \cdot \sqrt{\nu}$ and frequency is the principal variable, but for different materials ranging from dielectrics with $\rho_e \sim 10^{12}$ to conductors ranging to $\rho_e \sim 10^{-8}$ or less (ohm meters) with $\sigma = 1/\rho_e$, the material parameters influence the parameter x considerably. Thus for a glass or a semiconductor, a given x may correspond to very high frequencies, whereas for a conductor it will correspond to very low frequencies. Thus, the region $x < 1$ may range in the frequency from tens of cycles/sec to 10^9 or more cycles/second depending on the material.

4. Small x Power and Force Relations

It is found that for small x

$$F_1(x) \approx \frac{4x^4}{45 + 2x^4} \approx \frac{4x^4}{45} \quad (\text{very small } x) \quad (10)$$

$$G(x) \approx \frac{8x^4}{315 + 14x^4} \approx \frac{8x^4}{315} \quad (\text{very small } x) \quad (11)$$

and that at very small x , $F_1/G \approx 3.5$. This is shown in Figure VII-2 where below $x \approx 2.5$ the curve of F_1/G flattens out at the value 3.5.

For small x (actually it is found that this relation is fairly good out to $x \approx 2.5$), it is found that the power to acceleration ratio is

$$\frac{N}{g} = 3.22 R_2 \rho_g \rho_e \quad (12)$$

with $\left. \begin{array}{l} N/g \text{ in watts/(newtons/kgm)} \\ \rho_g \text{ in gm/cm}^3 \\ \rho_e \text{ in microhm-cm} \end{array} \right\} \text{ for convenience}$

For a specific material under a fixed force we can see that $N = \text{constant} \cdot R_2$ so that, for a given acceleration and a specific material, the absorbed eddy current power depends only on the sphere radius. For each material, then, the absorbed power will depend only on the sphere radius at small x , and the plot of N vs R_2 on log-log paper will be a straight line.

5. Positioning Control at Small x

Figure VII-3 shows the eddy current power absorbed by a free floating specimen when it is accelerated by an eddy current positioning device at a rate $10^{-6}g$ ($10^{-3} \text{ cm sec}^{-2}$). This acceleration

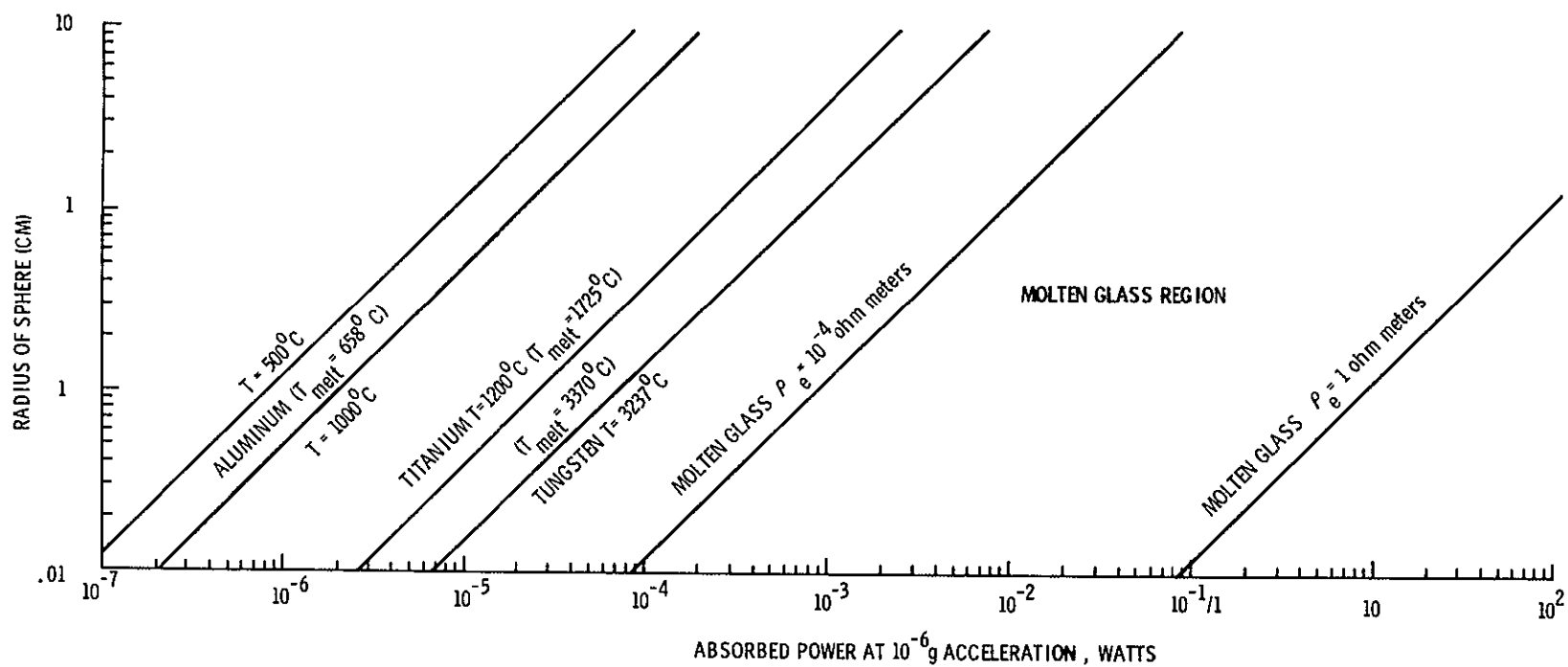


Figure VII-3. Eddy Current Power Absorbed by a Free Floating Specimen

is characteristic of the lower limit which may be achievable in lower altitude earth orbiting facilities unless compensation for deceleration due to air drag and gravity gradients are provided. The power requirement depends upon the sphere mass, density, electrical conductivity, and driving frequency. It also depends upon the magnetic permeability of the specimen, but our main interest is in molten materials which will be above the Curie temperature so that we may assume unit permeability. We see that the power is linearly proportional to the sphere radius and depends drastically upon the conductivity of the material. For example, minimum position control power for a one centimeter aluminum or molten glass sphere at an acceleration of $10^{-6}g$ ranges from 10^{-5} watts to 100 watts. For molten glass of relatively high conductivity, the corresponding power required for position control drops to 10 milliwatts. The corresponding frequencies required for position control range from the low audio range for metals to tens of megahertz for the molten glass of poorest conductivity.

For relatively small experiment vehicle carriers, such as the proposed dry work shop, astronaut body motions may occasionally impart accelerations to the vehicle approaching $10^{-4}g$ for short time periods. For most processes, sufficient free volume can be provided surrounding the specimen being processed so that it can remain free floating without seeing accelerations of this magnitude. Since these accelerations will average out to zero over a time period on the order of a minute or less, it is highly likely that rigid position control with respect to the vehicle will not be required. At least for short processing times, the operation of such accelerating forces could easily be inhibited until process completion. If it is desired to provide rigid positioning of free floating object with respect to the vehicle during accelerations as high as $10^{-4}g$, we can refer to Figure VII-4 for the required positioning powers. For the metals in the range up to ten centimeter radius, the positioning powers are essentially negligible (less than one watt). For high conductivity molten glass, the power requirement ranges up to only ten watts. For poorly conducting molten glass, required positioning powers can reach the multikilowatt region and hence it appears that eddy current position control is not a likely candidate in this extreme case unless simultaneous RF heating is used

Referring to Equations 7, 8 and 9, and using the small x approximation, we see that for $x < 1$ or $R_2/\delta < 1$

$$g = \left(\frac{0.0452 I_1^2}{\rho_g} \right) \left(\frac{8 x^4}{315} \right) = \text{constant} \cdot \frac{I_1^2 x^4}{\rho_g}$$

$$N = 4.16 \cdot 10^3 \rho_e I_1^2 R_2 \left(\frac{4 x^4}{45} \right) = \text{constant} \cdot \rho_g I_1^2 R_2 x^4$$

and for a fixed material, $x = \text{constant} \cdot R_2 \sqrt{\nu}$, so that

$$g \propto \frac{I_1^2 R_2^4 \nu^2}{\rho_g}$$

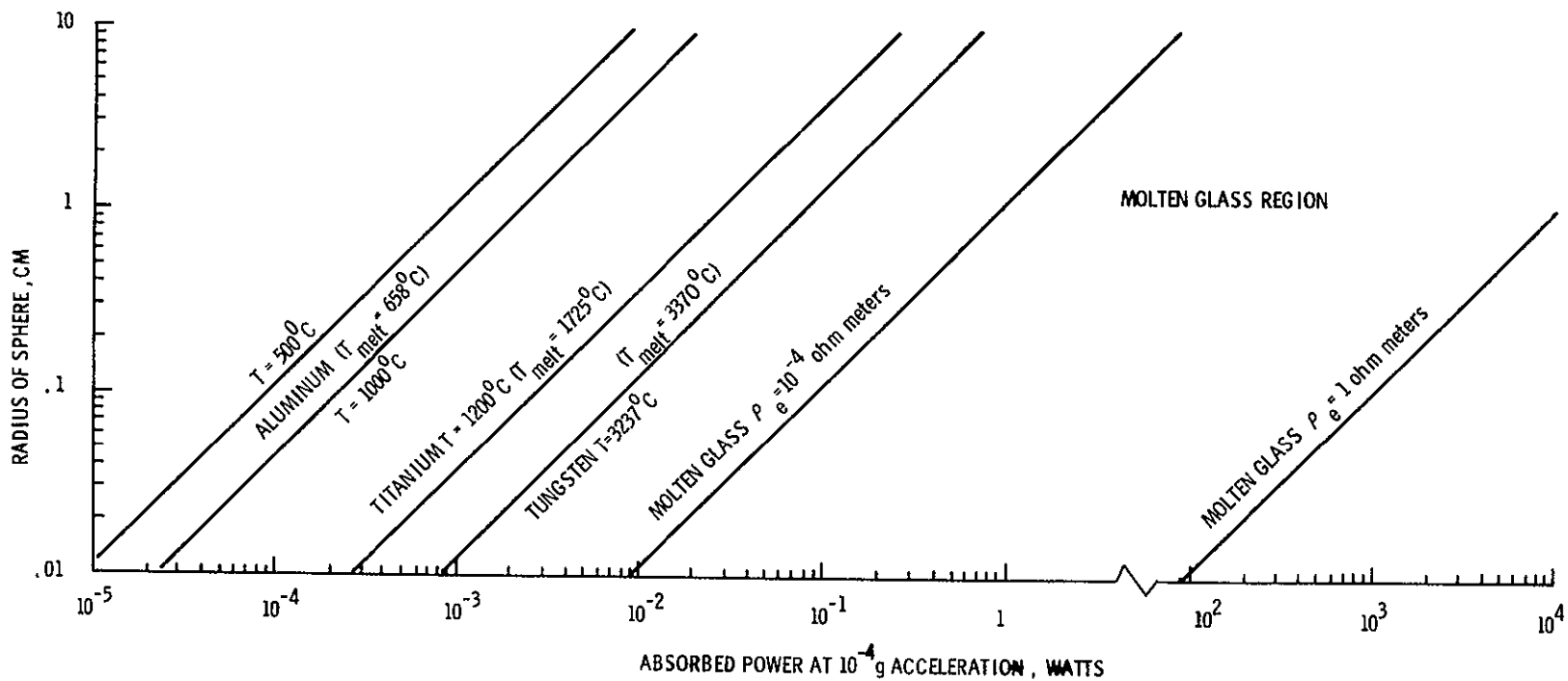


Figure VII-4. Rigid Positioning of Free Floating Object During Acceleration as High as $10^{-4}g$

$$N \propto I_1^2 \rho_e R_2^5 \nu^2$$

for small x . Small x ($x < 1$) means $R_2/\delta < 1$ so that the skin depth of penetration exceeds the sphere radius R_2 .

For the same material, then, for small x

$$g \propto \nu^2$$

$$N \propto \nu^2$$

Thus, for material conductivities, sphere radii, and driving frequencies such that the skin depth of penetration exceeds the sphere radius, a change in driving frequency will cause the acceleration and power dissipation to vary in the same proportion. Increasing the frequency so as to double the acceleration will also double the power dissipation.

6. *Positioning at Large x*

Curves showing the manner in which the acceleration and power dissipation vary with frequency are shown in Figure VII-2. These curves show that for frequencies and conductivities such that the skin depth is a small fraction of the sphere radius, the power dissipation increases with frequency more rapidly than acceleration. For the metals, positioning with negligible heating at low frequency is relatively simple. For a very poor conductor such as molten glass, an increase in frequency to at least the high audio range and even into the tens of megahertz range is required, hence, eddy current heating cannot be avoided. We have displayed the dependence of power dissipation, normalized per unit sphere surface area, as a function of driving frequency for metals and semiconductors in Figure VII-5. Figure VII-6 shows the range of frequencies of interest for positioning of metals and semiconductors.

For the molten metals of Figure VII-5, we can no longer assume, for practical frequencies, the regime of small x . Calculations for this plot are based on the full expression for $F_1(x)$ and $G(x)$, case $x \geq 1$ given earlier.

E. *Frequency Choice for Facilities*

Here we see that the choice of frequency for a positioning facility can be made conveniently in the audio region if the specimen is heated by some means other than eddy currents. In practice, we can select a frequency somewhat arbitrarily, such as ten kilohertz, for which requirements for electronic circuit design are extremely simple. The actual positioning forces obtained at a given driving field strength will then of course depend upon the resistivity and size of the material sphere being processed. In the servo positioning device which we are developing, the exact restoring force per

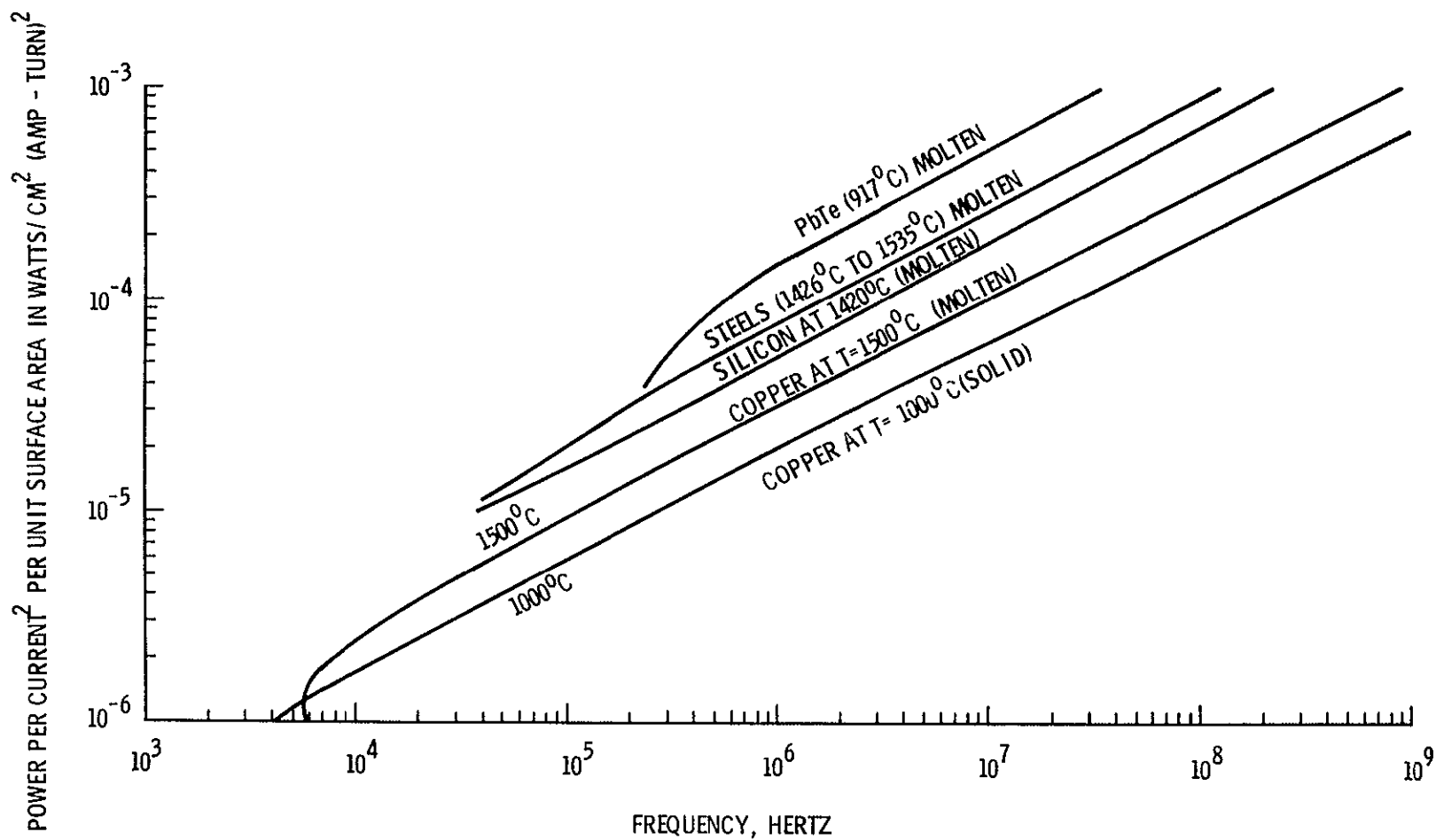


Figure VII-5. Power as a Function of Driving Frequency for Metals and Semiconductors

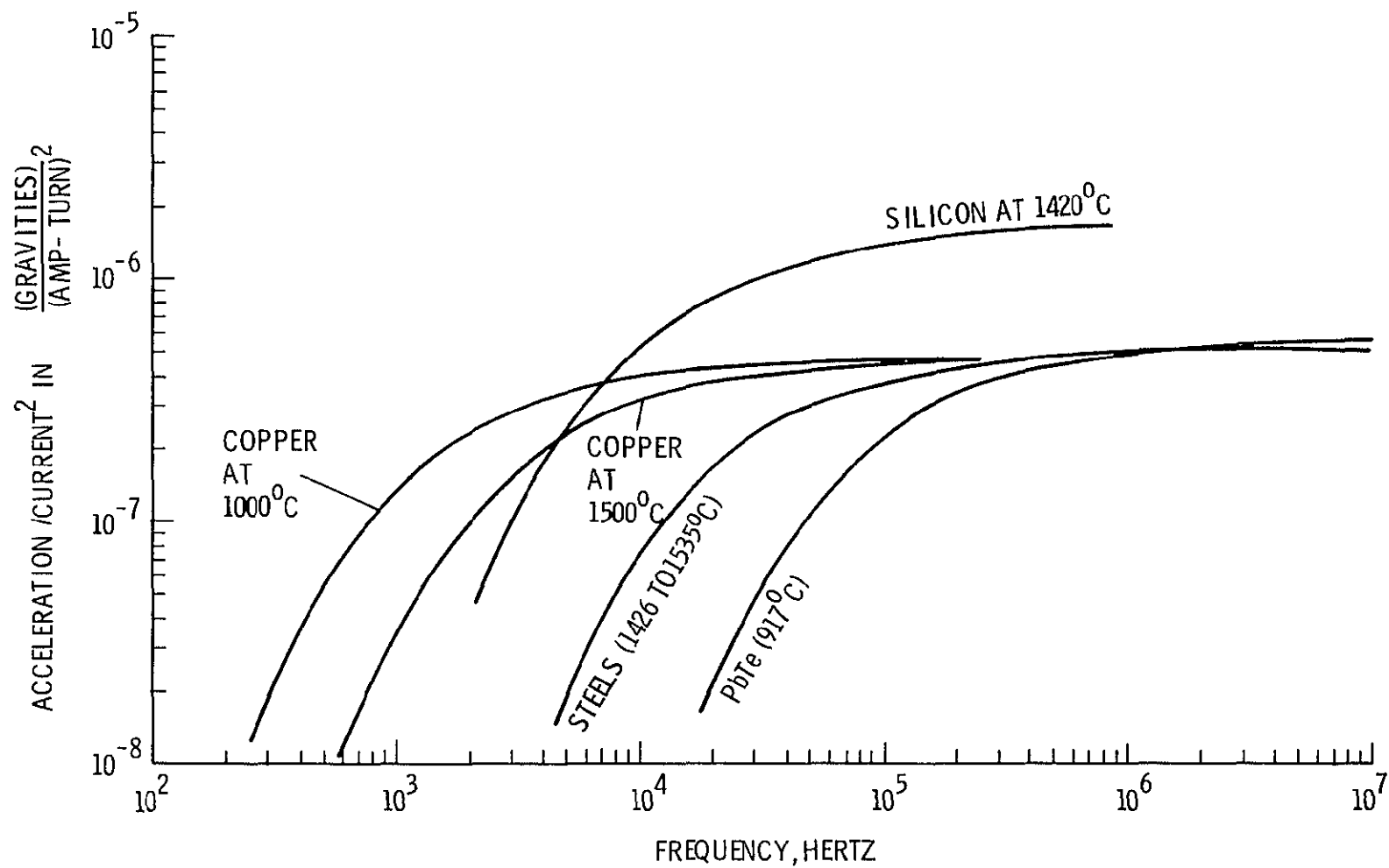


Figure VII-6. Acceleration as a Function of Driving Frequency for Metals and Semiconductors

unit position error is not particularly critical. Moreover, the servo loop gain can be varied quite easily, if desired, for different specimens by turning a knob to a precalculated position. In practice, such an adjustment would probably not be made unless the material resistivity varied extremely from one specimen to the next.

For molten glass (Figure VII-7), we see that the frequency required to obtain positioning accelerations of 10^{-6} g range from one kilohertz at 1,000 ampere turns and a resistivity 10^{-4} ohm meters to 100 megahertz for the case of a one ampere turn driving coil and glass of resistivity one ohm meter. It thus appears that, although eddy current positioning is feasible for molten glass, it may not be the optimum method in practice, especially for glass of poor conductivity. We have previously showed the skin depth as a function of frequency in Figure VII-I. Depending upon the frequency and conductivity, we see that the skin depth can range over 7 decades of variation, thus the ratio of skin depth to sphere radius can vary from values much less than unity to values much greater than unity for cases which will be of interest. This is in contrast to work in terrestrial levitation experiments where skin depths greater than the sphere radius are of little interest since they, in general, do not provide sufficient positioning force to levitate the material in the one g environment. The greater freedom of choice of frequency and skin depth for the case of materials which are processed in the zero gravity environment allows for eddy current heating which can be adjusted independently from the requirement for positioning.

F. Heating and Temperature Control

The minimum heating power which must be provided is that necessary to furnish surface radiation loss from the specimen. If a controlled atmosphere is utilized, additional power will be conducted away by the gas. In this connection it must be noted, however, that normal convection due to buoyancy of the heated gas will be absent and that, under these conditions, the gas will act as a good insulator. For many materials, including most metals, the choice of heating methods can be made independently of the choice for position control. For materials of very high resistivity such as glasses, the electromagnetic positioning can give rise to eddy current heating dissipations which can become significant so that it may be advantageous to consider RF heating, at least for things such as molten glass having reasonably good conductivity. One might be led to think, conversely, that the choice of eddy current or RF heating will lead to unavoidable positioning forces. However, if RF heating is provided by pairs of coils symmetrically disposed on either side of the specimen, no net translational force will be applied to the specimen when the coils are equally excited. With such an arrangement, if it is desired to impart a position control force, small differential excitations can be introduced into the coil excitations through a servo loop actuated by position or velocity errors in such a way that the total power dissipation in the specimen is unchanged. The specimen temperature can be controlled by raising or lowering the total coil excitation power.

Figure VII-8 simply illustrates the surface radiation loss, or minimum heating power required to achieve the melting or transition temperature for several materials of interest. By way of illustrating the relation between the heating power requirement, if this is provided by eddy currents, and the eddy current positioning requirements discussed earlier, we may consider the example of PbTe shown in Figure VII-8. This requires a minimum power dissipation in a one centimeter radius sphere of 130 watts. Referring back to Figures VII-5 and VII-6, we see that this requires a driving

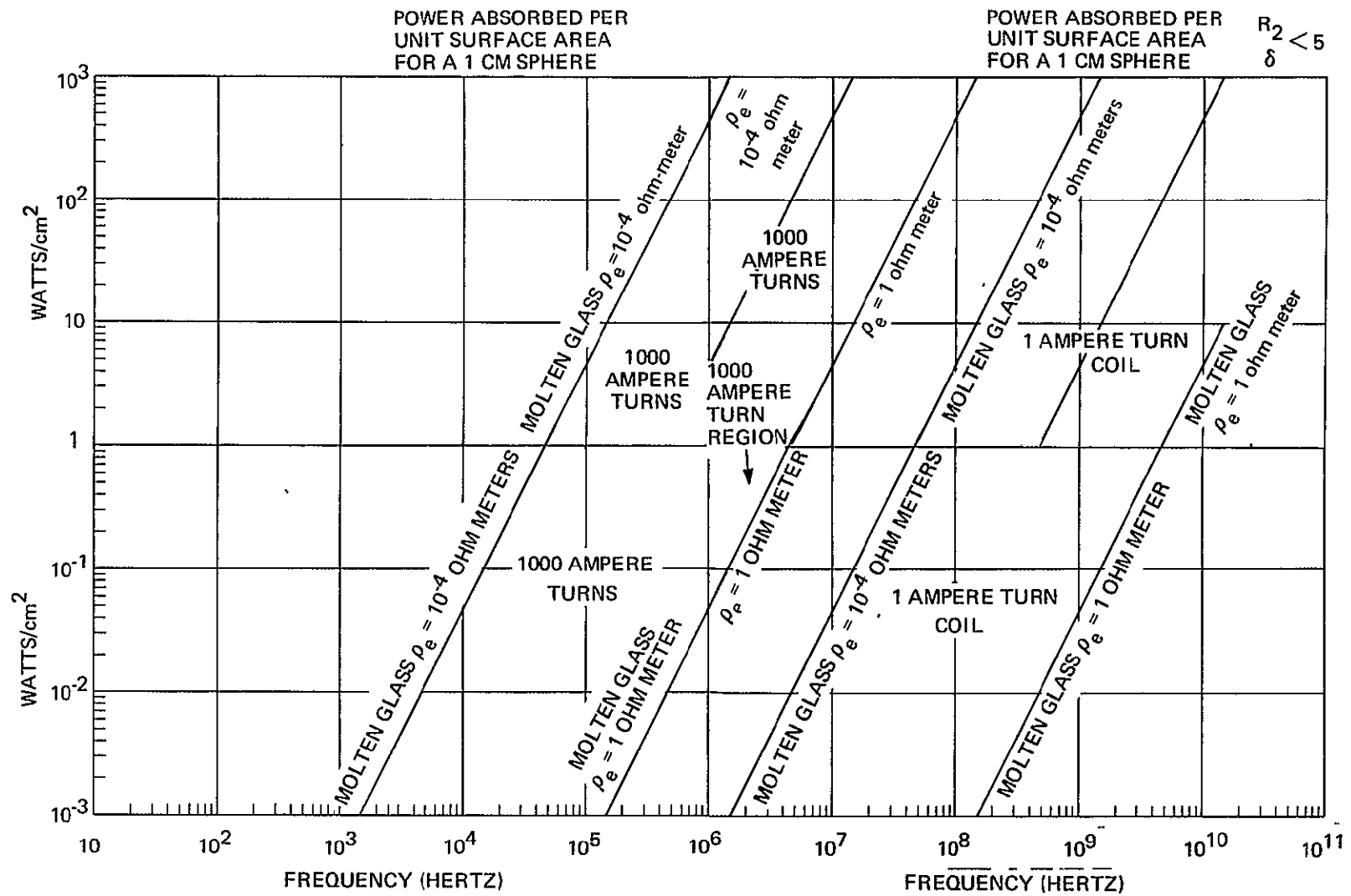


Figure VII-7. Power as a Function of Driving Frequency for Molten Glass

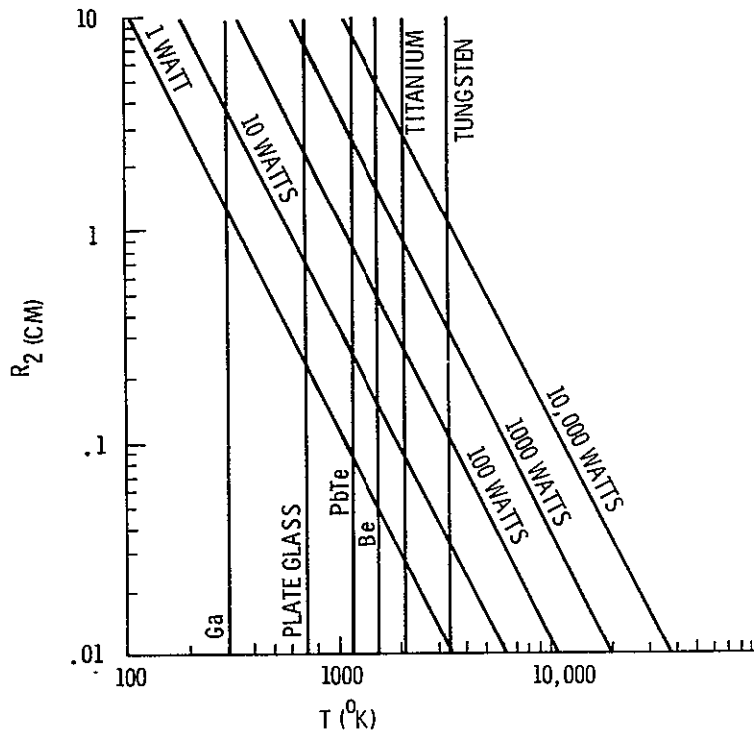


Figure VII-8. Minimum Heating Power Required to Achieve Melting Temperature for Several Metals of Interest

frequency of 600 kilohertz at 300 ampere turns, corresponding to a maximum acceleration of 0.04 g if all of the power is furnished by a single coil. Any lower value of position control acceleration can be provided by sharing the driving power between two coils, one on either side of the specimen

G. Position Sensing

A number of position sensing schemes are available which can be used for position control or handling of free floating solid or liquid materials. Besides the eddy current position sensor which we have developed and applied to sensing of metallic objects, one may also consider bolometers or other heat sensing detectors or changes in electrostatic capacitance. The latter would be a natural solution in the case of an electrostatic position control device.

Another possibility is optical sensing, either by emitted radiation from a hot object by interception of optical light beams, or visual or photographic observations. It is expected that visual observations of specimens during processing should be provided wherever possible, particularly in pilot experiments.

Any of the above position sensing methods, except photographic, can be used to actuate a position control servo in the same manner as is done in our demonstration electromagnetic device. It is quite likely that none of the above methods will be applicable to all processes, but each will have its own domain. It appears that these domains overlap. For many processes, either the eddy current position

sensor or the bolometer position sensor will be adequate. For samples of very high resistivity which must be positioned at temperatures too low for detection of emitted radiation, the electrostatic or optical methods can be considered. Normally, however, positioning of these specimens can perhaps be performed mechanically when they are removed from the processing chamber after cooling.

VIII. REFERENCES

- II-1. Prince, A., *Alloy Phase Equilibria*, Elsevier Publishing Company, Amsterdam – London – New York, 1966.
- II-2. Steurer, W. H., "Composite Casting Superior Structural Materials Through the Combined Application of Unique Zero Gravity Effects," *NASA Symposium, Space Processing and Manufacturing*, October 21, 1969.
- II-3. Frost, R. T., "Weightless, Containerless Melting and Solidification of Potential New Metals and Ceramic Products," *NASA Symposium, Space Processing and Manufacturing*, Marshall Space Flight Center, October 21, 1969.
- II-4. Utech, H. P., "Growing Crystals in Space," *NASA Symposium, Manufacturing Technology Unique to Zero Gravity Environment*, November 1, 1968
- II-5. Grodzka, P. G., "Gravity-Driven and Surface Tension-Driven Convection in Single Crystal Growth," *NASA Symposium, Space Processing and Manufacturing*, October 21, 1969.
- II-6. Hammalainen, M., "Segregation of Impurities in Molten Salts Induced by Cellular Convection and Its Effect on Crystal Growth," *J. Crystal Growth*, Volume 2, 1968, pp. 131–136.
- II-7. Deeg, E. W., "Glass Preparation in Space," *NASA Symposium, Space Processing and Manufacturing*, October 21, 1969.
- II-8. Blade, J. C., Clare, J. W. H., and H. J. Lamb, *J. Inst. Metals*, 88, 305, 1960.
- II-9. Brunst, W., *Die induktive Wärmebehandlung* (Berlin: Springer-Verlag), p. 42, 1957.
- II-10. Comenetz, G., and J. W. Salatka, *J. Electrochem Soc.*, 105, 673, 1958.
- II-11. Fogel, A. A., *Invest. Akad. Nauk, SSSR, OTN, Met.*, 1 Topl., 2, 24, 1958.
- II-12. Fromm, E., and H. Jehn, *Z. Metalk.*, 56, in the press, 1958.
- II-13. Harris, B., Price, E. G., and A. E. Jenkins, *Proc. Australian Atomic Energy Symposium*, p 221, 1958.
- II-14. Harris, B., and A. E. Jenkins, *J. Sci. Instrum.*, 36, 238, 1959.
- II-15. Hulsey, W. J., U. S. Atomic Energy Commission, Research and Development Report, Y-1413, 1963.
- II-16. Lewis, J. C., Neumayer, H. R. J., and R. G. Ward, *J. Sci. Instrum*, 39, 569, 1962.

- II-17. Okress, E. C., Wroughton, D. M., Comenetz, G., Brace, P. H., and I. C. R. Kelly, *J Appl Phys* , 23, 545, 1952.
- II-18. Polonis, D. H., Butters, R. G., and J G. Parr, *Research*, 7, 273, 1954.
- II-19. Scheibe, W., *Metall.*, 7, 751, 1953.
- II-20. Smythe, W. R., *Static and Dynamic Electricity* (New York: McGraw-Hill), 1950.
- II-21. Weisberg, L. R., *Rev. Sci Instrum* , 30, 135, 1955.
- II-22. Wroughton, D. M., Okress, E C., Brace, P. H., Comenetz, G., and I. C R. Kelly, *J Electrochem. Soc.*, 99, 205, 1952.
- II-23. Walker, J., "Influence of Large Amounts of Subcooling on Crystal Structure of Metals," *Journal of Physical Chemistry of Process Metallurgy*, Vol 2, 1961
- II-24. Bosier, L. and A. Befrain, *Bull. Soc. Fr. Mineral Crist.*, Vol. 88, p. 145, 1965.
- II-25. Olsen, R. P., "Containerless Production of New Glasses and Other Materials," *NASA Symposium, Manufacturing Technology Unique to Zero Gravity Environment*, November 1, 1968.
- II-26. Happe, R. A , "Possibilities for Producing New Glasses in Space," *NASA Symposium, Space Processing and Manufacturing*, October 21, 1969
- II-27. Witt, R., "Boron Filament Manufacture in Space — A Literature Feasibility Study," *NASA Symposium, Space Processing and Manufacturing*, October 21, 1969.
- II-28. Deeg, E W., "Glass Preparation in Space," *NASA Symposium, Space Processing and Manufacturing*, October 21, 1969.
- III-1. Rayleigh, Lord, *Theory of Sound*, Volume 1, Dover Publishing, 1945.
- III-2. Chandrasekhar, S., "Oscillations of a Viscous Liquid Globe," *Proceedings of London Mathematical Society*, Vol. 9, 1959.
- III-3. Benedikt, E., "Biological Effects of Weightlessness — Physical and Phenomenon," *Plenum Press*, N.Y., 1960.
- III-4. Reid, W H., "The Oscillation of a Viscous Liquid Drop," *Quarterly of Applied Mathematics*, Vol. 18, pp. 86–89, 1960.
- III-5. Lamb, H. J., *Hydrodynamics*, Dover Publications, New York, N.Y., 1945.

- III-6. Frost, R. T., "Crucibleless Melting, Purification and Solidification of Materials in Zero-G Environment," *NASA Symposium, Manufacturing Technology Unique to Zero Gravity Environment*, p. 86, November 1, 1968.
- IV-1 Okress et al, J., *Appl. Phys.*, 23, (1952) 545.
- IV-2. Fromm and Jehn, *Brit./Appl. Phys*, 16, (1965) 653.

APPENDIX A

MEASUREMENT OF SMALL FORCES

The forces of repulsion measured in 1969 were initially of the order of hundreds and thousands of dynes. After a series of refinements were made, forces as low as five dynes were measured acting upon an aluminum sphere of 13.5 gram mass (force/weight ratio equaled 4×10^{-4}). With the intention of attaining force weight ratios closer to 10^{-5} as our goal, the techniques available were recently reviewed more closely. The techniques examined were

1. Sphere free to roll on a flat surface.
2. Simple pendulum.
- 3 Sphere suspended in a liquid.
4. Torsion balance.
5. Electromagnetic levitation.

In each case it was assumed that the mass being pushed by the divergent electromagnetic fields was a 30-gram steel sphere with a 1-cm radius.

1. Sphere Free to Roll on a Flat Surface

It had been planned to employ a plate glass tilt table as soon as possible in the measurement of small forces, but it was soon evident that, for speeds and forces with which we wanted to work (e.g., 0.1 cm/sec and 10^{-4} g), the presence of dust presented a problem. Also, it turned out to be desirable to use a good conductor such as aluminum to facilitate position control at low frequencies and a sufficiently high quality aluminum sphere was not readily available. The use of the glass plate was set aside, then, and we turned to the simple pendulum described in the quarterly report of November 15, 1969. This rolling technique has now been reconsidered in more detail and the following limitations have been recognized.

- a. Dust - In a laboratory in which no special attempt is made to clean or filter the air, a rough estimate of the force required to start a perfect sphere rolling on a perfect surface might be as high as 100 dynes. Use of a moderately clean-room environment could reduce it to something more like 0.1 to 10 dynes. The dust particle density requirement for several classes of clean rooms is given in Figure A-1. Sampling of the air in such a room must produce data points which lie below the proper line in this figure. Assume that the surface upon which the sphere is to roll is in a closed container (such as our Plexiglas pendulum box) which has been cleaned such that it meets the requirements of a class 100,000 clean room. Assume, also, that all the dust in the air in this container up to one inch above the surface, settles upon the surface. The remainder then clings to the walls or remains suspended in the air during the course of the experiment. The distribution of particles corresponding to the line for a class 100,000 clean room is

$$n = 10^{4.3} s^{-2.3}$$

where n is the particle density (ft^{-3}) and s is the particle size (microns). The particle density on the surface is then

$$N = \left(\frac{1}{12} \right) 10^{4.3} s^{-2.3}$$

where N is expressed in ft^{-2} . Let us now estimate to what size particle we must go, starting from the largest, to find a surface density sufficiently large, on the average, to prevent a sphere from rolling freely.

A sphere can be prevented from rolling freely if it is surrounded by three particles of equal size as shown in Figure A-2. The surface density corresponding to such a condition is A^{-1} (ft^{-2}), where A is defined in the figure. Thus, setting $N = A^{-1}$ and arranging for R to be in cm and s in microns:

$$s = [2.4 \times 10^{-4} R]^{-1.3}$$

If $R = 1 \text{ cm}$:

$$s = 0.002 \text{ micron}$$

The smallest force required to push the sphere away from the three trapping particles is approximately (for $s \ll R$):

$$F = \frac{W}{2} \sqrt{\frac{s}{R}}$$

and for a 30 gm sphere

$$F = 6 \text{ dynes}$$

Because the class 100,000 line in Figure A-1 is an upper limit for any particle count in the clean area and because of the inexact nature of this calculation, the starting force might better be given as probably in the range between 0.1 and 10 dynes depending upon the dust distribution on the surface.

- b. Sphericity - The best steel balls have a tolerance on their sphericity of ± 0.000010 inch. If an out-of-round condition of 0.000010 inch is assumed to be in the form of a flat spot, a force of 200 dynes will be needed to initiate rolling. In actuality, the out-of-roundness is not found to be in such an extreme and simple condition and a more realistic initiating force is probably in the range of 20 to 2 dynes. As in the case of dust, any out-of-round condition would affect the path of a slowly rolling sphere.

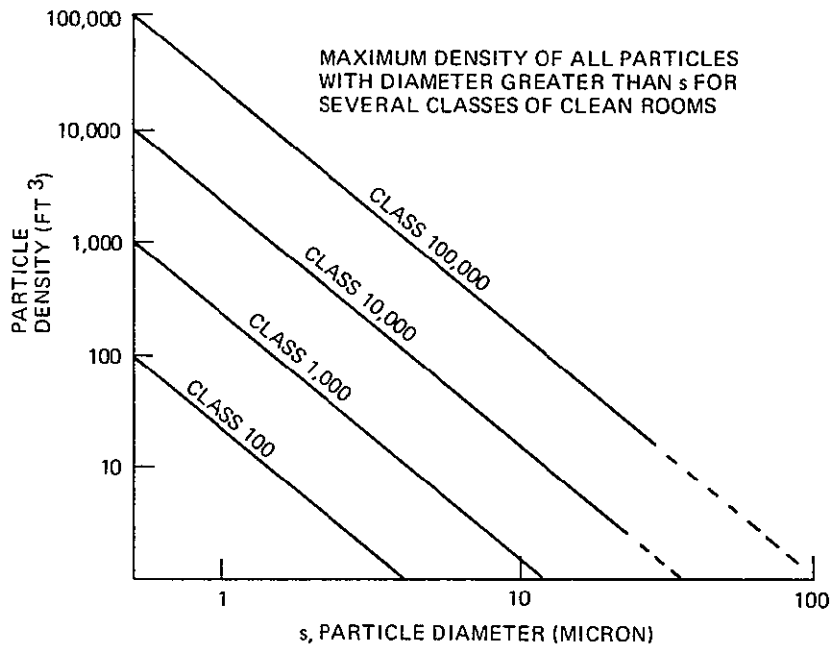


Figure A-1. Maximum Density of all Particles with Diameter Greater than s for Several Classes of Clean Room

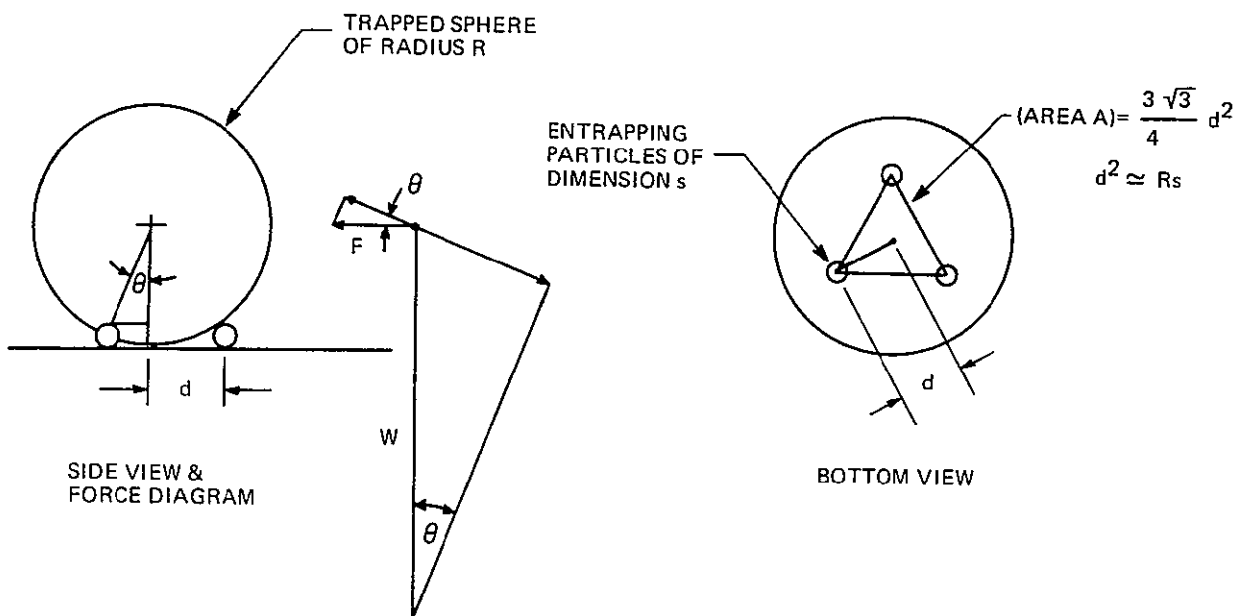


Figure A-2. Preventing a Sphere from Rolling Freely

- c. Friction - Data for steel spheres rolling on a glass surface have not been located but from data on similar materials it seems that a coefficient of rolling friction of 0.001 may be expected with no possibility of improvement beyond 0.0005. This provides a force/weight ratio of 10^{-3} to 0.5×10^{-3} and a force of 30 to 15 dynes for a 30-gram mass.

2 Simple Pendulum

A simple pendulum one meter long with its position observed through a microscope or telescope, as done previously, or via an optical lever (reflected light beam) may be just barely capable of measuring force/weight ratios of 10^{-5} . The feasibility depends upon the quality of the optical components used and largely upon the degree to which the effects of vibration can be minimized. Standard microscopy objectives cannot be used in the vicinity of the suspended sphere if conductive materials are to be prevented from distorting the electromagnetic field. If this technique were to be pursued, probably the layout of the apparatus would be as shown in Figure A-3.

3. Sphere in Liquid

To give a mass of material complete freedom to move in two dimensions it could be suspended by a float in a non-conducting liquid shown in Figure A-4. The equation of motion for small v is

$$m \frac{dv}{d\tau} + 3\pi \delta v \mu = F$$

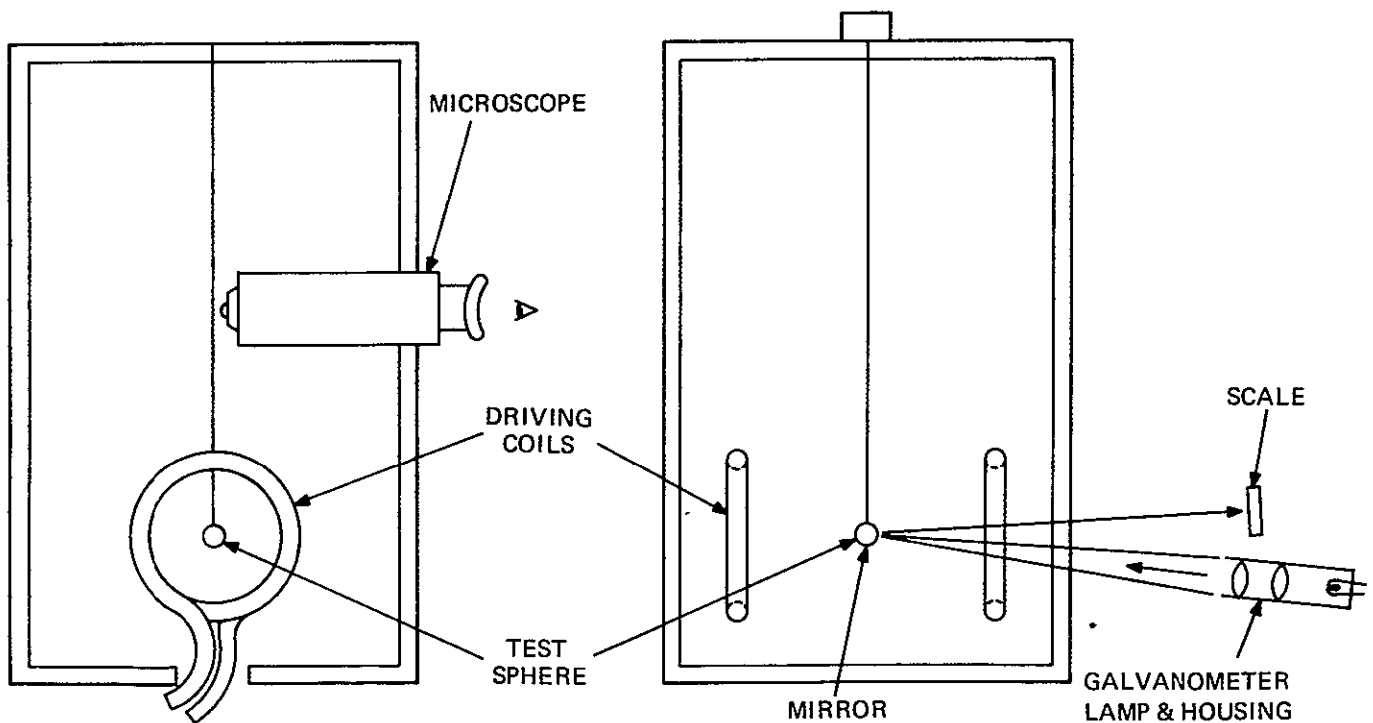


Figure A-3. Layout of Apparatus for Measurement of Small Forces with a Minimum of Electromagnetic Field Distortion

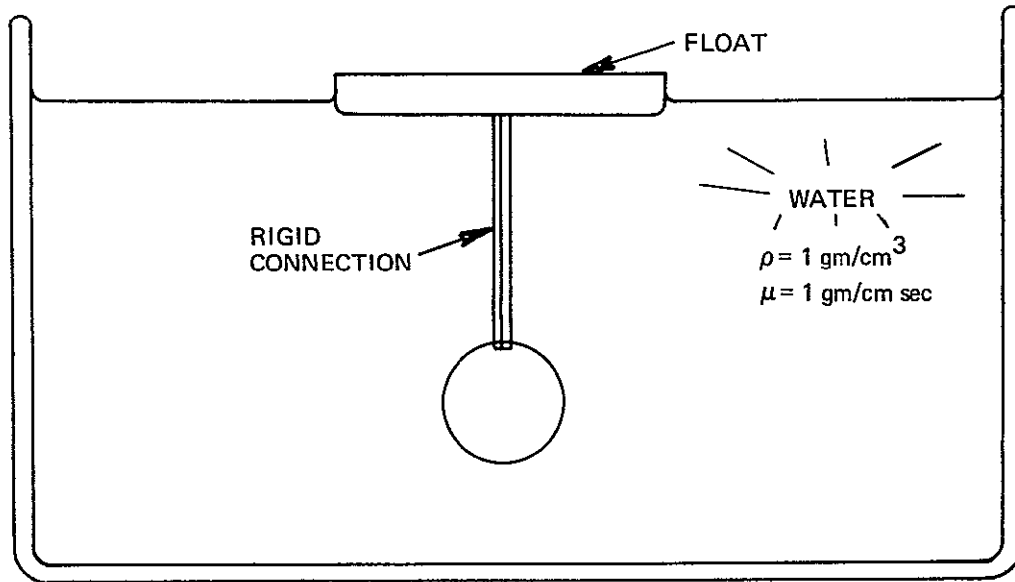


Figure A-4. Sphere Suspension

where v is the velocity of sphere relative to the fluid, δ is the diameter of the sphere, μ is the dynamic viscosity of the fluid, and F is the external force applied to the sphere. The second term of this equation is the drag force as given by Stoke's law which holds for Reynolds' numbers less than 0.5 and

$$\text{Reynold's number} = \frac{v \delta \rho}{\mu}$$

where ρ is the density of the fluid. One approach to this technique would be to observe the motion of the mass immediately after the initiation of the electromagnetic field, while v is very small and the viscous drag force exerted by the liquid upon the sphere is small compared to the applied force. During this period, the applied electromagnetic force would be accelerating the mass as if it were floating freely in space. However, the several requirements tended to be mutually contradictory.

For example, let it be required that a constant force F be applied to the initially stationary sphere and, at the end of the period of observation during which a distance s has been traversed, the drag force is still 10 times less than F . That is,

$$3 \pi \delta v \mu \leq 0.1 F$$

If $F = m \times 10^{-5}$ and $g = 0.3$ dyne for $m = 30$ gm in water

$$v \leq 0.003 \text{ cm/sec}$$

for which the Reynold's number is ≤ 0.006 . The distance s is 0.0005 cm which would be traversed during a period of 0.3 second. Measuring these last two quantities with reasonable accuracy is possible, but not without considerable difficulty and sophisticated specialized apparatus.

Observations can be made readily when the applied force equals the drag force. If the terminal speed thus attained produces a Reynold's number less than 0.5, then Stokes' Law would permit direct calculation of the average applied force during the period of observation. The drag force exerted upon a 2-cm diameter sphere in water, traveling at 0.05 cm/sec (for which Reynold's number is 0.01), is 0.1 dyne. The time to travel each of several 1-mm observation lengths of its path would be 20 seconds. The flotation device would add some drag which would have to be accounted for.

4 *Torsion Balance*

A highly sensitive torsion balance technique has long been used in our laboratory for measuring the force molecular beams exert upon a surface, and this technique should be adaptable to the needs of this program. For example, a tungsten filament 0.05 mm in diameter, 10 cm long, will provide a torsion constant of 0.13 dyne-cm/radian. If the mass upon which the electromagnetic field is acting is suspended on a 7.5-cm radius from the bottom of the tungsten filament, a force of 0.06 dyne will move the mass horizontally 2.5 mm (i.e., 0.02 dyne/mm). Such a force acting upon our 13.5 gm aluminum mass, for example, would produce an acceleration of $0.5 \times 10^{-5}g$ and upon a 30-gram mass, an acceleration of $0.2 \times 10^{-5}g$. The basis of this calculation and an estimation of the uncertainties involved are given below. The torque provided by a torsion balance is given by

$$T = \frac{\pi \theta E R^4}{2 L}$$

where θ is the angle of rotation, E is the shear modulus of the filament, R is the radius of the filament, and L is the length of the filament. If the mass is at the end of an arm of length λ from the filament's axis, then the force acting upon the mass is

$$F = \frac{\pi \theta E R^4}{2 L \lambda}$$

This equation is adequate for designing a torsion balance to measure small forces, but it does not lend itself to accurate force measurement because of the R^4 term. If the filament's diameter and its maximum uncertainty were 0.001 ± 0.00005 inch, the uncertainty in R would be 5 percent and the uncertainty in R^4 would be 20 percent. Add to this a total uncertainty of 5 to 10 percent for all the other terms and the force would be known within ± 25 to 30 percent. The calibration of this torsion technique is much improved if the period of a torsional oscillation of the system were measured with and without a mass of known moment of inertia. A cylindrical rod is very useful for this purpose and the force is given by

$$F = \frac{\pi m \theta \ell^2}{3 \lambda (t_r^2 - t_b^2)}$$

where m is the mass of the rod, ℓ is the length of the rod, t_r is the period of oscillation of the balance with the rod lying across it, and t_b is the period of the balance alone. Cumulative errors in this case should not exceed 10 percent, especially if m and ℓ are large.

The tensile strength of a 0.05-mm diameter tungsten filament has been estimated and, according to this estimation, it should be capable of suspending a 900-gram mass. For the purpose of this small force measurement, no more than about 20 percent of this limit would be required to suspend and balance a 30-gram mass, and an additional 10 to 20 percent would be used for the extra calibration rod.

A variation of this torsion balance which might be useful in demonstrating the dynamic behavior of a mass under the influence of small forces, much in the same manner that a long simple pendulum was used in our filmed demonstration with larger forces, is a mobile made up of two torsion balances, one suspended from the other. If sensitivity constants of the order of 0.002 dyne/mm are obtained by proper choice of parameters, the test mass would appear virtually free over a 1 cm x 1 cm range. A disadvantage to this mobile technique lies in the fact that the dynamics of the sphere would be tied to the moments of inertia of the system and not solely to its own mass.

5 *Electromagnetic Levitation*

Electromagnetic levitation usually is accomplished in such a manner that a potential well is formed at the top of the levitating field to keep molten levitated material centered in the field. We believe it is possible to produce a long level potential trough through use of a rectangularly shaped coil such that material suspended by it would behave as if it were at the end of an extremely long pendulum or on a slippery surface with an extremely low coefficient of friction. The degree to which this might be useful in small force measurement has not been investigated. Interactions between the levitating force field and the field creating the force to be measured may interfere with the measurement.

APPENDIX B

DIELECTRIC POSITIONING

The theoretical work on dielectric spheres in electromagnetic fields has not been advanced to the level where we have studied conducting spheres. An order of magnitude calculation has been made for the magnitude of the electric fields necessary to exert a few dynes of force on a Pyrex glass sphere of radius $a = 0.4125$ in. Consider a dielectric sphere in a time harmonic electric field. To the first order an induced polarization

$$\vec{P} = 4\pi \epsilon_0 a^3 |\vec{E}| \left[\frac{\eta_e - 1}{\eta_e + 2} \right] \hat{k}$$

will be induced in the sphere by a field $E \cos \omega t \hat{k}$, where

P is the induced polarization

ϵ_0 is the permittivity of free space

η_e is the relative permittivity of the dielectric.

To the first order the force acting on the dielectric sphere is $\vec{F} = (\vec{P} \cdot \nabla) \vec{E}$, and this is

$$\vec{F} = 4\pi \epsilon_0 R^3 \left[\frac{\eta_e - 1}{\eta_e + 2} \right] E \frac{\partial E}{\partial z} \hat{k}$$

We shall take a field whose gradient is given by $dE/dz = E/3$ (volts/cm/meter) or $E/3 \times 10^2$ volts/meter², where we have expressed E in volts/cm for convenience, since we are using apparatus of this size, so that

$$F_z = 4\pi \epsilon_0 \left[\frac{\eta_e - 1}{\eta_e + 2} \right] R^3 \frac{E^2}{3} \times 10^2.$$

Using

$$R_2 = 0.4125 \text{ in.} = 0.0104775 \text{ meters}$$

$$\eta_e = 5.1 \text{ for Pyrex glass}$$

$$\epsilon_0 = 8.854 \times 10^{-12} \text{ farads/meter}$$

we have

$$F = 2.46 E^2 \times 10^{-10} \text{ dynes.}$$

Therefore, to get a force of 2.46 dynes with a field having the above gradient, we would need $E = 10^5$ volts/meter or 10^3 volts/cm.

This result shows that dielectric positioning of a small Pyrex glass sphere requires fields of the order of 10^3 volts/cm to get a few dynes of force. For positioning in the weightless state, this is not an unreasonable field to generate.

APPENDIX C

SUPERPOSITION OF FORCES AND DISTRIBUTIONS CONTRIBUTED BY TWO COILS

Further insight was obtained into the addition of repulsion forces when more than a single control coil is excited. The body force due to eddy currents in the conducting sphere is proportional to the magnetic field strengths within the sphere, which determine the amplitude of the eddy currents, and the magnetic field gradient. The eddy current strength j_1 due to a single coil is proportional to the current i_1 flowing in that coil times a geometrical factor which can be written as $f(y_1)$; y_1 is the coil-to-sphere distance. Thus, $j_1 = i_1 f(y_1)$. For two coils, $j = i_1 f(y_1) + i_2 f(y_2)$. The gradient of the field is proportional to the current in a given coil times another geometrical factor which may be denoted as $g(y)$. Thus,

$$\frac{dB}{dy} = i_1 g(y_1) + i_2 g(y_2)$$

for two coils. When two opposing coils are excited, the total field at the sphere position depends not only on the amplitudes of the currents flowing in the two coils, but also on their relative phase. If we consider that the driving frequencies of the opposing coils are the same (such a servo design is possible, but has not yet been implemented in the laboratory), then the total field at the sphere position will depend on the constant phase differences between the two coil currents as well as the individual current amplitudes.

If we write, as an abbreviation, $i_1 g(y_1) = G_1 \cos \omega t$ and $i_1 f(y_1) = F_1 \cos \omega t$, etc., we can write the total eddy current force acting on the floating mass as $j \text{ grad } B = [F_1 \cos \omega t + F_2 \cos (\omega t + \Phi)] [G_1 \cos \omega t - G_2 \cos (\omega t + \Phi)]$, where we have assumed that the current in driving coil no. 2 leads by a phase Φ the current in driving coil no. 1. If we take the time average of this expression, we obtain the average body force:

$$\langle F \rangle = \frac{1}{2} (F_1 G_1 - F_2 G_2) + \frac{\cos \Phi}{2} (F_2 G_1 - F_1 G_2)$$

If we consider the total power dissipation in the floating mass, we can write:

$$P \sim j^2 = [F_1 \cos \omega t + F_2 \cos (\omega t + \Phi)]^2$$

for the instantaneous power and the average power becomes

$$\langle P \rangle = \frac{F_1^2 + F_2^2}{2} + F_1 F_2 \cos \Phi$$

We see, as the phase difference of the current in the two coils varies between zero and 180° , the average power varies between the limits:

$$(F_1 - F_2)^2 \leq \frac{P}{2} \leq (F_1 + F_2)^2$$

The average force over this same range of phase difference varies between the limits:

$$\frac{(F_1 + F_2)(G_1 - G_2)}{2} \leq F \leq \frac{(F_1 - F_2)(G_1 + G_2)}{2}$$

If we plot the average power as a function of phase difference we obtain the curve shown in Figure C-1. If we further make the assumption that the sphere is centrally located between two coils of symmetrical construction so that the difference between F_1 and F_2 and between G_1 and G_2 is due to different current amplitudes, we can write

$$\frac{F_1}{F_2} = \frac{G_1}{G_2}$$

The average force as a function of phase difference Φ gives the plot shown in Figure C-1.

It is thus apparent that considerable flexibility exists with this scheme for varying force and power dissipation individually. For example, if the sphere is centrally located between two coils with equal excitation and it is desired to apply a body force to the mass without changing the power dissipation in the mass, we can write

$$\Delta P = i_1 \Delta i_1 + i_2 \Delta i_2 + \cos \Phi (i_1 \Delta i_2 + i_2 \Delta i_1)$$

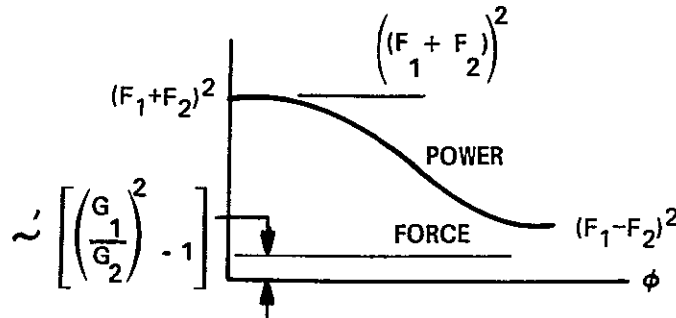


Figure C-1. Average Power as a Function of Phase Difference

where Δi_1 is a current increment.

For

$$i_1 = i_2, \Delta P = i_1 (\Delta i_1 + \Delta i_2) (1 + \cos \Phi)$$

If we select $\Delta i_2 = -\Delta i_1$, we see that there is no change in power dissipation, but a body force is obtained.

APPENDIX D

ELECTROSTATIC POSITIONING OF A DIELECTRIC

A thin walled, hollow glass sphere 3 cm in diameter, hanging on a fine wire about 300 cm long, was filled with tap water and placed among the electrodes shown in Figure D-1. The flat plates were four cm apart, the tip of the pointed electrode was 3 cm from each plate, and the sphere surface was 2 mm from the tip. (The dielectric constant of water and glass at room temperature are 80 and 5, respectively.) When 3000 volts were applied between the pointed electrode and the two flat plates, the uncharged sphere was repelled from the tip by approximately 2 mm which indicates a force of 10 dynes was acting upon it. Increasing the voltage to 5000 volts increased this deflection only slightly. One possible problem which can arise in the use of electrostatics was graphically shown when the sphere was made to swing such that it touched or very nearly touched the tip of the pointed electrode. It acquired a charge with each swing which by simple electrostatic repulsion caused the extent of each swing to become greater until finally, after 5 to 8 successively larger swings, the sphere was strongly attracted to one of the two plates, where it remained.

Pointed probes with spacings similar to those used above were used in place of the plates as shown in Figure D-2 without any obvious deflection for voltages up to 5000 volts.

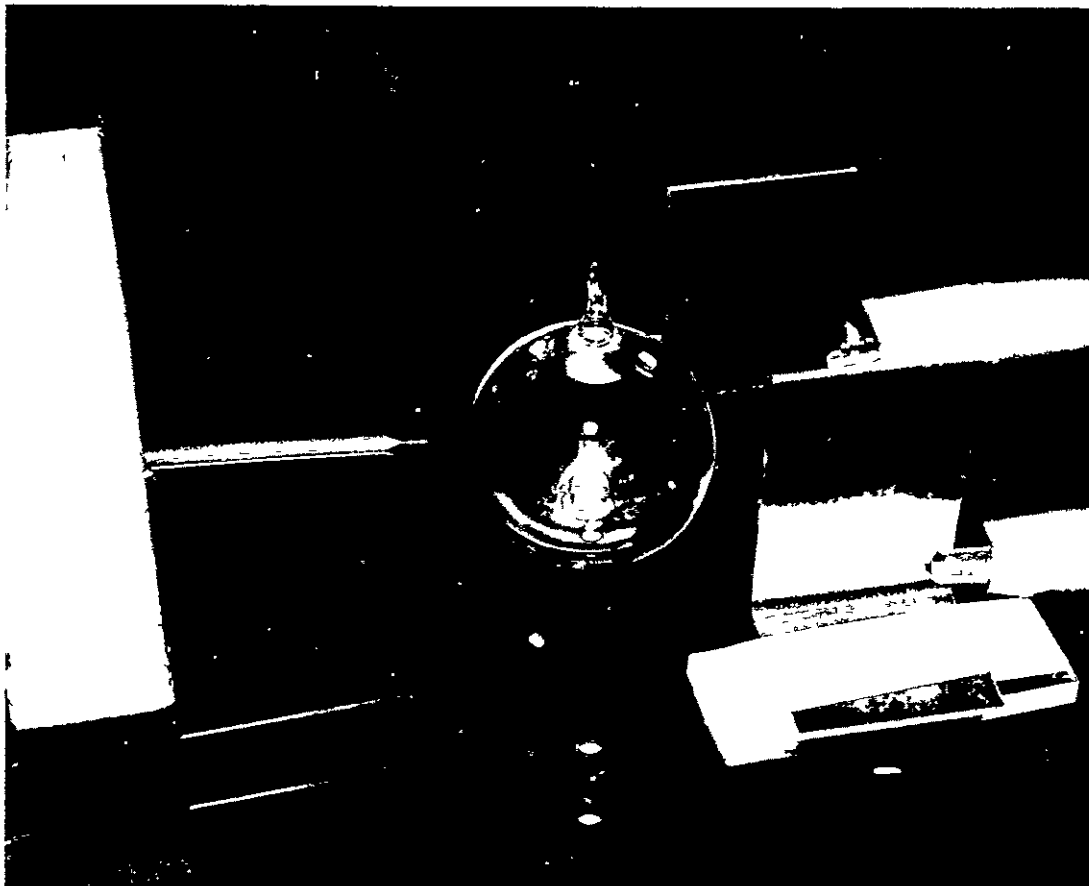


Figure D-1. Hollow Glass Sphere Filled with Water for Test of Electrostatic Repulsion with One Pointed Electrode

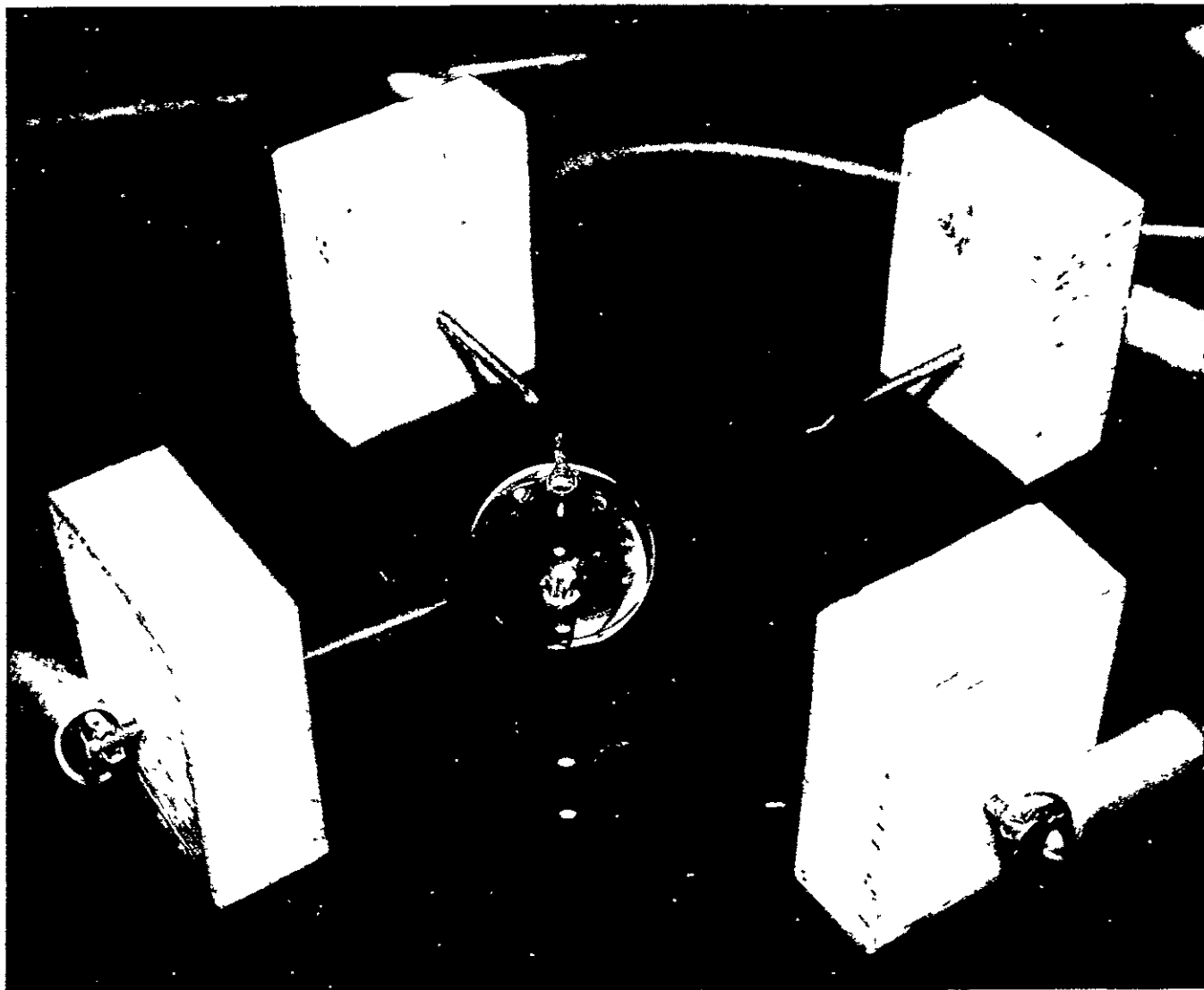


Figure D-2. Hollow Glass Sphere Filled with Water for Test of Electrostatic Repulsion with Four Pointed Electrodes

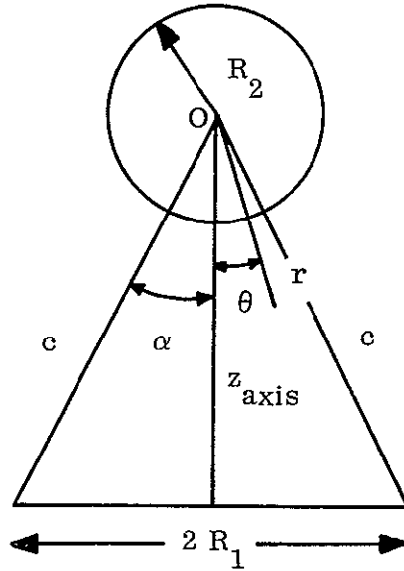
APPENDIX E

REFLECTED IMPEDANCE DUE TO EDDY CURRENTS

1. Introduction

In this appendix we shall develop more quantitatively the equations governing measurement of the position of a floating mass by electrical means. The simplest method, which has been described in this report and which served as a basis for the servo loop demonstration experiments, is to continuously monitor the fields generated by induced eddy currents in the floating mass. These fields will generate emf's in the control loops used to position the mass, and these emf's can be detected as equivalent changes in resistance and inductance of the coils. The induction effect follows from the fact that the eddy currents have, in general, a different phase than the coil excitation currents. In the main body of the report, circuits were described which detect these impedance changes independently of the level of coil excitation. In the following we develop the equations for the change in driving coil impedance due to the eddy currents.

Consider a single loop and a conducting sphere and let O at the sphere center be the origin of coordinates. Looking down on the subsystem, we have the illustration



where R_1 is the coil radius.

We may write the total vector potential \vec{A}_O outside the sphere as

$$\vec{A}_O = \vec{A}^c + \vec{A}^e$$

where A^c is the vector potential due to the exciting coil and \vec{A}^e is the vector potential due to eddy currents.

If we make the Fromm and Jehn approximation that "a current in a circular loop produces approximately the same field as a magnetic field uniform in space and sinusoidally oscillating with time" then

$$\vec{A}^e = \frac{DB_o}{2r^2} \sin \theta \hat{\phi}$$

where

$$D = \frac{(2\mu + \mu_o) v I_{-1/2}(v) - [\mu_o (1 + v^2) + 2\mu] I_{1/2}(v)}{(\mu - \mu_o) v I_{-1/2}(v) + [\mu_o (1 + v^2) - \mu] I_{1/2}(v)} R_2^3$$

with

$$v = \sqrt{j P} R_2, \quad P = \sigma \mu \omega,$$

and $I_{\pm 1/2}(v)$ denotes a Bessel function of order $\pm 1/2$.

The flux through the loop contributed by the eddy currents is just

$$\Phi = \int_S \int \vec{B}^e \cdot d\vec{S}$$

where S is a surface capping the loop. Using Stoke's Law,

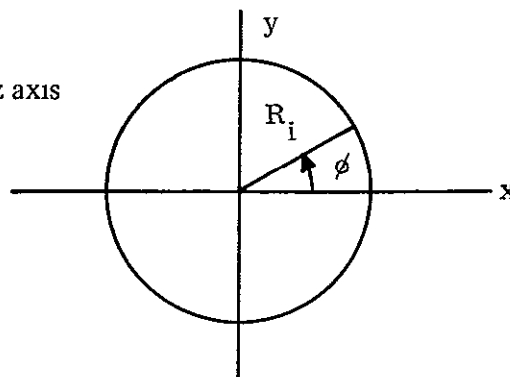
$$\Phi = \int_S \int \vec{B}^e \cdot d\vec{S} = \int_S \int \nabla \times \vec{A}^e \cdot d\vec{S} = \oint_{\ell} \vec{A}^e \cdot d\vec{\ell}$$

where ℓ is the path of the loop.

Then

$$\Phi = \frac{D B_o \sin \gamma}{2 c^2} \oint_{\ell} \hat{\phi} \cdot d\vec{\ell}$$

Looking at the loop along the z axis



$$\vec{R} = R_1 \cos \phi \hat{i} + R_1 \sin \phi \hat{j}$$

and

$$d\vec{R} = d\vec{\ell} = R_1 \left[-\sin \phi \hat{i} + \cos \phi \hat{j} \right] d\phi = R_1 d\phi \hat{\phi}$$

so that

$$\Phi = \frac{D B_o \sin \gamma}{2c^2} \oint_{\ell} R_1 d\phi$$

and

$$\Phi = \frac{2\pi R_1 D B_o \sin \gamma}{2c^2} = \frac{\pi R_1 D B_o \sin \gamma}{c^2}$$

$$\sin \gamma = \frac{R_1}{c}$$

and

$$c = \sqrt{R_1^2 + z^2}$$

$$\Phi = \left[\frac{\pi R_1^2 D B_o}{(R_1^2 + z^2)^{3/2}} \right] e^{j\omega t}$$

where the time dependence $e^{j\omega t}$ has been added and

$$E = \frac{-d\Phi}{dt} = \frac{-j\omega \pi R_1^2 D B_o}{(R_1^2 + z^2)^{3/2}}$$

is the induced voltage in the loop due to eddy currents in phasor form. Now letting B_o be the field due to the loop at the sphere center, if the sphere were not there

$$B_o = \frac{i_1 \mu_o}{2 R_1} \left\{ \frac{1}{(1+y^2)^{3/2}} \right\}$$

so that

$$E = \frac{-j \omega \pi R_1^2 D}{R_1^3 (1+y^2)^{3/2}} \left\{ \frac{\mu_o I_1}{2} \left[\frac{1}{(1+y^2)^{3/2}} \right] \right\}$$

and

$$E = \frac{-j \omega \pi \mu_o i_1 D}{2 R_1^2 (1+y^2)^3}$$

is the induced voltage in the exciting loop due to the flux arising from eddy currents.

Now $D = \text{Re}(D) + j \text{m}(D) = U + j W$

$$E = - \left\{ \frac{-\omega \pi \mu_o W}{2 R_1^2 (1+y^2)^3} + \frac{j \omega \pi \mu_o U}{2 R_1^2 (1+y^2)^3} \right\} i_1$$

which is the induced electromotive force rise in the circuit. The voltage drop is $-E$.

so we have

$$\Delta R = - \frac{\omega \pi \mu_o W}{2 R_1^2 (1+y^2)^3}$$

$$\Delta L = - \frac{\pi \mu_o U}{2 R_1^2 (1+y^2)^3}$$

as the reflected resistance and inductance, respectively.

In the high frequency limit as $\omega \rightarrow \infty$

$$\lim_{\omega \rightarrow \infty} U = -R_2^3$$

$$\lim_{\omega \rightarrow \infty} \omega W = \frac{3 \rho_e R_2 x}{\mu_o}$$

where

$$x = \frac{R_2}{\delta}$$

and

$$\delta = \sqrt{\frac{2}{\sigma \mu \omega}}$$

so that

$$\Delta L = \frac{-\pi \mu_o R_2^3}{2 R_1^2 (1 + y^2)^3}$$

$$\Delta R = \frac{3\pi \rho_e R_2 x}{2 R_1^2 (1 + y^2)^3}$$

Thus we have a decrease in the effective inductance and an increase in the effective resistance

For a loop of N turns $E = -N d\Phi/dt$ and if we assume that the loop is close wound so that the field B_o is approximately

$$B_o = \frac{N i_1 \mu_o}{2R_1} \left\{ \frac{1}{(1 + y^2)^{3/2}} \right\}$$

then

$$E = \frac{-j N^2 \omega \pi \mu_o i_1 D}{2 R_1^2 (1 + y^2)^3}$$

and

$$\Delta L = - \frac{\pi \mu_o N^2 R_2^3}{2 R_1^2 (1 + y^2)^3}$$

$$\Delta R = \frac{3 \pi \rho_e N^2 R_2^3}{2 R_1^2 (1 + y^2)^3}$$

2 Conclusion

Limited experimental tests were made for the effective change in inductance as the position of a conducting aluminum sphere was varied. Although the results varied with y in the way indicated from the formula above, a discrepancy of approximately a factor 2 was observed. This is considered to lie well outside of experimental errors and is thought to be attributable to the rather strong field gradient which was not taken into account in computing the dipole moment due to eddy currents.

APPENDIX F

ELECTRIC DISPLACEMENT CURRENT IN DIELECTRICS

When considering the properties of conductors and dielectrics, we must consider the form of Maxwell's equations within a material medium. The equation relating magnetic field intensity and current for linear, isotropic, nonpermeable media can be written as

$$\nabla \times (\mu_o \vec{H}) = \mu_o \vec{J} + \mu_o \kappa_e \epsilon_o \partial \vec{E} / \partial t$$

or

$$\nabla \times \vec{B} = \underbrace{\mu_o \vec{J}}_{\text{Conduction Current}} + \underbrace{\mu_o \kappa_e \epsilon_o \partial \vec{E} / \partial t}_{\text{Displacement Current}}$$

in the M.K.S. system of units, where $\mu_o = 4\pi \times 10^{-7}$ henry/meter and is the permeability of free space, $\epsilon_o = 8.854 \times 10^{-12}$ farad/meter and is the permittivity of free space, and κ_e is the relative permittivity of the linear, isotropic, homogenous, nonpermeable medium.

In a good conductor

$$\mu_o \vec{J} \gg \mu_o \kappa_e \epsilon_o \partial \vec{E} / \partial t$$

and in a poor conductor

$$\mu_o \vec{J} \ll \mu_o \kappa_e \epsilon_o \partial \vec{E} / \partial t$$

so that ratio

$$Q = \frac{\mu_o \kappa_e \epsilon_o \partial \vec{E} / \partial t}{\mu_o \vec{J}}$$

is a quantity which expresses the importance of conduction currents or displacement currents in a material. For a time harmonic field $\vec{E} = \vec{E} e^{j\omega t}$, and $\partial \vec{E} / \partial t = j \omega \vec{E}$, so with $\vec{J} = \sigma \vec{E}$, the ratio Q is just $\kappa_e \epsilon_o \omega / \sigma$.

The quantity $1/Q$ is the ratio of conduction to displacement currents. In a good conductor like copper, $1/Q$ will range from 10^{17} to 10^{12} as the frequency increases from 10 to 10^6 cps, while in a cold glass, $1/Q$ will range from 10^{-3} to 10^{-9} over the same range of frequencies. Figure F-1 shows the range of $1/Q$'s possible in the frequency range 10^3 to 10^6 cps for a molten glass. Here the range of conductivities is 1 mho/meter to 10^4 mho/meter, and taking a typical permittivity of $\kappa_e = 5$ (data show κ_e can vary from 3 to 18), the range of $\sigma/\kappa_e\epsilon_0$ is 2.26×10^{10} to 2.26×10^{14} and values of $1/Q$ within this rectangular region will range from about 1.59×10^4 to 1.59×10^{10} . It can be seen that as we go up in frequency, the quantity $1/Q$ decreases, since here displacement currents are becoming more and more important. We can also conclude that within this frequency band conduction currents still dominate appreciably. For intermediate temperatures, the conduction and displacement currents in glass will become of comparable magnitude.

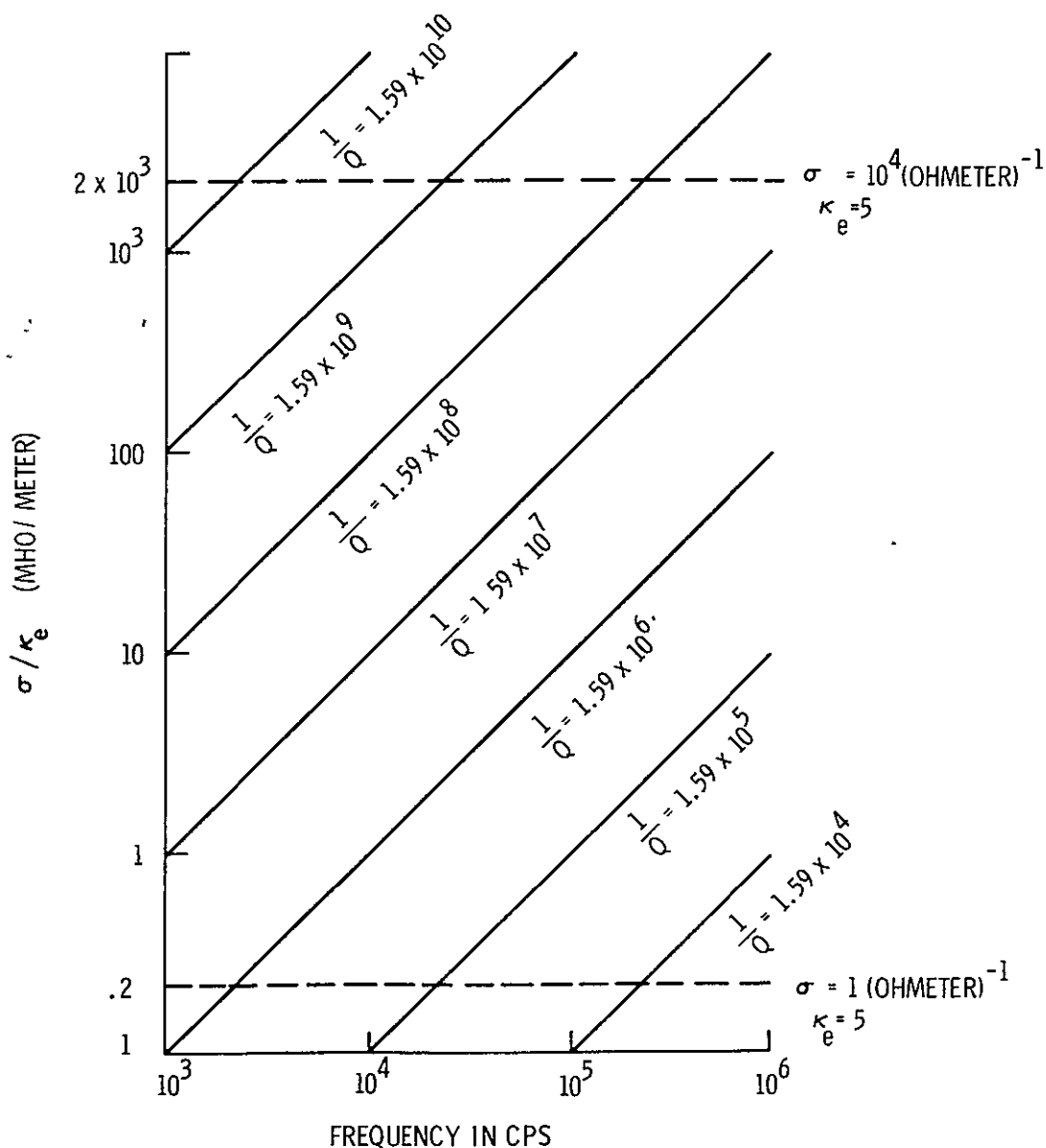


Figure F-1. Plot of $\rho/\kappa_e\epsilon_0 = (2\pi/Q) f$ with Dashed Lines a Molten Glass Region

APPENDIX G

CO-VARIANT SOLUTION OF ELECTROMAGNETIC EDDY CURRENT PROBLEM

In the previous quarterly report, expressions were derived for the magnetic field and current density inside a conducting sphere immersed within an otherwise uniform oscillating magnetic field. Because of the complexity of the mathematical expressions, a computer was used to calculate the distribution of fields and forces. Even these solutions, however, are highly idealized in that practical applications require utilization of nonuniform fields in order to obtain position sensing and control forces. An essential part of the complexity of the problem is related to the requirement for the use of spherical polar coordinates and the resulting complication in such mathematical expressions as the Laplacian ∇^2 and the curl. Because of the fact that expressions such as these have the same form independent of coordinate system when a covariant approach is taken to the solutions of the electromagnetic field and forces problem, this approach offers a hope for simplification of more complex problems such as those of nonuniform fields.

We will denote the components of the magnetic vector potential as A_μ , $\mu = 1, 2, 3$. The electromagnetic field components are represented by the antisymmetric tensor $\phi_{\mu\nu}$, where the indices μ and ν range over the values 1, 2, 3. The identification is made that $\phi_{23} = -B_\phi$, $\phi_{13} = B_\theta$, $\phi_{12} = -B_r$. Other quantities which we will require in the succeeding discussion are the following

The "metric tensor" components $g_{\mu\nu}$ and their inverses $g^{\mu\nu}$ relate the expression for arc length to the coordinate differentials. In spherical polar coordinates, these quantities are $g_{11} = 1$, $g_{22} = r^2$, $g_{33} = r^2 \sin^2 \theta$. The non-diagonal terms vanish

The determinant of the metric tensor, g , is in this case

$$g = r^4 \sin^2 \theta$$

The coordinates r, θ, Φ , are denoted as x_1, x_2, x_3 .

The electrical conductivity is denoted by σ and the magnetic permeability by μ .

Maxwell's equation for the curl of the magnetic field is then written simply as

$$\frac{\partial \Phi^{\mu\nu}}{\partial x_\nu} = J^\mu$$

where $\Phi^{\mu\nu}$ is the contravariant field tensor density $\sqrt{g} \phi^{\mu\nu}$, and J^μ is the contravariant current density.

If we assume that the only non vanishing component of A is A_3 and that this depends only on the coordinates x_1 and x_2 , the above expression reduces to

$$\frac{\partial}{\partial x_1} \sqrt{g} g^{33} g^{11} \frac{\partial A_3}{\partial x_1} + \frac{\partial}{\partial x_2} \sqrt{g} g^{33} g^{22} \frac{\partial A_3}{\partial x_2} = -\sigma \sqrt{g} g^{33} \frac{\partial A_3}{\partial j}$$

Introducing the more usual notation r, θ, Φ , assuming that A depends on the time as $\exp(i\omega t)$, and introducing the expression for skin depth $\mu\sigma\omega = 1/\delta$, we obtain

$$r^2 \frac{\partial^2 A}{\partial r^2} + \sin \theta \frac{\partial}{\partial \theta} \left(\frac{1}{\sin \theta} \frac{\partial A}{\partial \theta} \right) = -i \frac{r^2}{\delta^2} A_\phi$$

If we introduce $\xi = \sqrt{i} r/\delta$, this becomes

$$\xi^2 \frac{\partial^2 A}{\partial \xi^2} + \sin \theta \frac{\partial}{\partial \theta} \left(\frac{1}{\sin \theta} \frac{\partial A}{\partial \theta} \right) = -\xi^2 A_\phi$$

If we assume that A can be written as the product of separate functions of r and a function of θ , $A_\phi = R(r)\Theta(\theta)$, we obtain the pair of equations

$$\frac{1}{\theta} \sin \theta \frac{d}{d\theta} \left(\frac{1}{\sin \theta} \frac{d\Theta}{d\theta} \right) = \alpha$$

$$\frac{1}{R} \xi^2 \frac{d^2 R}{d\xi^2} + \xi^2 = -\alpha$$

where α is the separation constant. The separation constant satisfying the boundary condition of a uniform applied field gives $\alpha = -2$. This allows the angular equation to be integrated as

$$\Theta(\theta) = \text{const} \times \sin^2 \theta$$

The solution of the radiation equation is

$$R(r) = \sqrt{\xi} J_{3/2}(\xi)$$

where $J_{3/2}$ is a Bessel function of the first kind. The complete solution inside the sphere is then

$$A_3 = C \sin^2 \theta \sqrt{\xi} J_{3/2}(\xi)$$

The corresponding unitary magnetic vector potential is

$$A_{\phi}^u = \frac{A_3}{\sqrt{g_{33}}} = C' \frac{\sin \theta}{\sqrt{\xi}} J_{3/2}(\xi)$$

in accordance with the solution found by Smythe.

The expressions for the magnetic field components and the electromagnetic force can be written in very simple form in terms of the covariant component A_3 as follows:

$$\phi_{\mu\nu} = \frac{\partial A_{\mu}}{\partial x_{\nu}} - \frac{\partial A_{\nu}}{\partial x_{\mu}} \quad ; \quad \text{or} \quad \phi_{13} = -\frac{\partial A_3}{\partial x_1} \quad \text{and} \quad \phi_{23} = -\frac{\partial A_3}{\partial x_2}$$

$$F_{\mu} = \phi_{\mu\nu} J^{\nu}$$

The simplicity and symmetry of these expressions is evident and offers hope for simplification over the expressions in unitary form for more complicated problems, such as that of the nonuniform field. It must be remembered that the more familiar unitary force component per unit volume is related to the covariant force component by the expression

$$F_{\nu}^u = \frac{1}{\sqrt{g_{\mu\mu}}} F_{\mu}$$

